CORA Cork Open Research Archive
Cartlann Taighde Oscailte Chorcaí

Title	Acetylated microtubules are essential for touch sensation in mice
Authors	Morley, Shane J.
Publication date	2016
Original Citation	Morley, S. J. 2016. Acetylated microtubules are essential for touch sensation in mice. PhD Thesis, University College Cork.
Type of publication	Doctoral thesis
Rights	© 2016, Shane J. Morley. - http://creativecommons.org/licenses/by-nc-nd/3.0/
Download date	2026-11-01 23:54:18
Item downloaded from	https://hdl.handle.net/10468/4689



UCC
University College Cork, Ireland
Coláiste na hOllscoile Corcaigh

Acetylated Tubulin is Essential for Touch Sensation in Mice

By Shane J. Morley

Thesis presented for degree of Doctor of Philosophy

National University of Ireland, Cork

Department of Physiology

Head of Department: Prof. Ken O' Halloran

Supervisor: Dr. Mark Rae

December 2016

1 Table of Contents

Chapter 1: Introduction 2
1.1 The origin of mechanosensation 3
1.2 The structure of the peripheral nervous system (PNS) 7
1.2.1 Low-threshold fibres in glabrous skin 10
1.2.2 Low-threshold fibres in the hairy skin 14
1.2.3 High-threshold mechanosensitive (HTMR) fibres in glabrous and hairy skin 15
1.3 Dorsal root ganglia (DRG) 16
1.4 The spinal cord 18
1.5 Theories of peripheral sensory perception 20
1.6 Proprioception 23
1.7 Thermosensation 23
1.8 The molecular apparatus of mechanotransduction 24
1.8.1 Mechanosensitive (MS) ion channels 25
1.8.2 The gating of mechanosensitive ion channels 27
1.8.3 Microtubules as tether structures 32
1.9 Microtubules and mechanosensation 34
1.10 The role of Mec 17 and Atat1 in mechanosensation 36
2 Chapter 2: General Methods 39
2.1 Animal breeding and genetics 39
2.2 Statistical analysis and animal care 40
3 Chapter 3: Materials and Methods 42
3.1 Methods 42
3.1.1 Low-threshold mechanical assay I: tape response assay 42
3.1.2 Low-threshold mechanical assay II: cotton swab assay 42
3.1.3 High-threshold mechanical assay I: von Frey assay 42
3.1.4 High-threshold mechanical assay II: tail clip test 43
3.1.5 Thermal sensitivity assay I: hot plate assay 43
3.1.6 Thermal sensitivity assay II: tail immersion assay 43
3.1.7 Thermal sensitivity assay III: acetone drop test 44
3.1.8 Proprioceptive Assay I: Rotarod Assay 44

3.1.9 Proprioceptive assay II: grid walk balance assay 44
3.1.10 DRG neuronal culturing and transfection 45
3.1.11 Visualising the afferents peripheral nervous system in the skin 45
3.1.12 Electron microscopy of saphenous nerves 46
3.1.13 Measuring axon growth in DRG cells 46
3.1.14 Actin staining of DRG 46
3.1.15 Superresolution of DRG 47
3.1.16 Staining of the dorsal horn of the spinal cord 48
3.1.17 Microtubule axonal transport 48
3.1.18 Fluorescent recovery after photo-bleaching (FRAP) analysis of Piezo2-GFP transfected DRG neurons 49
3.1.19 Immunohistochemical labelling of microtubules in both MEF cells and DRG neurons 50
3.1.20 Visualisation of acetylated microtubules in peripheral corneal nerve fibres 50
3.1.21 Localisation of acetylated microtubules in the saphenous nerve 51
3.1.22 Atomic Force Microscopy (AFM) 51
3.1.23 Hyperosmotic Shock Cell Shrinking Assays 52
4 Chapter 4: Behavioral Characterisation of Atat^{cKO} Mice 54
4.1 Results 54
4.1.1 Assessing animal behavioural response to mechanical, thermal and proprioceptive tests 54
4.1.2 Atat1^{cKO} mice are insensitive to innocuous mechanical stimuli 54
4.1.3 Atat1^{cKO} mice are insensitive to noxious mechanical stimuli 56
4.1.4 Atat1^{cKO} mice showed no difference in thermal sensitivity relative to Atat1^{Control} 58
4.1.5 Atat1^{cKO} mice exhibited no deficits in proprioception 60
4.2 Discussion 62
4.2.1 Atat1^{cKO} mice are insensitive to low threshold mechanical stimuli 62
4.2.2 Atat1^{cKO} mice are insensitive to high threshold mechanical stimuli 63
4.2.3 No differences in thermal sensitivity were observed between the genotypes 64
4.2.4 Proprioceptive testing revealed no differences between the genotypes 65
4.2.5 Mechanosensitivity was restored by genetically mimicking Atat1 activity 66
4.2.6 Genetically mimicking Atat1 activity restored mechanosensitivity 69
5 Chapter 5: Examining the structural and functional characteristics of the PNS 71
5.1 Aims: Examining the structural and functional characteristics of the PNS 71
5.2 Results 71
5.2.1 The structure of the PNS in skin / saphenous nerve was unaltered between genotypes 71

5.2.2 Axonal outgrowth length was unaltered between Atat1^{Control} and Atat1^{cKO} DRG 74
5.2.3 The actin cytoskeleton appeared unaltered in DRG from both genotypes 76
5.2.4 Superresolution microscopy of α tubulin network in DRG neurons revealed no differences between the groups 78
5.2.5 Spinal cord morphology was unaltered between the groups 81
5.2.6 Axonal Transport in DRG Neurons was not different between the genotypes 83
5.2.7 Fluorescence recovery after photobleaching (FRAP) analysis of Piezo2-GFP in transfected DRG neurons revealed no differences in membrane ion channel trafficking..... 85
5.3 Discussion: Atat1^{cKO} mice show no alterations in gross PNS morphology / function relative to Atat1^{Control} 87
6 Chapter 6: Examining the role of Atat1 in regulating the membrane rigidity of DRG neurons 92
6.1 Aims: Examining the role of Atat1 in regulating the membrane rigidity of DRG neurons 92
6.2 Results 92
6.2.1 Acetylated microtubules have a sub-membrane localization in corneal peripheral afferents 94
6.2.2 Acetylated microtubules have a sub-membrane localization in saphenous nerve tissue .. 96
6.2.3 Atat1^{cKO} DRG neurons have stiffer membranes relative to control cells 98
6.2.4 Atat1^{cKO} DRG afferents and internal microtubule networks exhibit greater resistence to shrinking than their Atat1^{Control} counterparts 100
6.3 Discussion: Atat1 is essential for regulating the membrane rigidity of DRG and their associated afferents 102
7 Conclusions 108
8 Future directions 110
9 References 114
10 Appendix 136

Declaration

I hereby declare that the arrangement of this thesis is entirely my own work. Elements of this study have been published as a manuscript which appears as a pre-print in the appendix. I confirm that this thesis has not been submitted to any other institution for the reward of a PhD.

Acknowledgements

I would like to thank Dr. Paul Heppenstall for his mentorship and scientific guidance throughout my Ph.D. training. I also wish to thank Dr. Cornelius Gross, Dr. Darren Gilmour and Dr. Gordon Reid for their scientific input throughout my studies. I extend extra thanks to Dr. Mark Rae for his guidance and support while preparing this manuscript.

Acknowledgement of Copyright

I hereby confirm that I have received permission from the respective authors / publishers to re-produce all of the images contained within this document.

List of Abbreviations

Atat1	Alpha tubulin acetyltransferase 1
Mec17	Mechanosensory abnormality protein 17
MScL	Mechanosensitive ion channel large conductance
MScS	Mechanosensitive ion channel small conductance
MS- channels	Mechanosensitive - channel
LTMRs	Low threshold mechanosensory fibre
HTMRs	High threshold mechanosensory fibre
IB4	Isolectin B4
CGRP	Calcitonin gene related peptide
CLTMRs	C fibre low threshold mechanosensory fibre
SAM	Slowly adapting mechanosensory fibre
RAM	Rapidly adapting mechanosensory fibre
RAI / II	Rapidly adapting mechanosensory fibre type I /II
SAI / II	Slowly adapting mechanosensory fibre type I / II
DRG	Dorsal root ganglion
PNS	Peripheral nervous system
ASIC	Acid sensing ion channel
TRPC1	Transient receptor potential ion channel 1
NOMPC	No mechanoreceptor potential C
SLP3	Stomatin like protein 3
ARs	Ankyrin repeats
TRPV1	Transient receptor potential cation channel subfamily V member 1
TRPM8	Transient receptor potential cation channel subfamily M member 8
PTMs	Post-translational modification
MAP	Microtubule associated protein
GNAT	GCN5-related N-acetyltransferase domain
TRNs	Touch responsive neurons
Avil	Advillin
RPM	Rotations per minute
K40	Lysine 40
GFP	Green fluorescent protein
YFP	Yellow fluorescent protein
BG	Benzilguanine
BSA	Bovine serum albumin
dSTORM	Direct stochastic optical reconstruction microscopy
MT	Microtubule
FRAP	Fluorescence recovery after photobleaching
PGP 9.5	Protein gene product 9.5
NGF	Nerve growth factor
Q-dot	Quantum-dot
TH	Tyrosine hydroxlase
MEF	Mouse embryonic fibroblast
PFA	Paraformaldehyde
CB	Cytoskeleton buffer
NGS	Normal goat serum
SiR	Silicone rhodamine
MBP	Myelin basic protein
AFM	Atomic force microscopy

cKO	Conditional knock-out
MSC	Mechanosensitive ion channel
SNI	Spared nerve injury

List of Figures and Tables

Figure 1	A hypothetical model of mechanosensation in proto-amoeboid cells.
Figure 2	A diagram representing the constituent components of the peripheral nervous system.
Figure 3	Diagram illustrating the types of fibres and end organs found in the glabrous and hairy skin.
Figure 4	An image and diagram of the spinal cord outlining the sub-division of this structure into various laminae.
Figure 5	Diagrams representing the structure and mode of action of the duel-tether type model of mechanical gating.
Figure 6	Diagrams representing the structure and mode of action of the single tether type model of mechanical gating.
Figure 7	Diagram representing the components and ultrastructure of microtubules.
Figure 8	Low-threshold mechanical touch assays carried out on $Atat1^{Control}$ and $Atat1^{cKO}$ mice respectively.
Figure 8.1.	High-threshold mechanical assays carried out on $Atat1^{Control}$ and $Atat1^{cKO}$ mice respectively.
Figure 8.2.	Temperature testing assays carried out on $Atat1^{Control}$ and $Atat1^{cKO}$ mice respectively.
Figure 8.3.	Proprioception assays carried out on $Atat1^{Control}$ and $Atat1^{cKO}$ mice respectively.
Figure 8.4.	Whole cell patch-clamp recording from transfected $Atat1^{cKO}$ DRG to detect restoration of mechanosensation
Figure 9.0.	Analysis of peripheral nerve afferents / end organs in whole mount skin of $Atat1^{Control}$ and $Atat1^{cKO}$ animals.
Figure 9.1.	Electron microscopy images and analysis of saphenous nerve taken from $Atat1^{Control}$ and $Atat1^{cKO}$ mice.
Figure 9.2.	Mosaic images and analysis of axon outgrowth from whole mount DRG explants after 7 days in culture.
Figure 9.3.	Cytoskeleton (actin) organization in DRG neurons derived from $Atat1^{Control}$ and $Atat1^{cKO}$ mice.
Figure 9.4.	Superresolution imaging and analysis of the microtubule network of $Atat1^{Control}$ and $Atat^{cKO}$ – derived DRG neurons.
Figure 9.5.	Representative images of spinal cord staining from $Atat1^{Control}$ and $Atat1^{cKO}$ mice.
Figure 9.6.	Single particle NGF / receptor complex axonal transport in $Atat1^{Control}$ and $Atat^{cKO}$ DRG cells.
Figure 9.7.	FRAP analysis of Piezo-GFP in transfected $Atat1^{Control}$ and $Atat1^{cKO}$ DRG neurons.
Figure 10.0.	Staining and analysis of the distribution of acetylated and non-acetylated α tubulin in $Atat1^{Control}$ DRG neurons and MEFs.
Figure 10.1.	Representative confocal fluorescence image of sensory affernts immunohistochemically labelled for SNAP and acetylated tubulin.
Figure 10.2.	Staining of $Atat1^{Control}$ saphenous nerve with anti-acetylated tubulin and myelin basic protein.
Figure 10.3.	Graph summarising AFM results measuring the pressure required to indent the membranes of $Atat1^{Control}$ and $Atat1^{cKO}$ DRG neurons to specific degrees.

Figure 10.4.	Figure showing axonal shrinking and microtubule network integrated density following hyperosmotic shock of $Atat^{Control}$, $Atat^{cKO}$ DRG neurons transfected with the K40Q amino acid mimic.
Table 1	A scheme representing the proposed sub-populations of DRG based on single-cell RNA sequencing data

Abstract

The sense of touch depends upon the transformation of mechanical energy into electrical signals by peripheral sensory neurons and associated cells in the skin. This conversion is thought to be mediated by a complex of proteins in which ion channels such as Piezo2 function as mechanotransducers. However, how mechanical energy is transmitted into mechanosensitive ion channel opening, and how cellular components such as the cytoskeleton influence this process, is largely unknown. Here we show that mice lacking the tubulin acetyltransferase, Atat1, in sensory neurons display profound deficits in their ability to detect mechanical touch and pain. In the absence of Atat1, behavioural responses to innocuous and noxious mechanical stimuli are strongly reduced in multiple assays while sensitivity of mice to thermal stimuli is unaltered. In *ex vivo* skin-nerve preparations, the mechanosensitivity of all low- and high- threshold mechanoreceptor subtypes innervating the skin is substantially decreased in Atat1 conditional knockout mice. In cultured dorsal root ganglion neurons, both slowly- and rapidly- adapting mechanically- activated currents are absent or reduced upon Atat1 deletion with no effect on other neuronal functions. We establish that this broad loss of mechanosensitivity is dependent upon the acetyltransferase activity of Atat1, and that by mimicking α-tubulin acetylation genetically by substituting the lysine amino acid for a structurally similar glutamine, mechanosensitivity can be restored in Atat1- deficient sensory neurons. Finally, we demonstrate that acetylated microtubules localize to a prominent band under the membrane of sensory neuron cell bodies and axons, and in the absence of Atat1 and acetylated α-tubulin, cultured sensory neurons display significant reductions in their membrane elasticity. Our results indicate that the microtubule cytoskeleton is an essential component of the mammalian mechanotransduction complex and that by influencing cellular stiffness, α-tubulin acetylation can tune mechanical sensitivity across the full range of mechanoreceptor subtypes.

It is a profound and necessary truth that the deep things in science are not found because they are useful; they are found because it was possible to find them”

- Robert Oppenheimer

Chapter 1: Introduction

Traditionally there are thought to be five sensory faculties: sight, smell, taste, hearing and touch. These separate sensory faculties have evolved to detect a diverse array of physical signals, such as photons (sight) or gaseous molecules (smell). Taken together, these systems give life forms the information they require to survive in dynamic, ever changing environments. Amongst all of the senses, it might be argued that touch, or mechanosensation, by virtue of its early emergence in the tree of life, is among the most fundamental (Martinac and Kloda, 2003). Indeed, it was Aristotle himself who declared in his work 'De anima' (On the Soul) translated by J.A. Smith in 1994, that 'the primary form of sense is touch, which belongs to all animals', (Aristotle, 1994). In the Aristotelian context 'touch' is considered to be a response to physical or mechanical stimuli. In modern times, touch is likewise defined; however, it now falls under the broader umbrella term of somatosensation, which encompasses other types of sensations such as temperature (thermosensation), body orientation (proprioception) and the itch (prurioception) response to mechanical / chemical irritants. As a whole, these separate somatosensory modalities allow an organism to extract important information from all the solids, liquids and gases which it will encounter in the world. In this work, I shall focus my attention almost exclusively on the somatosensory sub-modality of mechanosensation, exploring from a 'ground-up' perspective our current molecular understanding of this, the most ancient of senses.

Touch or mechanosensation can be best defined as the conversion of physical force into electrical or chemical signals (Martinac and Kloda, 2003). Despite the early evolutionary origin of mechanosensation; outside of prokaryotes surprisingly little is known about the basic molecular underpinnings of this modality in comparison with many of the other sensory systems (Kung, 2005; Chalfie, 2009). Moreover, what little is known, even in 'simple' multicellular organisms such as *C.elegans* paints a complex picture, involving a myriad of interdependent intracellular, extracellular

and membrane associated proteins (Chalfie, 2009). Given then that mechanosensation is such a complex topic, I will now briefly outline the structure and content of the introduction section.

As mentioned, I intend to take a 'ground-up' approach to examining mechanosensation. Therefore, I will begin with a discussion of the evolutionary origins of this sensory modality in our early ancestors. Following this, I will then move on to discuss the anatomy of the peripheral nervous system (PNS). In this section, I will highlight the most recent molecular and genetic studies which have given us an unprecedented understanding of the diversity and intricacy of this system. I will then devote a section to discussing some of the molecular machinery, such as ion channels, components of the lipid membrane and other proteins, which function to directly detect, or aid detection of, mechanical events in the PNS. Next, I will turn my attention to microtubules and our current understanding of the role of these important proteins in mechanosensory biology. Finally, I will discuss our current understanding of the role of MEC17 / Atat1 (Mechanosenory abnormality protein 17 / alpha-tubulin acetyltransferase 1) in mechanosensation, which is a topic that we have been able to shed light upon with our own work.

1.1 The origin of mechanosensation

"All the essential problems are already solved in the one-celled…protozoan and these are only elaborated in man or in the other multicellular animals".

(Simpson, 1949)

The first living systems are thought to have appeared on the Earth between 4.1 – 3.5 billion years ago (Ohtomo *et al.*, 2014; Bell *et al.*, 2015). Since their emergence, living systems have evolved an incredible repertoire of perceptive capacities that allow them to sense the various properties of their surrounding environments. One of these sensory systems was a sense of touch or mechanosensation. This modality primarily allows living systems to detect and respond to physical stimuli exerted upon the interface between the organism and its environment. The most recent picture of the phylogenetic

tree of life encompasses three principle domains, namely, the eukarya, bacteria and Archaea respectively. Mechanosensitive ion channels (MS-channels) have been identified in members of all three of these domains, thus indicating an early origin for these proteins in life on this planet (Martinac and Kloda, 2003). The regulation of water levels across the cell membrane of these early organisms may have provided the necessary selective pressure to drive the origin of the earliest MS-channels (Kung, 2005). Water is vital for life on Earth; however too much or too little water and an organism will quickly succumb to lysis or dehydration, respectively. Therefore, the regulation of the concentration of water across the membrane of cells is vital for the survival of living systems (Kung, 2005).

Work, starting in the 1950s, with the bacterium *Escherichia coli* (*E. Coli*) demonstrated that these organisms were capable of releasing their solutes into their extracellular environment in response to an increase in extracellular water, thus preventing the bacteria from bursting due to increased turgor pressure (Kung, 2005). Two channels discovered in 1987 (Martinac *et al.*, 1987), MscL and MscS (mechanosensitive channel of large or small unitary conductance, respectively) were postulated to act as solute 'release valves' that prevent *E.coli* from lysing in these circumstances. However, it was not until 1999, when work carried out on *E. coli* harboring non-functioning mutant copies of these channels, demonstrated that these cells were overly prone to lysis in aqueous solutions (Levina *et al.*, 1999). The mechanism of action of the MscL and MscS channels is deceptively simple. Following the exposure of *E.coli* to a hypotonic solution, the bacteria begin to swell as liquid passed through the ever-stretching plasma membrane by osmosis. MS-channels are forced open by this stretching, thereby allowing an efflux of solutes which reduces the osmotic gradient across the bacterial membrane and thereby equilibrates the intra / extracellular concentration of water, preventing the cell from bursting (Kung, 2005). Moreover, the MS-channels were also shown to produce ionic currents when a suction based mechanical stimulus was applied to the membrane of *E. coli* cells (Martinac *et al.*, 1987). Additionally, further work on purified MscL proteins, which were reconstituted within simplified lipid membranes, demonstrated that this channel remains sensitive to membrane

perturbation in this setting (Perozo, Cortes, *et al.*, 2002; Perozo, Kloda, *et al.*, 2002). Therefore, it was concluded that MscLs were capable of functioning in biologically reduced systems, and that the channel can be fully activated by stretching of the membrane, independently of other proteins (Perozo et al. 2002).

Given the simplicity of their mechanism of action, coupled with their vital role in maintaining homeostasis, it is probable that the MS-channels present in *E.coli* are the ancestors of earlier molecules which served the same function in their forebears (Martinac and Kloda, 2003). Indeed, phylogenetic analysis has revealed that certain domains within MscL are conserved across gram-positive and gram-negative bacteria, indicating regions of the proteins which may well be indispensable for its mechanosensory function (Moe, Blount and Kung, 1998). Linking back to G.G. Simpson's earlier assertion, that all of the essential problems associated with an organisms' survival are already solved in single celled life and merely elaborated on in higher organisms, it seems that sensing stretch of the lipid membrane (the bilayer mechanism) is at the heart of all MS-channel functioning from prokaryotes onwards. Therefore, any elaborate adaptations now being discovered in eukaryotes such as the interaction with cytoskeletal and extra-cellular matrix proteins, function only to finesse the sensitivity of this fundamental mechanism (Martinac and Kloda, 2003).

Moving from prokaryotes to the first eukaryotes, an interesting hypothesis was forwarded recently to explain how guarding against the influx of calcium may have provided the selective pressure required to evolve some of the 'elaborate adaptations' observed in eukaryotic MS-channels (Brunet and Arendt, 2016). Cells spend a substantial amount of energy maintaining a huge (~20,000 fold) difference in the concentration of calcium between their extracellular (high calcium) and intracellular (low calcium) environments (Clapham, 2007). This difference is maintained to guard against the cytotoxic effects generated by excessive quantities of calcium within the cytosol. Specifically, due to its propensity for forming precipitates with phosphate (Clapham, 2007), chronically elevated intracellular calcium can interfere with vital metabolic processes within the cell. As a result, any opening induced by damage to the cell membrane must be quickly sealed. In order to achieve this,

two systems have evolved to quickly plug a hole in the cell membrane and remove the excess calcium invading the cell and these mechanisms are conserved across all eukaryotic organisms. These mechanisms are **(1)** closure of the puncture (hole) by contraction of an actomyosin ring (Abreu-Blanco, Verboon and Parkhurst, 2011) and **(2)** removal of excess calcium by exocytosis of vesicles (Reddy, Caler and Andrews, 2001). Given that these strategies are designed to close a gap in the cell membrane, it is not surprising to learn that both systems are activated by the inevitable rise of intracellular calcium which would accompany such an insult (Idone, Tam and Andrews, 2008; Abreu-Blanco, Verboon and Parkhurst, 2011). It is well known that eukaryotic transient receptor potential (TRP) channels, as well as the recently discovered Piezo family of MS-channels, are either partly or exclusively permeable to calcium (Clapham, 2003; Syeda *et al.*, 2015). The authors suggest that such Ca^{2+} permeable MS-channels were recruited as part of an 'early warning system' to detect the initial influx of calcium, before a catastrophic tear could form in the membrane (Brunet and Arendt, 2016). They further suggest that the initial influx of calcium through these channels then activates the aforementioned puncture repair mechanisms in order to stem any further influx.

Indeed the authors cite the sub-membrane position of the actomyosin network in all eukaryotic cells as strong evidence for a cross-interaction between the channels and the network (Brunet and Arendt, 2016). Finally, as shown in figure 1, the authors suggested that by coupling mechanical sensation with a contractile actomyosin network, proto-amoeboid cells would have been equipped with an apparatus to sense and move away from forces exerted upon their surface without the need for even a simple nervous system (Brunet and Arendt, 2016).

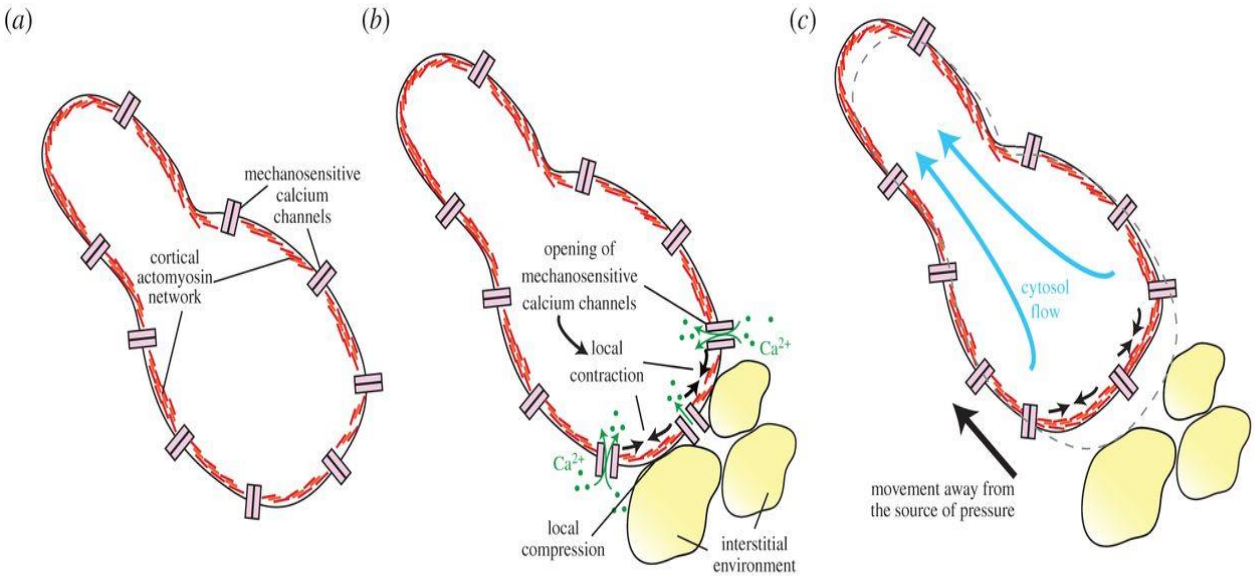


Figure 1. A hypothetical model of mechanosensation in proto-amoeboid cells. (a), Calcium sensitive MS-channels are co-opted into a partnership with the actomyosin network in the membranes of these cells. **(b)**, Upon receipt of a mechanical stimulus, extracellular calcium flows through the channels, leading to a localised contraction in the actomyosin network. **(c)**, This contraction induces a flow of current in the cytosolic fluid which propels the cell away from the site of mechanical stimulation. Taken from (Brunet and Arendt, 2016).

Having discussed some of the basic ideas and molecules involved in mechanosensation in primitive organisms, I will now turn my attention to higher organisms. Here I will discuss in detail the structure of the PNS, as well as a brief discussion of some of the other sensory modalities associated with this system. Following this, I will briefly outline the various theories pertaining to perception in peripheral afferents. Finally, I will provide an outline of some of the key molecular players within these elements which act to detect mechanical stimuli.

1.2 The structure of the peripheral nervous system (PNS)

The PNS is composed of three major constituent parts as illustrated in figure 2. These are; the nerve fibres in the skin, the dorsal root ganglia (DRG) neurons and the spinal cord (Todd, 2010). The perception of externally-derived mechanical stimuli begins with the activation of specific populations of sensory afferents in the skin. These afferents then project back to neurons in the DRG which then

further relay this signal to specific layers (laminae) within the dorsal horn of the spinal cord (figure 2) (Todd, 2010). I will now discuss the anatomical heterogeneity of these three component parts, beginning with the skin.

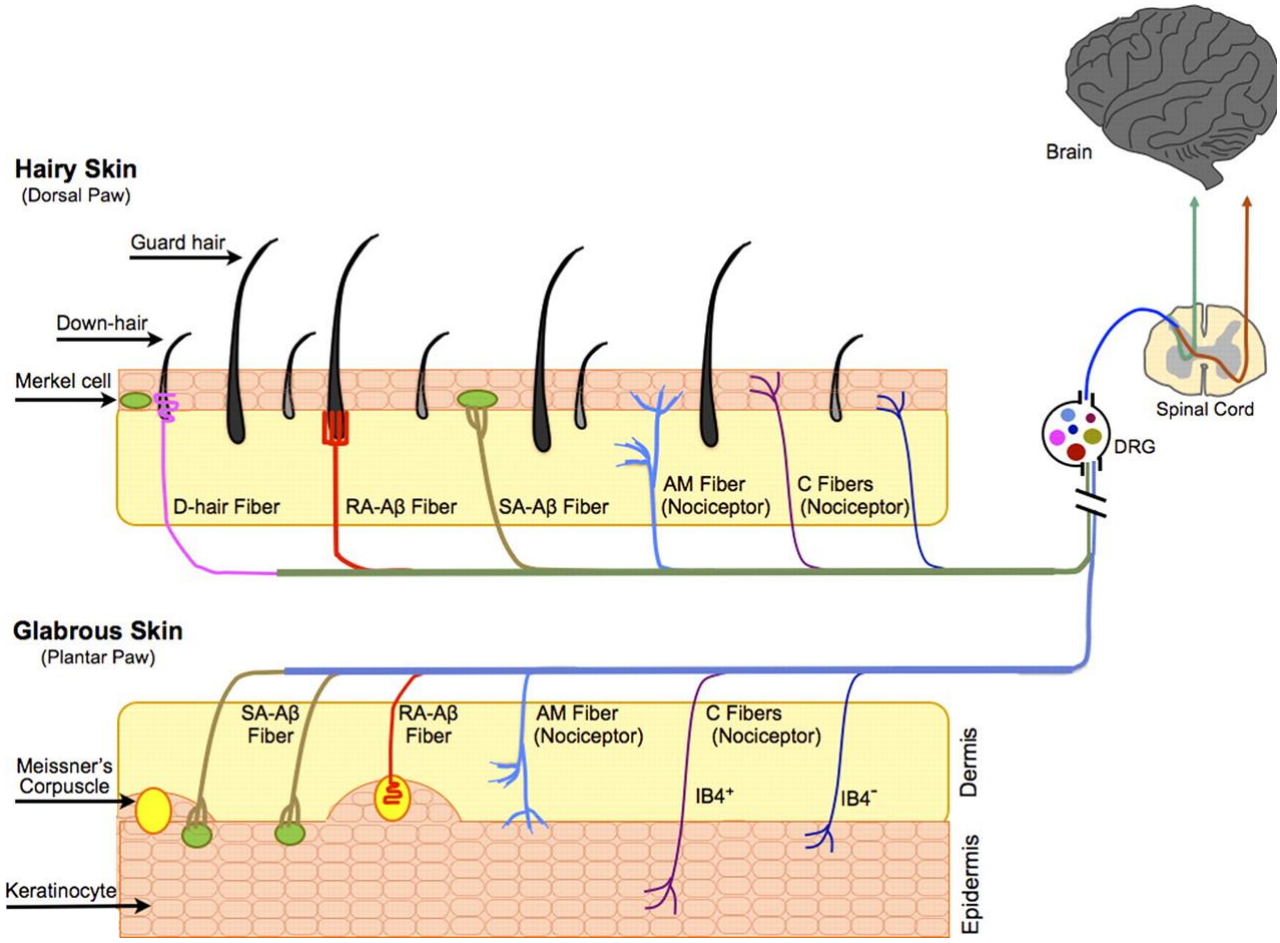


Figure 2. A diagram representing the constituent components of the peripheral nervous system. The PNS is composed of a number of distinct structures: the skin, DRGs and the spinal cord. Skin can be divided into glabrous (non-hairy) and hairy. Both glabrous and hairy skin are innervated by distinct populations of fibres which are tuned to respond to both innocuous and noxious stimuli. These fibres originate from DRG neurons, which are divided into sub-populations based on the nature of the stimuli they are hardwired to perceive. Finally, central projections emanating from DRG neurons pass to particular layers of the spinal cord where the information is processed before being relayed to the brain. Taken from (Garrison, Dietrich and Stucky, 2012).

Over the past century, our knowledge of the anatomy of afferent fibres innervating the skin and the particular tactile events that they detect has dramatically improved. The pioneering electrophysiological studies from people like Ainsley Iggo (Iggo and Muir, 1969), Vernon Mountcastle (Talbot *et al.*, 1968) and others, as well as microneurography studies carried out in humans and non-human primates, transformed our understanding of cutaneous mechanosensation. Now, using mouse models and modern molecular biology tools, it is possible to genetically manipulate and visualise the fibres that these early pioneers first recorded from.

The sensory afferents associated with mechanosensation in skin can be separated into three groups, Aβ, Aδ and C fibres (Zimmermann *et al.*, 2009). A multitude of parameters such as the size of the cell body, the degree of myelination and conduction velocities, differ between these various fibre types and thus allow us to delineate these three sub-populations of fibres (Zimmermann *et al.*, 2009). Aβ type afferents project to the skin from large body DRG neurons. These fibres are thickly myelinated and have very fast conduction velocities of between 16-100 m/s. For the most part, Aβ afferents detect low-threshold mechanical stimuli and are therefore often referred to as mechanoreceptors (Zimmermann *et al.*, 2009).

Aδ fibres are associated with DRG cell bodies of medium size, and while these afferents are also myelinated, the degree of myelination is not as thick as that found around Aβ nerve afferents (Zimmermann *et al.*, 2009). Moreover, Aδ fibres are characterised by a conductance velocity of 5-30 m/s (Zimmermann *et al.*, 2009).

Finally, C fibres, which represent the most abundant type of innervating fibre in the skin, project from small body DRG neurons, lack myelination and have the slowest conduction velocity (0.2-2 m/s) of any of the three fibre types (Zimmermann *et al.*, 2009). Moreover, Aδ and C fibres diversify into sub-populations which are able to detect either low (mechanosensitive) or high-threshold (nociceptive) mechanical stimuli, respectively. So-called Aδ-low threshold mechanoreceptors (LTMRs), sometimes referred to as D-hair afferents, and C-LTMRs respond to physical stimuli that are far below the nociceptive threshold (Brown and Iggo, 1967; Burgess, Petit and Warren, 1968). The other

members of the Aδ and C fibre populations respond to mechanical stimuli in the nociceptive range. Finally, both Aδ and C fibres also respond to noxious heat and cold (Abraira and Ginty, 2013).

As well as diverse fibre types that are based upon their structural / functional features, as shown in figure 3, the skin that the nerves innervate can also be divided into two types, namely glabrous (non-hairy) and hairy skin (Lechner and Lewin, 2013). I will now start with an overview of low-threshold mechanosensitive afferents and their associated end organs in glabrous skin.

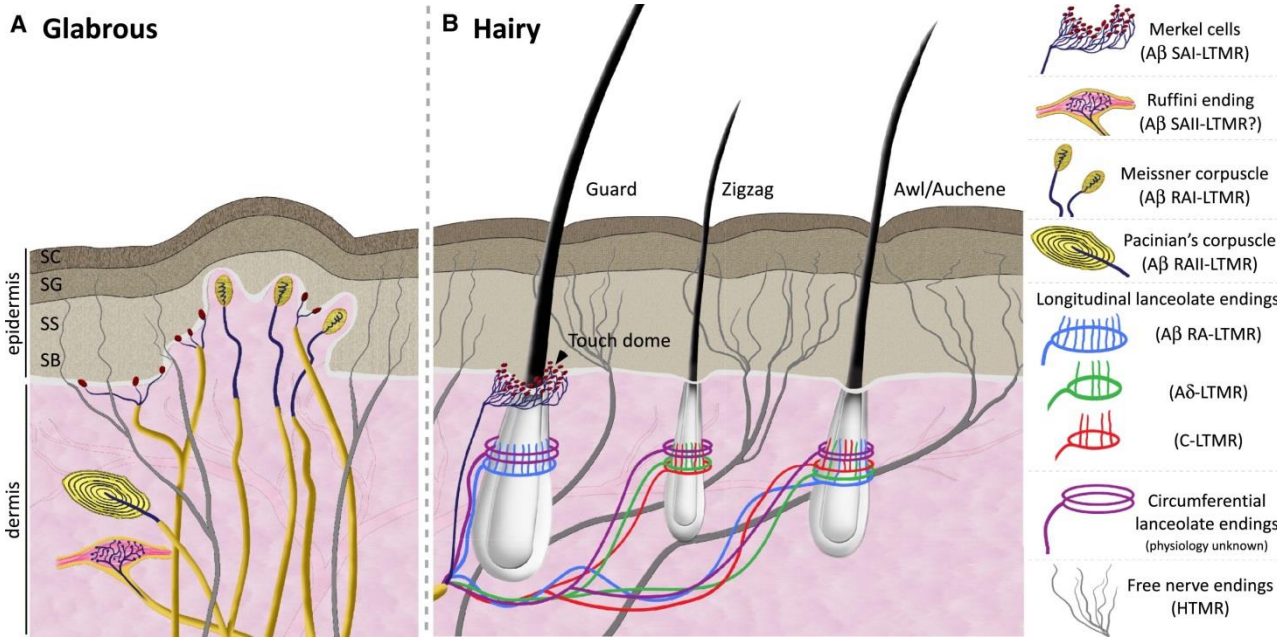


Figure 3. Diagram illustrating the types of fibres and end organ structures found in glabrous and hairy skin. **(a)**, Glabrous skin is innervated by both low-threshold and high-threshold mechanosensitive afferents. The LTMRs innervate a variety of end organ structures in this type of skin, including Meissner's and Pacinian corpuscles as well as Ruffini ends. **(b)**, Hairy skin contains three types of hair follicles named guard, awl / auchene and zigzag. These structures are innervated by different combinations of LTMRs and are associated with end organ structures like Merkel cells. Both glabrous and hairy skin are densely innervated by HTMRs which terminate as free nerve endings in this the skin. Taken from (Abraira and Ginty, 2013).

1.2.1 Low-threshold fibres in glabrous skin

As shown in figure 3, LMTRs innervating glabrous skin can be divided into four types, based on the nature of mechanical stimuli they are tuned to respond to, as well as their association with particular mechanosensitive end organ structures. These four types are: slowly adapting I (SAI), slowly adapting

II (SAII), rapidly adapting I (RAI) and rapidly adapting I (RAII)-LTMRs (Zimmermann *et al.*, 2009). SAI and II type fibres are characterised by their sustained firing throughout the duration of a mechanical event. SAI type fibres have Aβ range conduction velocities, are highly sensitive to small (< 15μm) displacements of the skin in humans, and are especially sensitive to the curvature and topography of materials (Woo *et al.*, 2014). Moreover, these afferents exhibit exceptional spatial resolution and are particularly adept at detecting the velocity of mechanical stimuli (Woo *et al.*, 2014). SAI-LTRMs are usually associated with Merkel cells (first identified in 1875 by Friedrich Merkel) which form end organs near nerve fibres in the skin (Merkel, 1875). Much later these fibres were shown to be SAIs (Iggo and Muir, 1969; Munger, Pubols and Pubols, 1971). Merkel cells exist in close proximity to the terminal end of SAI afferents and display a branching structure, with separate terminals innervating clustered groups of Merkel cells (Paré, Smith and Rice, 2002; Woodbury and Koerber, 2007). The concentration of Merkel cells in glabrous skin is greatest in highly sensitive areas such as the lips and fingertips (Maricich *et al.*, 2009a; Woo *et al.*, 2014).

Due to this close relationship between SAIs and Merkel cells, a question arises: is the mechanical response initiated in the afferent or the end organ? By phototoxically-ablating Merkel cells, one study rendered SAIs incapable of responding to stimulation (Ikeda *et al.*, 1994), while another obtained data to the contrary (Mills and Diamond, 1995). Other studies focused on removing the transcription factor Atoh1, which enables the selective deletion of Merkel cells. These studies found that in the absence of these structures, mice were unable to perceive textured surfaces with their feet (Maricich *et al.*, 2012). Furthermore, skin-nerve analysis revealed that SAI fibres from these mice did not respond to mechanical stimuli (Maricich *et al.*, 2009b). However, such developmental deletions have been called into question by data which suggests that altering skin / Merkel cell development might have adverse effects on the proper growth and maintenance of sensory afferent fibres (Krimm, Davis and Albers, 1999). Whatever the case, it is clear that this SAI / Merkel cell pairing imbues glabrous skin with an important perceptual capacity.

SAII-LTMR also possess Aβ type conduction velocities and show strong responses to skin indentation (Zimmermann *et al.*, 2009). These fibres display a lower density of skin innervation, considerably larger receptive fields, and are also considerably more sensitive to skin stretch than SAI afferents (Johansson and Vallbo, 1980; Edin, 1992). There is some controversy over which organisms harbour this particular type of afferent, as human studies have identified the population (Goodwin, Macefield and Bisley, 1997), but work in non-human primates has not (Johnson and Lamb, 1981). A population of afferents matching the characteristics of SAII-LTMRs has been identified in mice (Wellnitz *et al.*, 2010). However, unlike the well-defined SAI / Merkel cell interaction previously discussed, the partner end organ (if any) of this population of nerves has not yet been clearly defined. One candidate cell type may be the so-called Ruffini corpuscle which was first identified by the Italian histologist Angelo Ruffini in 1894 (Ruffini 1894). It has been suggested that collagen fibres associated with Ruffini corpuscles can undergo displacement-induced stretching (Rahman *et al.*, 2011). Therefore, given the exceptional sensitivity of SAII type fibres to this type of stimulus, they would make an excellent pairing with this end organ. However, the presence of Ruffini corpuscles has not been confirmed in rodents and the existence of an SAII / Ruffini pairing remains controversial (Abraira and Ginty, 2013).

RAI and RAII LTMRs fire in very fast, short bursts of activity only at the onset and completion of a mechanical event (Abraira and Ginty, 2013). RAI-LTMRs were initially associated with the detection of rapid movement of mechanical stimuli against the skin and therefore became associated with the detection of low-frequency vibration type stimuli (Torebjörk and Ochoa, 1980). RAI type fibres exhibit far greater sensitivity than SA type fibres, yet they are far less adept at spatially localising a sensory stimulus. Furthermore, RAI fibres respond quickly and often to short bursts of mechanical motion exerted upon the skin, whilst simultaneously not responding to long term indentation (Abraira and Ginty, 2013). These properties make such afferents excellent candidates for sensing the slippage of an object being gripped within the hand (Johansson and Vallbo, 1979; LaMotte and Whitehouse, 1986).

It is no surprise then to discover that these fibres are associated with mechanical end organs, termed Meissner's corpuscles, which are highly enriched in the fingerprint skin in human hands as well as on the soles of the feet (Abraira and Ginty, 2013). The way that the structure of Meissner's corpuscles respond to physical force compliments the type of stimuli RAIs are best able to detect. Thus, upon mechanical indentation of the glabrous skin, collagen fibres which link the corpuscle to the surrounding environment, act to distort this structure. This in turn induces the innervating RAI afferents to activate in a short burst that quickly ceases as a consequence of the rapidly adapting nature of their firing properties (Zimmermann *et al.*, 2009). When the indentation finally ceases, the corpuscle reforms, leading to another short burst of firing by the sensory afferents (Abraira and Ginty, 2013). Work in primates has shown that 30-80 such corpuscles can be innervated by a single RAI-LTMR afferent (Bolton, Winkelmann and Dyck, 1966; Paré, Smith and Rice, 2002).

We now arrive at the final type of fibre innervating glabrous skin, the RAII-LTMR. This type of afferent is characterised by its unrivalled ability to detect high-frequency vibration-type stimuli(Zimmermann *et al.*, 2009). Again, this fibre type is associated with an end organ, which in this case is termed the Pacinian corpuscle. These corpuscles are quite large in diameter (~1mm) and are therefore visible to the naked eye (Halata, 1977). Consequently it is possible to directly stimulate this end organ whilst recording from the RAIIs that innervate them (Bell, Bolanowski and Holmes, 1994). RAII-LTMRs are incredibly sensitive to very small mechanical perturbations on a nanometer scale (Janig, Schmidt and Zimmermann, 1968). The Pacinian corpuscles that RAIIs innervate are localised deep in the dermis of the skin and are especially concentrated in fingers (Bell, Bolanowski and Holmes, 1994). However, their positioning results in these structures having very large receptive fields, rendering them poorly equipped for detecting spatial properties of physical stimuli (Bell, Bolanowski and Holmes, 1994). That being said, the RAII /Pacinian corpuscle complex is exquisitely (Paré, Smith and Rice, 2002) sensitive to vibration, with some suggesting it rivals the auditory system's capacity to detect / differentiate between sound waves (Formby *et al.*, 1992).

1.2.2 Low-threshold fibres in the hairy skin

Recently, a detailed study of the low-threshold mechanosensitive afferents in the hairy skin of mice, revealed a complex innervation pattern that rivals that of glabrous skin for intricacy (Li *et al.*, 2011). Although previously discussed mechanical end organs such as Merkel cells also occur in hairy skin (Woo *et al.*, 2014), the main focus of this section will be to discuss the innervation of distinct population of hair follicles by LTMRs in this skin region as shown in figure 3.

The three distinctive types of hair follicles found in hairy mouse skin are guard, zigzag and awl / auchene (Li *et al.*, 2011) (figure 3). These follicles differ from one another in terms of size (length), numbers and the type of LTMR fibres that innervate them (Li *et al.*, 2011). Like glabrous skin, the fibres innervating hairy skin can be sub-classified into three types, Aβ, Aδ and C fibres respectively (Lechner and Lewin, 2013). I will begin with a discussion of Aβ type LTMRs.

Like glabrous skin, Aβ-LTMRs in hairy skin can be sub-divided into two classes, SA and RA mechanoreceptors, based upon their adaptation rates (Zimmermann *et al.*, 2009). The SAI type fibres in hairy skin innervate Merkel cells which cluster around guard hair follicles in regions termed 'touch domes' (Lechner and Lewin, 2013) **(**figure 3**)**. In hairy skin, the activation of RA-LTMRs has been observed upon displacement of hair follicles (Brown and Iggo, 1967). In mice these fibres form so-called 'lanceolate endings' around the base of guard and awl / auchene hair follicles (Li *et al.*, 2011) where they appear as 'picket' -like innervations surrounding the circumference of the base of the hair follicles. Their orientation makes these structures excellent candidates for detecting mechanically-induced deflections in the hair follicles that they associate with (Takahashi-Iwanaga, 2000). Moreover, the hair follicles themselves vary in the density of their distribution (Li *et al.*, 2011; Wu, Williams and Nathans, 2012), ranging from lone isolated hair follicles to clustered groups (Li *et al.*, 2011). These arrangements are likely to be important for the types of stimuli these follicles are tuned to detect.

Aδ type (D-hairs) fibres also innervate hair follicles in the skin (Li *et al.*, 2011). The types of hair follicle that these fibres innervate, often referred to as D-Hair units, were first identified by examining

the electrical responses produced by movement of down hairs in cat and rabbit skin (see review by (Abraira and Ginty, 2013). Work in mice and cats demonstrated that Aδ-LTMRs exhibit exceptional sensitivity to very fine mechanical stimuli; they are consequently considered to be the most sensitive afferent type in the skin (Brown and Iggo, 1967; Burgess and Perl, 1967). A study by Li et al. 2011 utilised molecular genetic strategies in mice to label Aδ-LTMRs which revealed a lanceolate-type innervation around the base of zigzag and awl / auchene type hair follicles.

Hairy skin also harbours a population of C-LTMRs which are absent from glabrous skin (Li *et al.*, 2011). The presence of a C fibre which responds to mechanical, rather than nociceptive-type, stimuli was first observed by Yngve Zotterman in 1939 (Zotterman, 1939). These C-LTMR fibres, which express tyrosine hydroxylase (TH) are found in much higher abundance than their myelinated counterparts (Li *et al.*, 2011), and are highly sensitive to slowly moving mechanical stimuli exerted across their receptive fields (McGlone, Wessberg and Olausson, 2014). For this reason, these fibres were thought to detect 'stroking'-type stimulation of the skin. Indeed, experiments in human individuals who lacked myelinated fibres revealed that these people reported perceiving a 'pleasant' type sensation when the skin was stimulated to induce activity of C-LTMRs (Olausson *et al.*, 2002). Some experimenters have even suggested that these fibres play a role in so-called 'emotional touch' (Löken *et al.*, 2009; McGlone, Wessberg and Olausson, 2014). The C-LTMRs and Aδ-LTMRs co-localise to form intertwining lanceolate type endings around the base of awl / auchene and zigzag type hair follicles, respectively (Li *et al.*, 2011).

1.2.3 High-threshold mechanosensitive (HTMR) fibres in glabrous and hairy skin

High-threshold afferents innervate both glabrous and hairy skin, and occur in two main subtypes: Aδ and C fibres (see review by (Lechner and Lewin, 2013)) These fibre types perceive damage-inducing stimuli and are therefore essential for an organism's survival.

The first type, Aδ-HTMRs, have conduction velocities of intermediate speed and mediate the rapid perception of noxious mechanical / thermal stimuli (Abraira and Ginty, 2013). In contrast, C-HTMRs

have slower conduction velocities and respond solely to mechanical insults (Bessou and Perl, 1969). These nociceptive fibres have been sub-classified into two groups based upon whether or not they express the neuropeptides, substance P and calcitonin gene related peptide (CGRP) (Zylka, Rice and Anderson, 2005). Those which express the neuropeptides are termed 'peptidergic' and innervate deeper regions of the epidermis (Zylka, Rice and Anderson, 2005). Conversely, so-called non-peptidergic fibres innervate the epidermis at sites closer to the skin surface and display strong binding to isolectin-B4 (IB4), a glycoprotein isolated from the *Griffonia simplicifolia* plant species (Zylka, Rice and Anderson, 2005). This disparity in localisation likely serves to facilitate the detection of different types of noxious stimuli (Zylka, Rice and Anderson, 2005). Selective ablation of non-peptidergic nociceptors leads to a selective loss of the perception of pain-inducing mechanical stimuli (Cavanaugh *et al.*, 2009), whilst similar experiments with peptidergic nociceptors resulted in the loss of noxious thermal sensitivity (Cavanaugh *et al.*, 2009).

A third group of HTMRs also exist, termed Aβ type myelinated fibres (Burgess and Perl, 1967; Woodbury and Koerber, 2003). These fibres innervate both glabrous and hairy skin regions and respond to both noxious mechanical and thermal stimuli. Currently, the morphology of these afferents in the skin is unknown (Abraira and Ginty, 2013).

Having discussed the major fibre types of LTMRs and HTMRs in the skin, I will now turn my attention to a brief discussion of the different populations of neurons found within dorsal root ganglia (DRG), from which the peripheral sensory afferents I have just discussed emanate.

1.3 Dorsal root ganglia (DRG)

DRG neurons are the primary cells of the somatosensory system. They are pseudounipolar, extending one branch towards the skin (periphery) and another branch centrally to the grey matter of the spinal cord (Vriens, Nilius and Voets, 2014) **(**see figure 2**)**. Neurons within DRGs can be divided into diverse sub-populations based upon their ability to detect distinct type(s) of sensory stimuli, such as temperature, innocuous / noxious mechanical stimuli, chemical irritants and body position

(proprioception) (Marmigère and Ernfors, 2007). This ability is due to the fact that distinct populations of DRG neurons express unique populations of receptors / ion channels (Usoskin *et al.*, 2015).

The specific fate of individual DRG neurons is determined at an early stage in the developing organism with stringently controlled signaling factors being released from the neural tube which facilitate the release of neural crest cells from this structure. These cells then migrate ventrally to form the DRGs (Le Douarin and Kalcheim, 1999). As neural crest cells migrate and coalesce to form DRGs, they are subject to tightly regulated spatiotemporal signaling from factors released by the adjacent spinal cord. Following this process the neurons diversify into their respective sub-populations which pre-dispose them to detect discrete forms of sensory stimuli (Marmigère and Ernfors, 2007). After specification, diverse populations of DRG neurons express different receptor tyrosine kinases (Trk) that can be used as markers to classify DRG neurons into groups dependent upon how they respond to different types of sensory stimuli (Marmigère and Ernfors, 2007). For example, TrkA-positive DRG cells mostly respond to noxious type stimuli, while TrkB- and TrkC-positive populations predominantly respond to mechanical and proprioceptive stimuli (see figure 4**)**, respectively (Marmigère and Ernfors, 2007).

Whilst a large cohort of molecular markers have been identified that label sub-populations of DRG neurons (such as IB4 for non-peptidergic nociceptors) (Zylka, Rice and Anderson, 2005), recent single cell RNA sequencing analysis undertaken by Patrik Ernfors, allows for the unbiased categorisation of DRG neurons into sub-groups based upon their molecular expression profiles (Usoskin *et al.*, 2015). By carrying this out on some 600+ DRG neurons and clustering the results in an unbiased manner, Ernfors and colleagues produced a catalogue of eleven DRG neuronal populations based upon their expression of key genes such as *ntrk1* (TrkA), *ntrk2* (TrkB) and *ntrk3* (TrkC) **(**figure 4**)**. The existence of these eleven neuronal populations was verified by conventionally staining the DRG neurons with antibodies against population specific markers which emerged from the sequencing data (Usoskin *et al.*, 2015). It is worth noting here that this analysis was carried out

on DRGs extracted only from the lumber portion of the spinal cord (Usoskin *et al.*, 2015), and as such other distinct neuronal populations may be present in the mouse that are not enriched in DRG from the lumbar region. Nevertheless, these data represent the most comprehensive single catalogue of DRG neuronal sub-populations available to date.

Having briefly outlined the function of DRG neurons I will now move on to discuss the general innervation pattern of different populations within another main structure of the PNS, the spinal cord.

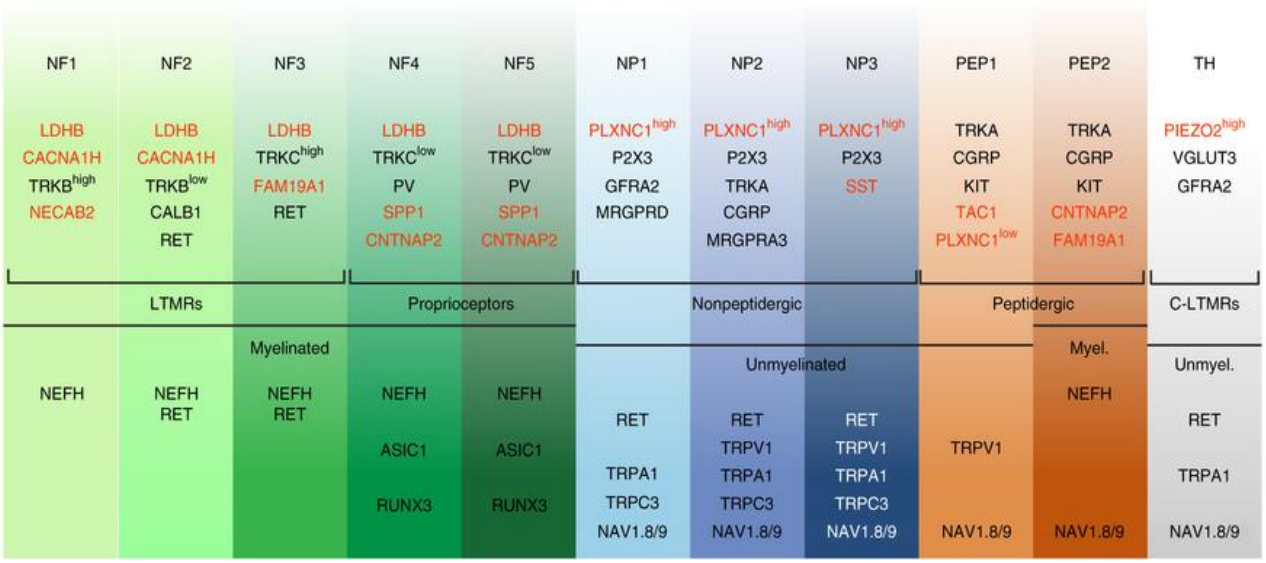


Table 1. A schematic representing the proposed sub-populations of DRG based on single-cell RNA sequencing data. The populations of different DRG can be divided into eleven distinct classes based upon their expression of common receptors, ion channels and other proteins. The populations can be further sub-divided by the sensory modality they detect such as LTMRs, proprioceptors and nociceptos (peptidergic and non-peptidergic). Adapted from (Usoskin *et al.*, 2015).

1.4 The spinal cord

The dorsal horn of the spinal cord is innervated by afferents emanating from neurons within DRGs (figure 2). These afferents synapse with cells within specific layers (laminae) of the cord in a pattern which reflects the type of stimuli (noxious or non-noxious) that the DRG neurons detect (Todd, 2010) see figure 5b. These laminae were first described in the spinal cord of cats, based upon differences in the size and concentration of neurons within each lamina (Rexed, 1952) as illustrated in figure 5a.

The signals from the peripheral afferents are received by dorsal horn neurons which make up part of a complex circuit, composed of both excitatory (glutamatergic) and inhibitory (GABA / glycinergic) interneurons (Todd, 2010). It is imperative that a tight control is maintained over the levels of excitation and inhibition within these circuits, as blocking of inhibitory transmission can lead to the development of disorders such as mechanical allodynia, a condition in which low threshold (innocuous) mechanical stimuli are perceived as painful (Sivilotti and Woolf, 1994), inflammatory and/or neuropathic pain (Todd, 2010).

Under ordinary conditions, once a signal is received at the level of the spinal cord, these circuits project the signal to cells called projection neurons which relay the information to different brain regions (Todd, 2010).

The general innervation pattern of the spinal cord dorsal horn **(**figure 5b**)**, which is the point at which almost all of the fibres associated with the detection of innocuous and noxious mechanical and thermal stimuli terminate, is as follows. Fibres which detect noxious stimuli innervate lamina I and II respectively. LTMRs innervate the inner region of lamina II (IIi) through to lamina V respectively (Todd, 2010) **(**see figure 5b**)**. It has also been observed that myelinated and unmyelinated LTMRs innervating the same portion of skin innervate the dorsal horn in structures which are referred to as 'somatotopically arranged LTMR columns' (Abraira and Ginty, 2013). These innervation columns span several laminae and it has been suggested by David Ginty that processing of the aggregate of signals originating from different afferent types by interneurons within these columns may influence the final firing pattern of projection neurons, and therefore the signal passed to the brain (Abraira and Ginty, 2013). Currently, our knowledge of the heterogeneity of cells within the spinal cord, especially interneurons, is sparse (Maxwell *et al.*, 2007; Yasaka *et al.*, 2007). As such, new genetic markers are required to identify these populations in order to better understand how these cells process and relay messages from the periphery (Todd, 2010).

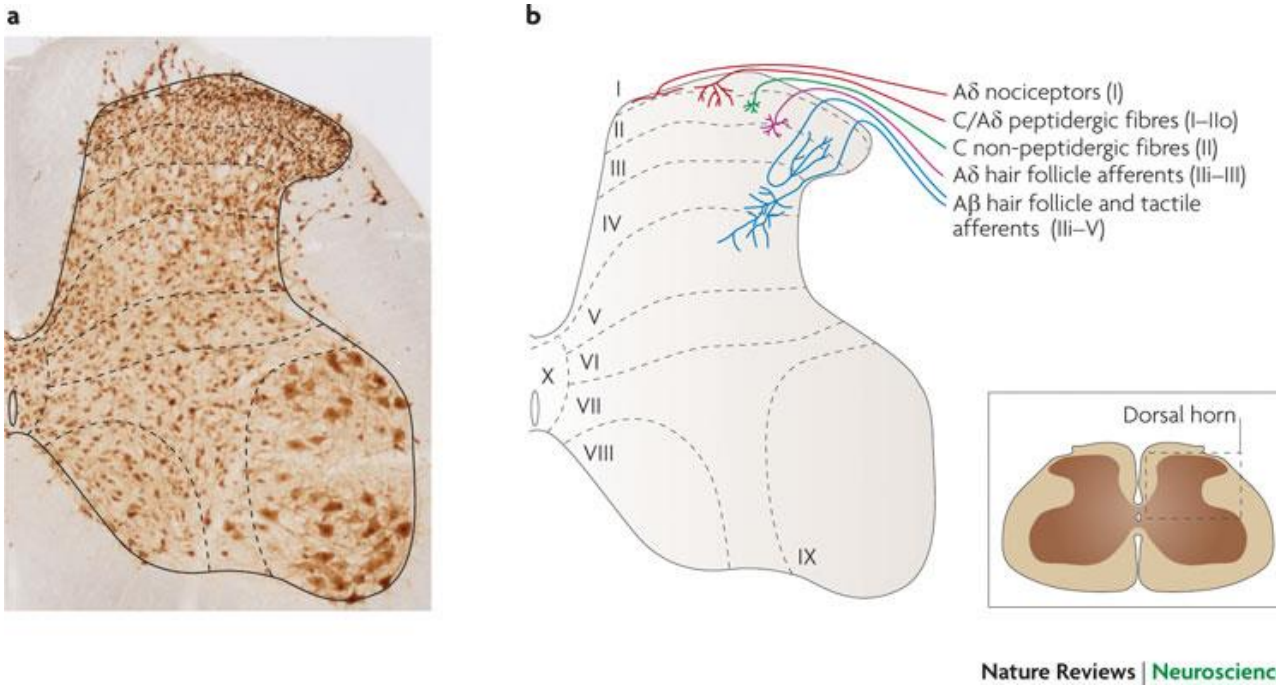


Figure 4. An image and diagram of the spinal cord outlining the sub-division of this structure into various laminae. (a), A section of the rat spinal cord stained with the neuronal marker NeuN. The dashed lines mark the demarcation between the various different laminae. **(b)**, A diagram showing the division of the spinal cord into various laminae (regions I –IX). Colour coded representations of various types of fibres innervating the spinal cord dorsal horn, which is highlighted in the inset image. Taken from (Todd, 2010).

Having discussed in some detail the anatomy and function of the primary elements of the PNS, I will next briefly summarise the various theories, both historical and contemporary, which have endeavored to explain the how the PNS functions.

1.5 Theories of peripheral sensory perception

For centuries, philosophers and scientists have discussed and debated, how the body perceives and delineates between discrete ranges of force applied to its surface. Historically speaking, much of these discussions have focused upon how the body detects pain (both mechanically-induced and otherwise); although more modern contributors have also integrated the detection of low-threshold stimuli into their hypotheses (Melzack and Wall, 1965). There are four major theories which attempt to explain

how the PNS detects these stimuli, named the specificity (labelled line) theory, the intensity theory, the pattern and the gate control theory (Moayedi and Davis, 2013). I will discuss, briefly, each of these theories below.

The specificity or labelled line theory, which was originally postulated by Charles Bell, suggests that the PNS is composed of a heterogeneous mix of fibre types which only detect one specific type of stimuli (Bell and Shaw, 1868). Within such a system it is proposed that there are dedicated fibres which, for example, can detect and transmit only painful stimuli. In its modern guise, proponents of this idea suggest that all of the stimuli perceived by the somatosensory system are detected by dedicated fibres, which harbour distinctive receptors that determine their unique perceptual ability. The discovery in the 19th century of a cohort of low-threshold touch receptor organs in the skin such as Meissner's and Pacinian corpuscles, as well as Merkel cells and Ruffini end organs, bolstered the specificity theory, as these structures were proposed as the unique elements designed to detect particular types of stimuli (Moayedi and Davis, 2013). With the later discovery of peripheral sensory fibres dedicated to the detection of discrete types of stimuli (e.g. myelinated fibres which respond exclusively to noxious stimuli (Burgess and Perl, 1967)), along with the discovery of nociceptors and high-threshold mechanoreceptors (Bessou and Perl, 1969), the specificity theory seemed to be vindicated. However, as will be discussed later, the advent of the gate control theory saw a decline in the popularity of the labelled line theory.

The intensity theory posits that a painful type sensation can be evoked in any of the somatosensory modalities as long as a critical threshold of activation is met. According to (Moayedi and Davis, 2013) this idea can be traced back to Plato who defined pain not as a unique sensory stimulus but rather as an emotional response to a supra-normal stimulus. This idea was picked up and expanded on by Rene Descartes, who suggested that nerve fibres were tube-like structures that could be physically 'pulled' by sensory stimuli (Descartes *et al.*, 1664). In Descartes' model, a nerve fibre that was pulled at a normal level would evoke a non-painful sensation. However, with severe stimulation, these neuronal tubes would 'sever' leading to the perception of pain (Moayedi and Davis, 2013). Experiments from

the 19th century carried out by Bernhard Naunyn and first cited by Dallenbach almost a century later (Dallenbach, 1939), demonstrated that repeated light tactile stimulation of patients suffering from syphilis resulted in the perception of pain. Based on this work, the German physiologist Arthur Goldscheider posited that the signals from concurrent non-painful stimuli could 'summate' in the spinal cord resulting in the sensation of pain (Moayedi and Davis, 2013). Eventually however, due to the increasing weight of evidence for the specificity theory, intensity theory fell out of favour.

The third hypothesis, pattern theory, is quite similar to that of intensity theory. In this case, proponents of the idea suggested that practically all nerve fibres are the same, but rather than fibres responding differently to stimuli of different intensities, this model posits that the spatio-temporal firing profile of the fibre is important for determining the type of perception detected (Moayedi and Davis, 2013).

The gate control theory, which was first proposed in 1965 (Melzack and Wall, 1965), changed the way that we currently understand the interaction between low-threshold (non-noxious) and high-threshold (noxious) stimuli in the PNS. Essentially, what Melzack and Wall proposed was as follows; low-threshold and high-threshold detecting afferents synapse onto two discrete regions within the dorsal horn of the spinal cord, the substantia gelatinosa and the transmission cells, respectively (figure 5b). The 'gate' of the gate control theory is the substantia gelatinosa. Cells within this region modulate the flow of signals from primary afferents to the transmission cells, which are the final arbiters for transmitting an action signal. Signals from large afferent (low-threshold) fibres act to hold the gate shut, while those of small afferent (high-threshold) fibres actively open the gate. When noxious signals reach a critical threshold they overcome the inhibitory signal of the large afferent fibres, opening 'the gate', and thereby leading to the perception of painful stimuli (Melzack and Wall, 1965; Moayedi and Davis, 2013).

None of these theories however adequately explains all of the phenomena observed in the PNS related to mechanosensation. For example, even the gate control theory, which has become a cornerstone of modern peripheral sensory physiology, only deals with the transmission of acute pain

and therefore does not directly contribute to an understanding of the mechanisms involved in chronic and neuropathic pain states (Moayedi and Davis, 2013).

Although my own work is primarily concerned with cutaneous mechanosensation I will include here a very brief discussion on the role of the PNS in proprioception and thermosensation, as experiments pertaining to these systems appear in the Results section of this thesis.

1.6 Proprioception

Proprioception is a somatosensory modality encoded by the PNS which allows an organism to feel the relative position(s) of its body and/or limbs (Proske and Gandevia, 2012). This modality is encoded for by a specific sub-population of DRG neurons which project their afferents to end organ structures called muscle spindles and Golgi tendon organs, which reside within muscles and their associated tendons, respectively (Woo *et al.*, 2015). The proprioceptive afferents which innervate muscle spindles detect longitudinal stretch of these structures, whereas Golgi tendon organs respond to variations in the tension of tendons (Proske and Gandevia, 2012; Bewick and Banks, 2014). Without proprioception, seemingly mundane actions such as standing and walking are severely curtailed (Akay *et al.*, 2014).

1.7 Thermosensation

The ability of an organism to sense temperature is called thermosensation. Sensory afferents within the skin harbour ion channels which allow these structures to respond to thermal stimuli (Vriens, Nilius and Voets, 2014). Certain subtypes of the transient receptor potential (TRP) superfamily of ion channels act as molecular thermometers such as TRPV1, TRPM3 and TRPM8, with different members of the family responding to different degrees of heat or cold (Vriens, Nilius and Voets, 2014). Thermosensitive afferents in the skin of humans may encounter a wide array of different temperatures on a daily basis, with a temperature of ~33ºC being considered thermo-neutral, while

temperatures below ~15ºC and above ~45ºC usually being perceived as noxious (Basbaum *et al.*, 2009). DRG neurons which respond to extremes of heat and cold are able to rapidly generate action potentials when exposed to a noxious temperature stimulus (Zimmermann *et al.*, 2009), and exhibit minimal adaptation to prolonged stimuli (Torebjork, LaMotte and Robinson, 1984; Frölich *et al.*, 2010).

Having outlined the broad structure of the mechanosensory elements of the PNS, as well as the basic principles of both proprioception and thermosensation, I will now move on to a detailed discussion of the molecular apparatus within sensory fibres which allow these afferents to sense mechanical stimuli.

1.8 The molecular apparatus of mechanotransduction

As discussed previously, mechanosensation is best defined as the conversion of physical force into electro / chemical signals which can be interpreted by the organism (Chalfie, 2009). The detection of such mechanical signals is vital for the function of a wide array of biological processes such as touch, hearing, locomotion and the regulation of blood pressure (Chalfie, 2009) A seminal paper published in 1979 by Corey & Hudspeth demonstrated that movement of hair bundles within the inner ear of the bullfrog (*Rana catesbeiana*) produced an exceptionally rapid electrical response (Corey and Hudspeth, 1979). To put this into context, the latency to the electrical response they recorded was 40μs, which is orders of magnitude faster than the tens of milliseconds required by channels in the vertebrate retina to respond to light, a process which was then known to involve chemical messaging (Hagins, 1972; Penn and Hagins, 1972). Corey and Hudspeth therefore proposed that the process that they were witnessing must have been due to direct gating of a transduction channel. Subsequent results of other experiments carried out in sensory organs derived from *Drosophila* and *C. elegans* uncovered similarly rapid electrical response rates (Walker, Willingham and Zuker, 2000; O'Hagan, Chalfie and Goodman, 2005; Albert, Nadrowski and Göpfert, 2007). As a result, research efforts were

focused upon trying to identify the channel(s) and other potential partner proteins which would allow a sensory system to be directly activated by a mechanical stimulus. To this end, I will now discuss the identity of mechanosensitive ion channels (MS-channels) before then moving onto discuss other partner proteins involved. Finally in this section, I will discuss the role that the cytoskeleton plays in this process.

1.8.1 Mechanosensitive (MS) ion channels

There are four criteria which a candidate protein must meet to be considered a *bona fide* mechanosensitive channel: **(1)** it should be present in the appropriate sensory type cell, and be suitably localised within these cells, **(2)** the presence of the protein must be necessary to elicit an electrical response in the sensory cell, **(3)** if the protein is placed in a simplified lipid bilayer or expressed in heterologous *in vitro* or ectopic cells *in vivo* the current observed should be the same as that seen in the native cell type, and **(4)** mechanical force should activate the protein in native cells as well as under the conditions of point **(3)** (Katta, Krieg and Goodman, 2015). A number of proteins fit some, but not all, of these parameters for mechanosensation and can therefore be considered as candidate MS ion channels. One such candidate is the acid-sensitive ion channel (ASIC). The ASICs are part of the degenerin / epithelial sodium channel (DEG /ENaC) family and their members are expressed in the sensory neurons of a wide array of animals, including *C. elegans* (Árnadóttir and Chalfie, 2010), *Drosophila* (Zelle *et al.,* 2013) and mammals (Lin, Sun and Chen, 2015). Although three ASIC channels are known to be expressed in DRG neurons, removing two of these did not produce mechanosensory deficits (Drew *et al.,* 2004). The same cannot be said for other members of the DEG /ENaC family such as MEC-4 which, when mutated in *C. elegans,* leads to touch insensitivity (Chalfie and Au, 1989) and abolishes mechanical currents *in vivo* (O'Hagan, Chalfie and Goodman, 2005). However, it has so far proven to be impossible to record currents from MEC-4 expressed in heterologous expression systems (Katta, Krieg and Goodman, 2015).

In contrast, the Drosophila protein, dTRPN1, is one such protein that does fit the four parameters required to be considered a MS channel. This protein, which is more commonly referred to as No mechanoreceptor potential C (NOMPC), is a member of the TRP family. NOMPC channels are necessary for both the detection of touch (Walker, Willingham and Zuker, 2000; Cheng *et al.*, 2010; Tsubouchi, Caldwell and Tracey, 2012; Yan *et al.*, 2013) and hearing (Kamikouchi *et al.*, 2009; Effertz, Wiek and Göpfert, 2011; Zhang *et al.*, 2013). I will discuss this particular channel later in the section entitled 'Microtubules as tether structures'.

Another TRP channel, TRPC1, contributes to low-threshold mechanical sensation in mice (Garrison, Dietrich and Stucky, 2012). TRPC1 is known to be enriched in myelinated A-type fibres as well as non-peptidergic C fibres and Merkel cells, thereby suggesting a potential role in the detection of both innocuous and noxious stimuli for this candidate MS channel (Elg *et al.*, 2007). The results from (Garrison, Dietrich and Stucky, 2012) showed a significant decrease in the number of mechanically-elicited action potentials in Aβ and Aδ-LTMRs in whole animal knock-outs of TRPC1 relative to controls. Furthermore, behavioural analysis revealed a mechanical insensitivity phenotype in TRPC1 knock-out mice during experiments testing low-threshold mechanosensitivity (Garrison, Dietrich and Stucky, 2012). Despite the expression of TRPC1 on non-peptidergic nociceptors, no differences in the response of the animal groups to noxious mechanical or thermal tests were observed. However, it has been impossible to record mechanical currents from TRPC1 expressed in heterologous expression systems (Gottlieb *et al.*, 2008), therefore its role as a canonical MS channel has yet to be confirmed.

Relatively, recently another pair of potential mechanosensitive ion channels, Piezo1 and Piezo2, have been identified and are currently the focus of intense research. The Piezo proteins are enormous, containing over 30 transmembrane domains (Coste *et al.*, 2012). First identified in 2010, these channels are capable of generating mechanical currents very similar to those seen in their native tissues when expressed in HEK293T cells (Coste *et al.*, 2010). Furthermore, Piezo2 is expressed in a subset of DRG neurons that project afferents to the skin. This was demonstrated via the generation of

a transgenic mouse line which produced endogenously green fluorescent protein (GFP)-tagged Piezo2. Using this animal it was possible to visualise GFP in skin in a variety of MS structures such as lanceolate endings, circumferential endings, Meissner's corpuscles and Merkel cells (Ranade *et al.*, 2014; Woo *et al.*, 2014). Constitutively deleting Piezo2 resulted in lethality; therefore an inducible Cre which selectively removes Piezo2 only from the PNS was employed (Ranade *et al.*, 2014). Using this tool, Patapoutian and colleagues observed a severe and selective loss of mechanical sensitivity in slowly and rapidly adapting LTMRs, with little or no change to the sensitivity of nociceptors (Ranade *et al.*, 2014). More recently, using similar strategies, Patapoutian and colleagues have highlighted the importance of Piezo2 in proprioception (Woo *et al.*, 2015). Thus, mice lacking Piezo2 in proprioceptors suffered from severe deficits in locomotion. Recently published work on human patients who carry defective variants of the Piezo2 gene, also revealed deficits in touch and proprioception, although they were not nearly as severe as the phenotypes exhibited by Piezo2 $^{-/-}$ mice (Chesler *et al.*, 2016).

Following the above discussion on some candidate and canonical MS channels, I will now discuss the various gating mechanisms which enable force-mediated activation of these structures.

1.8.2 The gating of mechanosensitive ion channels

There are three proposed gating models for MS channels, namely, the **(1)** force membrane model, **(2)** duel-tether model and **(3)** single-tether model (Chalfie, 2009) which I will discuss in turn below.

The force membrane model postulates that upon the receipt of a mechanical stimulus, changes in the force within the cell membrane change the conformation of the MS channel(s), thereby activating it. This model is the most simplistic of the three, as the mechanism of action requires only the membrane and MS channels. The bacterial channels MscS and MscL are two examples of this type of channel gating, as they require only force-mediated changes in the cell membrane to be activated (Perozo, Cortes, *et al.*, 2002; Perozo, Kloda, *et al.*, 2002; Kung, 2005). Work on the structure of MscS in

particular, suggests that this channel is activated when protein helices linking the channel to the adjacent membrane undergo conformational changes as a result of membrane stretch (Wang *et al.*, 2008; Vásquez, 2009). Recent work on the Piezo1 channel by Cox et al. (2016) suggested that this channel may also be activated exclusively by membrane-gating (Cox *et al.*, 2016). A number of different approaches were taken in this study in order to define the contributions of the membrane and cytoskeletal components (actin and microtubules) to the activation of Piezo1. Thus, recording of Piezo1 activity from mechanically-activated 'blebs' or bulges within the lipid membrane which have no cytoskeletal elements (Charras, 2008; Charras *et al.*, 2008), demonstrated that this channel can be activated by the lipid membrane alone. Moreover, in experiments measuring the mechanical activation of Piezo1 in cells where the polymerization of actin and microtubules was disrupted through treatment with cytochalasin D and colchicine respectively, this channel was once again activated normally by membrane gating alone (Cox *et al.*, 2016). This type of membrane gating of Piezo1 is further supported by the recently discerned structure of this channel which highlighted the presence of flexible blade regions surrounding the putative pore domain of the channel (Ge *et al.*, 2015). These blades are located at the protein / membrane interface (Ge *et al.*, 2015) and therefore may respond to force-induced changes in the lipid membrane.

A protein that directly influences the activation / gating of Piezo2 specifically is stomatin-like protein 3 (SLP3). SLP3 is the murine orthologue of the MEC-2 gene first identified in *C. elegans*. Studies using this model indicated that MEC-2 was required for touch sensation in these animals (Huang *et al.*, 1995; O'Hagan, Chalfie and Goodman, 2005). In *C. elegans* MEC-2 is proposed to function as part of a mechanosensory complex associated with DEG/ENaC channels (Chelur *et al.*, 2002; Ernstrom and Chalfie, 2002; Goodman *et al.*, 2002). Further, Lewin and colleagues found that SLP3 was expressed in DRG neurons (Mannsfeldt *et al.*, 1999). Follow up studies demonstrated that SLP3-deficint mice were insensitive to low-threshold mechanosensation (Wetzel *et al.*, 2007). Skin-nerve electrophysiological analysis of the SLP3-deficient mice also demonstrated a profound increase in

the percentage mechanically insensitive Aβ and Aδ fibres compared to those in wildtype mice (Wetzel *et al.*, 2007), a finding that was supported by their behavioural studies of the SLP3 knock-out mice (Wetzel *et al.*, 2007). However, no deficiencies in the detection of noxious stimuli or proprioception were observed.

More recently, SLP3 was shown to 'tune' the activity of Piezo channels (Poole *et al.*, 2014). Using a novel 'pillar array' apparatus, which allows for the discrete mechanical stimulation of small regions of cells which are cultured atop these structures, it was possible to measure very finely mechanically-induced currents from various cell types. This study demonstrated that both Piezo 1 and 2 were much more sensitive to nanometer range displacements in the presence of SLP3 (Poole *et al.*, 2014). In terms of how SLP3 actually physically facilitates mechanosensation, Qi et al. (2015) have proposed that SLP3 assists mechanosensitivity by recruiting cholesterol to the cell membrane, thereby altering its mechanical properties (Qi *et al.*, 2015). Using atomic force microscopy (AFM) the authors demonstrated that DRG neurons derived from mice lacking SLP3 had softer membranes which exhibited less tension than control neurons. They therefore concluded that the softer membranes were less capable of transferring force-derived tension to MS channels such as Piezo, thereby negatively influencing their activation (Qi *et al.*, 2015). These findings add support to the hypothesis that the activation of the Piezo channels is driven primarily by membrane induced tension upon these channels.

The second postulated model of MS channel activation, the duel-tether model, proposes that activation of MS channels is through the stretching of interlinked intra- and extra-cellular assemblies (Chalfie, 2009) (see figure 6). Therefore, the role of the lipid membrane in this model is negated. This model is perhaps best exemplified *in vivo* by the structure involved in vertebrate hair cell transduction (Chalfie, 2009), an apparatus which is thought to underlie the sense of hearing. In this model, the MS channel is linked via tethers to intra- and extra-cellular surfaces (Gillespie and Walker, 2001). These tethers link the MS channel intracellularly to the actin cytoskeletal network and

extracellularly to adjacent stereocilia (Gillespie and Walker, 2001). When a mechanical force is exerted, the ion channel, which is 'locked' between these elements, is pulled open by the stretching of the tethers as illustrated in figure 6b. Due to this arrangement, the transduction of force is said to be unidirectional, as the tethers can only pull open the channel during stretching, but not compression. The basis for this arrangement comes from electron microscopy observations which showed filament type structures, referred to as 'tip links', connecting neighbouring stereocilia in hair cells within the inner ear of guinea pigs (Pickles, Comis and Osborne, 1984). Further evidence for this model of mechanotransduction comes from calcium imaging experiments which show that calcium enters stereocilia at these tip regions when they are mechanically stimulated (Denk *et al.*, 1995). Furthermore the loss of these tip links prevents signal transduction (Assad, Shepherd and Corey, 1991). It is worth noting here that the ion channel associated with this structure has yet to be identified (Chalfie, 2009).

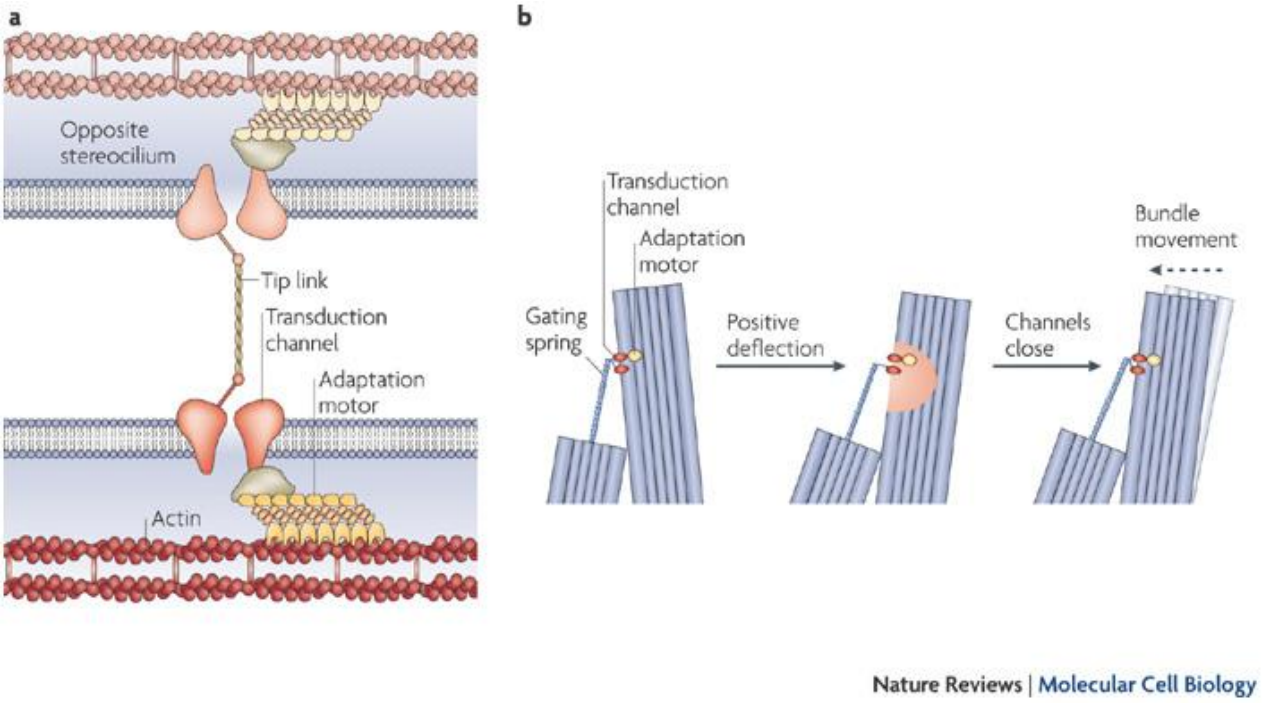


Figure 5. **Diagrams representing the structure and mode of action of the duel-tether type model of mechanical gating.** This type of system is best exemplified by the vertebrate hair cell transduction apparatus. **(a)**, Diagram showing the various components of the mechano-transduction apparatus associated with specialised hair cells within the inner ear. The transduction channels are directly tethered via a tip link to the actin cytoskeleton and adjacent stereocilium. **(b)**, Upon mechanical stimulation of this system, the tip links pull open the transduction channel to thereby enable the perception of force (sound). Taken from (Chalfie, 2009)**.**

Finally, the theory underlying the single-tether model, as illustrated in figure 7, lies somewhere between that described for the two previously postulated models. Originally proposed by Kung (Kung, 2005), the essential difference between it and the force membrane model is that rather than the channel being solely activated by membrane-induced tension, here the channel is opened by a change in its position within the membrane governed by the tether links. This change in localization alters the forces exerted by the membrane upon the channel (Chalfie, 2009). In this scenario a channel can be activated when its position is moved up or down within the lipid bilayer (figure 7). The requirement for a tether structure in this system might go some way to explaining why many candidate MS channels are not readily activated when expressed in heterologous systems (Chalfie, 2009).

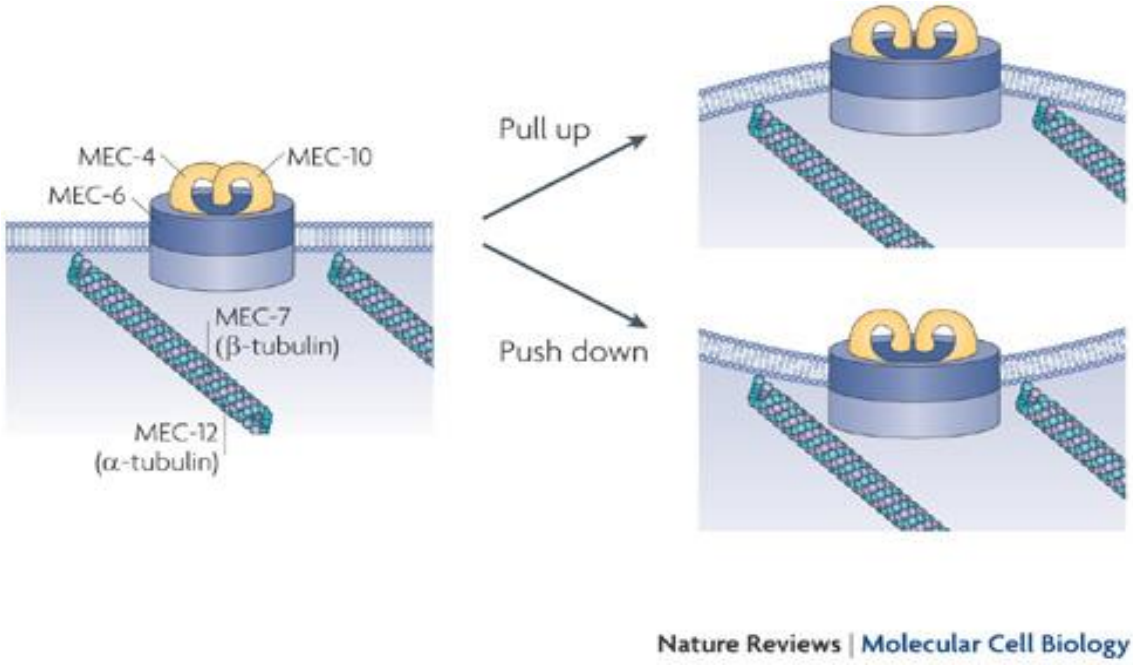


Figure 6. **Diagrams representing the structure and mode of action of the single tether type model of mechanical gating.** This type of mechanical gating involves a synergistic relationship between the lipid membrane and tether structures which position the MS channel within this structure. These images show the proposed components of the DEG / ENaC channel in the model organism *C. elegans*. Upon mechanical stimulation the tether structures react by changing the position of the ion channel within the cell membrane. This process leads to a change in the forces acting from the membrane to the channel, thereby facilitating channel activation. The model allows for channel activation upon receipt of mechanical forces that both bulge and indent the membrane. Taken from (Chalfie, 2009).

1.8.3 Microtubules as tether structures

As previously discussed, the NOMPC channel functions as a mechanosensor in *Drosophila* (Walker, Willingham and Zuker, 2000; Cheng *et al.*, 2010; Tsubouchi, Caldwell and Tracey, 2012; Yan *et al.*, 2013). More recently, work on this channel has revealed that it is tethered to the sub-membrane microtubule network by a multitude of N-terminus protein domains called ankyrin repeats (ARs) (Zhang *et al.*, 2015). This elegant study demonstrated for the first time a direct linkage between an MS channel and the microtubule cytoskeleton. The AR domains which link the NOMPC channel to microtubules had long been proposed to act as elastic tethers or 'gating springs' which act to pull open the respective MS channel upon mechanical stimulation (Howard and Bechstedt, 2004; Jin,

Touhey and Gaudet, 2006; Gaudet, 2008). Of all the TRP channels, NOMPC has the largest number of ARs (29) (Montell, 2005). Past observations from sensory structures present on *Drosophila* wings revealed filament-like connections between the membrane and the underlying microtubule network, known as membrane-microtubule connectors (MMCs) (Liang *et al.*, 2013). These connections were shown to be ARs linking between the cytoskeleton and the NOMPC channel (Zhang *et al.*, 2015). The importance of these ARs was illustrated when their removal from NOMPC prevented the channel from being activated. Moreover, removing these domains resulted in an increase in the space between the cell membrane and the underlying microtubules, suggesting that ARs pull the membrane and the cytoskeleton closer together (Zhang *et al.*, 2015). Perhaps the most convincing experiment carried out in this study was to confer mechanosensitivity to the non-mechanosensitive K^+ channel Kv2.1 by creating a chimeric protein that fused the ARs of NOMPC to the transmembrane domain of the Kv2.1 (Zhang *et al.*, 2015).

Work carried out on osmosensory neurons (ONs) located in the hypothalamus of rats, revealed an interaction between the transient receptor potential vanilloid type-1 (TRPV1) channel and microtubules (Prager-Khoutorsky, Khoutorsky and Bourque, 2014). These neurons detect increases in the osmolality of extracellular fluid as a result of dehydration, which leads to a decrease in cell volume. This physical response induces an increase in the firing rate of these neurons which then promotes the release of vasopressin. This hormone subsequently enhances the reabsorption of water by the kidneys (Bourque, 2008). TRPV1 had previously been shown to be important for sensing the stretch of the bladder urothelium in mice (Birder *et al.*, 2002). Moreover, previous work on osmosensitive cells from the hypothalamus of TRPV1 knockout mice, had shown that they were incapable of changing their membrane conductance and forming depolarising potentials in response to a hyperosmotic shock (Sharif Naeini *et al.*, 2006).

However, the mechanism by which TRPV1 allowed neurons to respond to mechanical pressure associated with cell shrinking, was not revealed for another eight years. Experiments carried out by

Prager-Khoutorsky *et al.* (2014) revealed that a TRPV1-microtubule cytoskeleton interaction was essential for the detection of mechanical stimuli in ONs (Prager-Khoutorsky, Khoutorsky and Bourque, 2014). The study found that cells which had been treated with the microtubule depolymerizing agent nocadazole were incapable of increasing their firing patterns in response to an extracellular increase in osmolality (Prager-Khoutorsky, Khoutorsky and Bourque, 2014). By carrying out co-immunoprecipitation and proximity ligation assay experiments, they found that TRPV1 and microtubules directly interact with one another. Moreover, the number of interactions was almost doubled in ONs treated with the microtubule stabilizing agent taxol (Prager-Khoutorsky, Khoutorsky and Bourque, 2014). Previous work by others suggested that the site(s) at which TRPV1 interacts with microtubules are located on a C-terminus cytoplasmic domain of the TRPV1 channel (Goswami, Hucho and Hucho, 2007). By designing peptides which bind to these domains and applying them to ONs, the co-immunoprecipitation of TRPV1 and microtubules, as well as the excitation response to mechanical stimuli, were negatively affected (Prager-Khoutorsky, Khoutorsky and Bourque, 2014). The study proposed that at rest TRPV1 channels in the membrane of ONs are largely inactive, however upon shrinking, the force of the membrane collapsing downward upon the microtubule cytoskeleton leads to a counteracting push force from the microtubules which leads to activation of TRPV1 channels.

Microtubules have therefore been conclusively shown to be important elements of the mechanotransductory apparatus associated with certain channels. I will now discuss how the presence / absence of acetylation on microtubules in *C. elegans* effects the mechanical sensitivity of these animals.

1.9 Microtubules and mechanosensation

Microtubules are composed of repeating heterodimers of α and β tubulin, which form long intracellular chains termed protofilaments as shown in figure 8. These protofilaments link together to

form long hollow tubes which play a role in a number of key cellular processes such as cell division, migration and intracellular transport respectively (Cueva et al. 2012). Microtubules are dynamic structures that continually cycle through phases of assembly (polymerization) and disassembly (de-polymerization) (Mitchison and Kirschner, 1984).

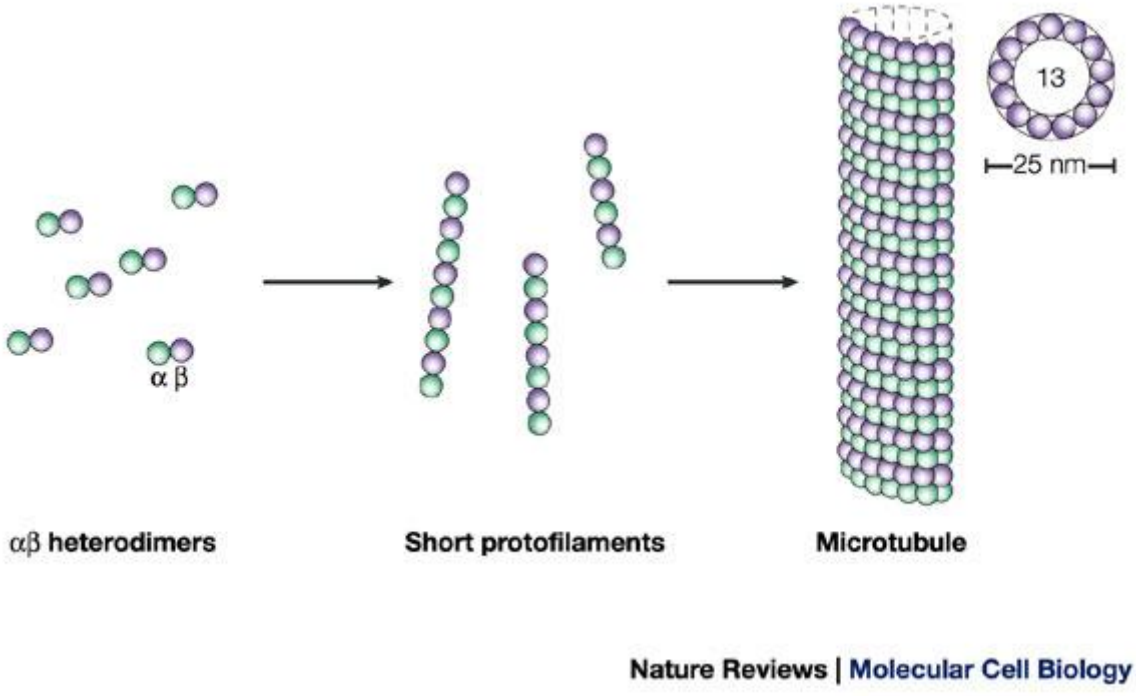


Figure 7. Diagram representing the components and ultrastructure of microtubules. Microtubules are composed of repeating heterodimers of α and β tubulin linked together to form long rod shaped protofilaments. The protofilaments then link together to form enclosed tube structures which comprise the microtubule ultrastructure. Taken from (Westermann and Weber, 2003).

Microtubules interact with a multitude of different microtubule associated proteins (MAPs) which can stabilise (*e.g.* tau protein, MAP1 and MAP2), or destabilise (*e.g.* spastin and katanin) these structures, respectively (Roll-Mecak and McNally, 2010; Kadavath *et al.*, 2015). The function and activity of microtubules is regulated by different forms of post-translational modifications (PTMs) such as acetylation, phosphorylation and detyrosination, among others (Janke & Bulinski 2011). These PTMs are mediated by enzymes, and involve the covalent addition of a functional group to a translated protein. The PTM of α and β tubulin is believed to increase the heterogeneity of these

structures, specialising them for the diverse range of roles they undertake within cells (Janke, 2014). The particular tubulin PTM my own work is concerned with is acetylation, which was first identified in the single celled green algae, *Chlamydomonas reinhardtii* (L'Hernault and Rosenbaum, 1983). Here, acetylation was associated with a lysine residue residing on the α tubulin subunit of microtubules (L'Hernault and Rosenbaum, 1985; Piperno, LeDizet and Chang, 1987). We now know that this acetylated lysine residue (K40), resides on the inner lumen of microtubules (Nogales *et al.*, 1999) and that, to the best of my knowledge, is to date the only PTM located in this region.

1.10 The role of Mec 17 and Atat1 in mechanosensation

Initially, the biological function of tubulin acetylation was unclear as mutant *Tetrahymena thermophila*, a free living protazoa which lacked acetylation on its microtubules, were shown to be perfectly viable (Gaertig *et al.*, 1995). However, genetic screens carried out to find touch-insensitive mutants in *C. elegans* identified a mechanoinsensitivity phenotype associated with a mutant copy of a gene called *mec-17* (Chalfie and Au, 1989). In follow up work, the gene locus was sequenced and the expression of *mec-17* was found to be specific to the six touch responsive neurons (TRNs) present in *C. elegans* (Zhang *et al.*, 2002). A subsequent bioinformatic analysis of the MEC-17 protein highlighted its distinct similarity with members of Gcn5-related N-acetyltransferase (GNAT) superfamily of proteins, suggesting that MEC-17 might act as an acetyltransferase (Steczkiewicz *et al.*, 2006). This was confirmed in 2010, when two independent papers established, in both invertebrates and vertebrates, that MEC-17 and its mammalian orthologue, alpha-tubulin acetyltransferase 1 (Atat1) act as acetyltransferase(s) that specifically target the lysine 40 (K40) residue of α-tubulin (Akella *et al.*, 2010; Shida *et al.*, 2010).

Subsequent to this, a flood of work relating to the activity of these enzymes, as well as the effect of knocking them out in *C. elegans* and mice followed. Papers were published on the cellular localisation of Atat1 in cells (Montagnac *et al.*, 2013), its dynamics and targeting (Szyk *et al.*, 2014), as well as

how this protein gains access to its target, K40, on the inner lumen of microtubules (Coombes *et al.*, 2016). Work in mice which were genetically deficient in Atat1 demonstrated that the sperm of male animals were less motile than those of wildtype males, with a consequent decrease in the fertility of these animals (Kalebic *et al.*, 2013).

Work on MEC-17 revealed that knocking this enzyme out in the touch-responsive neurons of *C. elegans* resulted in a change in the protofilament number of microtubules, from the usual 15 to a wider distribution ranging from 10 – 16 in these cells (Topalidou et al. 2012; Cueva et al. 2012). Moreover, processes emanating from TRNs MEC-17 mutants showed morphological deficits such as bulges and breaks in their structure (Topalidou *et al.*, 2012). Finally, the touch insensitivity phenotype observed in MEC-17 mutants could be rescued by transforming an enzymatically inactive form of the enzyme into the animals' TRNs. However, the enzymatic mutant did not restore the protofilament number within TRNs, suggesting that the 15-protofilament microtubules commonly observed is not essential for functional mechanosensation (Topalidou *et al.*, 2012). Intriguingly, computational simulations of intra- and inter- protofilament salt bridge formation in microtubule ultrastructures in the TRNs of MEC-17 wildtype and mutant *C. elegans* respectively, reveal that acetylation of the K40 residue leads to a greater abundance of these linkages between amino acids on adjacent protofilaments, which confers increased stability to these structures (Cueva, et al. 2012).

Acetylation is not the only type of PTM that changes the structural mechanics of microtubules. Recent work published on microtubule networks in cardiomyocytes revealed an interaction between the microtubule cytoskeleton and desmin intermediate filaments that was dependent on the detyrosination state of the microtubules (Robison *et al.*, 2016). Desmin intermediate filaments are known to link with the Z-disc (Konieczny *et al.*, 2008), and also form detyrosination-dependent linkages with microtubules. Therefore, desmin acted as an anchoring bridge between the microtubules and the Z-disc. When detyrosination was low, the interaction between the microtubules and the Z-disc became weaker, which enabled the myocytes to contract more readily. Conversely, when detyrosination was

high, these linkages were more robust, rendering a greater physical rigidity to the network (Liao and Gundersen, 1998), subsequently impeding contraction (Robison *et al.*, 2016).

Thus, PTMs can markedly affect the rigidity of microtubules and, consequently, the cells in which they reside. I will now discuss the results of my own work, in which I investigated the role of Atat1 in the peripheral nervous system of mice.

The aim of our work was to assess the role of Atat1 in mechanosensation of mice. To do this we utilised a conditional knock-out transgenic mouse line which specifically removes Atat1 from the peripheral nervous system. Our aim was to assess whether mice which were knockout for Atat1 in their peripheral nervous systems were touch insensitive. We also wanted to assess the sensitivity of these animals and their wildtype counterparts to other types of peripherally encoded stimuli such as temperature and proprioception. Finally, if such a deficit was found to be present, we next aimed to systematically evaluate the structure and function of the peripheral nervous system of these knockout mice at both the whole animal and the molecular level to uncover the mechanism behind this deficiency.

2 Chapter 2: General Methods

2.1 Animal breeding and genetics

In order to ascertain the effect on touch sensitivity of deleting the *atat1* gene, Atat1 $^{fl/+}$ mice (Kalebic et al., 2013) were crossed with mice which have the peripheral nervous system specific Cre-driver line Avil$^{cre/+}$. By driving the expression of Cre from the PNS specific promoter Advillin, it was possible to create a conditional knock-out mouse line which lacked Atat1 in the structures of the PNS including the sensory nerve afferents, DRG and the trigeminal ganglia (Zurborg *et al.*, 2011). To generate Avil-Cre::ATAT1$^{fl/+}$ (control), and upon further crossing of these animals, Avil-Cre::ATAT1$^{fl/fl}$ (cKO) animals. These mice were then bred with ROSA26::SNAP-CAAX animals (Yang *et al.*, 2015) to genetically label the peripheral nervous system. The mice were genotyped as described previously (Zurborg *et al.*, 2011; Kalebic *et al.*, 2013; Yang *et al.*, 2015). A description of the primer sequences and the expected band sizes of the respective genotyping strategies are included below. Age-matched male adult (> 6 weeks) mice were used for all experiments, as female mice have been shown to have modified responses to mechanical stimuli as a result of their estrous cycle (Mogil, 2012).

Genotyping of mice

Mice were genotyped according to the following strategy:

<u>Avil-Cre</u>

Primers – Cre:

Cre3 - GCACTGATTTCGACCAGGTT

Cre4 - GAGTCATCCTTAGCGCCGTA

PCR program: CRE2

94ºC 2 min, (94ºC 30s, 55ºC 1 min, 72ºC 1 min) x 39 cycles followed by 72ºC 5 min 4°C forever.

Band size of Cre: 408 base pairs (bp)

Avil-Cre::ATAT1$^{fl/fl}$

Primers – ATAT1$^{fl/fl}$:

Rikwt fw – CCTCCCACTATTGTCTCTCATTA

Rikwt rev2 – CCTGGAGATGGGTGCATATAAAC

PCR program: Genorik

95ºC 3 min, (95ºC 10s, 60ºC 30s, 72ºC 30s) x 54 cycles followed by 72ºC 5min 4°C forever.

Band size of ATAT1: Wild-type 156bp; Flx 230bp

ROSA26::SNAP-CAAX

Primers – ROSA26::SNAP-CAAX

HL54 – TAAGCCTGCCCAGAAGACTCC

HL152 – (Fwd common) AAGGGAGCTGCAGTGGAGTA

HL MP – GGCGTTACTATGGGAACATAC

Pcr Program: RosaCAG"

95°C 5min (94°C10s, 62°C 30s, 72°C 30s) x35 cycles followed by ,72°C 2min 4°C forever.

Band size of ROSA26:: SNAP-CAAX: Wild-type 209bp; Mutant 361bp.

The relevant genotyping was carried out on all mice that were used in experiments.

2.2 Statistical analysis and animal care

All of the statistical analyses are presented as standard error of the mean (SEM), along with the number of samples analyzed (n). Student's t-test, unpaired t-test, Fisher's exact test, Mann-Whitney test and 2-way repeated measures (RM) ANOVA were used as appropriate and $P<0.05$ was considered statistically significant. In order to power our studies the 'resource equation' method was utilised (Charan and Kantharia, 2013). Using this method an E value between 10 and 20 was considered within the acceptable range to extract robust statistical information from an experiment

(Charan & Kantharia, 2013). The E value was calculated as follows E = (number of mice x number of experimental groups) – number of experimental groups (Charan & Kantharia, 2013).

Animal housing, care and ethics

The mice were maintained at the EMBL Mouse Biology Unit, Monterotondo, Italy, in direct accordance with Italian legislation (Art. 9, 27. Jan 1992, no 116) under license from the Italian Ministry of Health. Mice were maintained in plexiglass cages in a temperature controlled room with a 12-hour light / dark cycle. Food and water was available to the mice *ad libitum* and daily visual inspections of the mice's general health were conducted by the animal caretakers. Mice were euthanized for experiment by CO_2 inhalation. For experiments involving the injection of dyes into live mice, the animals were first anaesthetized using 5% Avertin in a weight to dosage dependent manner.

3 Chapter 3: Materials and Methods

3.1 Methods

3.1.1 Low-threshold mechanical assay I: tape response assay

This test was designed to assay the response of the mice to an innocuous mechanical stimulus. Male $Atat1^{Control}$ and $Atat1^{cKO}$ mice were exclusively used for all behavioral tests. The mice were placed into transparent plexiglass containers (30cm x 30cm) and allowed to habituate for 15 minutes. Subsequently, a 3cm long by 1cm wide piece of tape (Identi tape, Valtec, Co, U.S.A.) was placed along the spinal column on the lower back of the animals. The mice were then allowed to roam freely for 5 min and the numbers of attempts to remove the tape were recorded. Three distinct actions were considered as attempts to remove the tape, these being biting, hind-paw flick and vigorous shaking (Garrison, Dietrich and Stucky, 2012). The experiment was carried out using the following number of animals n = 8 $Atat1^{Control}$ and 7 $Atat1^{cKO}$.

3.1.2 Low-threshold mechanical assay II: cotton swab assay

This test was designed to assay the response of the mice to an innocuous mechanical stimulus. Mice were placed into plexiglass transparent containers (30cm x 30cm) which were positioned atop an elevated surface with a mesh grid base. They were allowed to habituate to this setting for 30 minutes. Subsequently, a cotton swab (Q-tip) which had been 'puffed' out to increase its size was touched against the right and then the left hind-paw of the mice in a light brushing manner. A quick retraction of the touched paw was considered a positive response (Garrison, Dietrich and Stucky, 2012). The experiment was carried out using the following number of animals n = 9 $Atat1^{Control}$ and 9 $Atat1^{cKO}$.

3.1.3 High-threshold mechanical assay I: von Frey assay

This test was designed to assay the response of the mice to punctate noxious stimuli. Mice were placed inside transparent plexiglass containers (30cm x 30cm) and allowed to habituate for 1 hour. A series of von Frey filaments (North Coast Medical, NC12775-99, Ca, U.S.A.), producing forces

ranging from 0.02g to 1g were applied to animals' hind-paws in an alternating right / left pattern. A withdrawal of the hind -paw was considered a positive response. The frequency of responses of $Atat1^{cKO}$ mice never reached 100%, even using the von Frey with the largest force. Therefore, a threshold was calculated based on the force required to produce a response 50% of the time. n = 8 $Atat1^{Control}$ and 8 $Atat1^{cKO}$.

3.1.4 High-threshold mechanical assay II: tail clip test

This test was designed to assay the response of the mice to a noxious stimulus. Mice were placed into transparent plexiglass containers and allowed to habituate for 10 minutes. A crocodile clip with a rubber ending (to reduce tissue damage) and a measured constrictive force of 400g was placed on the base of the animal's tail. The mice were allowed to freely roam until they visibly responded to the presence of the clip. The latency to response was recorded (Ranade *et al.*, 2014). n = 7 $Atat1^{Control}$ and 7 $Atat1^{cKO}$

3.1.5 Thermal sensitivity assay I: hot plate assay

This test was designed to assay the response of the mice to a range of different standard noxious thermal stimuli. For this assay, mice were placed onto a pre-heated metal pad (Hot plate Ugo Basile, 35150) which had a fixed temperature of 50, 52.5 or 55°C respectively. The latency to response for each mouse was recorded. A response was considered to have occurred when an animal jumped, flicked and or licked itself. In the absence of a response the animal was removed after 30s. n = 6 $Atat1^{Control}$ and 6 $Atat1^{cKO}$

3.1.6 Thermal sensitivity assay II: tail immersion assay

This test was designed to assay the response of the mice to a range of different noxious thermal stimuli. Mice were habituated over the course of a week into voluntarily climbing headlong into a mesh restrainer. The exposed tail region was then dipped into the water of a pre-heated water bath set

to a temperature of 46, 48 or 50°C respectively. A response was recorded when the animal's tail flicked, and the latency was recorded. n = 6 Atat1^{Control} and 6 Atat1^{cKO}.

3.1.7 Thermal sensitivity assay III: acetone drop test

This test is designed to assess responses to a noxious cold stimulus via evaporative cooling. For this, mice were placed into transparent plexiglass containers atop an elevated surface on a mesh grid base. Using a syringe, ice cold acetone was sprayed onto the hind-paws of the mice in a right / left alternating manner. The strength of response was recorded based on a four-point scale (Choi et al., 1994). n = 6 Atat1^{Control} and 6 Atat1^{cKO}

3.1.8 Proprioceptive Assay I: Rotarod Assay

A version of the rotarod test (Rotarod 3375-5 TSE systems) was carried out on the animals to assess their general locomotion. Firstly, the mice were allowed to habituate to balancing on stationary dowels for 5 minutes. Each subsequent habituation or test phase was followed by a 5 minute rest period where animals were placed back into their cages with food and water *ad libitum*. The animal's locomotion was tested at 5, 10, 15, 20 and 25 rotations per minute (RPM) respectively with a total of two minutes per trial. The latency to failure was measured. A fall from the dowels or two full rotations whilst the animal gripped the apparatus was considered a fail during the test. n = 12 Atat1^{Control} and 9 Atat1^{cKO}

3.1.9 Proprioceptive assay II: grid walk balance assay

This test was designed to assay fine proprioception. A grid walk assay was performed on the mice to assess their capacity for fine proprioception. The mice were allowed to freely roam for 2 minutes on a metal grid (30cm x 30cm) which consisted of evenly interspersed metal rungs ~2cm apart. The number of total steps and slips for all paws was recorded. n = 11 Atat1^{Control} and 10 Atat1^{cKO}

3.1.10 DRG neuronal culturing and transfection

Mice were sacrificed by CO_2 inhalation. Cultures of dissociated DRG neurons from adult mice (> 6 weeks) were prepared as follows. DRGs were dissected from mice and placed in a solution of ice cold phosphate-buffered saline (PBS). The tissue was then enzymatically digested using collagenase IV (1 mg/ml) for 25 min at 37ºC and subsequently with trypsin (0.05%) for 25 min at 37ºC. The DRG was then mechanically treated by triturating the cells with a P1000 pipette to facilitate the dissociation of individual neurons. The dissociated DRG neurons were then plated in Dulbecco's Modified Eagles Medium containing 10% foetal bovine serum (FBS Sigma-Aldrich) and 1% penicillin / streptomycin referred to as 'DRG medium' onto poly-L-lysine (200 mg / ml) and laminin (20 µg / ml) coated coverslips within 35mm dishes. These dishes were then transferred to a humidified incubator set to 37ºC with 5% CO_2. For transfection, prior to plating on poly-L-lysine / laminin coated coverslips, the cells were suspended in 20µl of Mouse Neuron Nucleofector solution and transfected using the small cell number (SCN) Nucleofector kit (Lonza AG) with 4-5µg of plasmid DNA at room temperature. The solution was transferred to a cuvette and electroporated (AMAXA Nucleofector AAFD-10015 Transfector) using the pre-set program SCN Basic Neuron 6. Following this the cells were transferred to an eppendorf containing 500µl of RPMI 1640 medium (Gibco) for 10 min at 37°C. The cells were then plated onto glass coverslips coated with poly-L-lysine (200 mg/ml) and laminin (20 µg/ml) in Roswell Park Memorial Institute (RPMI) 1640 medium containing 10% FBS. The medium was replaced with standard DRG medium 3-4 hours after plating.

3.1.11 Visualising the afferents peripheral nervous system in the skin

$Atat1^{Control}$ and $Atat1^{cKO}$ mice which express the SNAP-tag (a genetically encoded membrane protein) (Yang *et al.*, 2015) specifically in the PNS, were used to visualise the peripheral nervous system in hairy skin taken from the digits of the hind-paw(s) of these animals. Mice were first anaesthetised with ketamine. Subsequently, ~10µl of BG TMRstar (a fluorescent dye which binds specifically to the SNAP-tag) (2µM) (New England Biolabs) was delivered via intradermal injection to hairy skin

of the finger. Following a 5 hour waiting period, the animals were sacrificed and the injected skin regions were removed and mounted on glass with 80% glycerol to preserve the sample for imaging.

3.1.12 Electron microscopy of saphenous nerves

Dissected saphenous nerves were post-fixed for 24 hours with fresh 4% paraformaldehyde (PFA), 2.5% glutaraldehyde (Sigma-Aldrich) in 0.1 M phosphate buffer at 4°C. The samples were then incubated for 2 hours with 1% osmium tetroxide (OsO_4) which was supplemented with 1.5% potassium ferrocyanide. Afterwards, the samples were dehydrated in ethanol and infiltrated with propylene oxide / Epon (Agar) (1:1) followed by embedding in resin. Ultrathin sections were cut (Ultracut S, Leica), and counter stained with uranyl acetate and lead citrate to add contrast to the images. The samples were then subsequently observed with a Transmission Electron Microscope (TEM) Jeol 1010 equipped with a MSC 791 CCD camera (Gatan).

3.1.13 Measuring axon growth in DRG cells

Wholemount *ex-vivo* DRG explants from $Atat1^{Control}$ and $Atat1^{cKO}$ mice were extracted and grown for one week in a matrigel matrix in DRG medium. To allow the axons time to develop, the explants were allowed to grow for one week. Following this, the samples were fixed with 4% PFA for 10 min, subsequently washed with PBS three times and then stained with (PGP 9.5 which stains neuronal cell bodies and axons) 1:200 (Agilent DAKO) to visualise the outgrowths. All images were acquired with a Leica LMD 7000.

3.1.14 Actin staining of DRG

Phalloidin staining was carried out to visualize the distribution of actin in cultured DRG cells using Alexa488-phalloidin (0.5 μg/ml) (Lifetechnologies). In summary, cells were then fixed with 4% PFA (EM grade, TAAB) in cytoskeleton buffer (10mM MES, 138mM KCl, 3 mM MgCl, 2 mM EGTA) supplemented with 0.3 M sucrose, permeabilized in 0.25% Triton-X-100 (Sigma-Aldrich), and

blocked with 2% BSA (Sigma-Aldrich). Imaging was carried out on a Leica SP5 confocal microscope.

3.1.15 Superresolution of DRG

Cultured DRG neurons were washed with PBS before fixation and permeabilization for 2 minutes in cytoskeleton buffer (CB) containing 0.3% glutaraldehyde and 0.25% Triton X-100. The cells were then post-fixed for 10 minutes in a CB containing 2% glutaraldehyde and then treated for 7 minutes with 0.1% Sodium Borohydride ($NaBH_4$) in PBS. Afterwards cells were washed three times for 10 minutes with PBS. Primary antibody staining with mouse anti-α-tubulin (Neomarker 1:500) was then carried out for 30 minutes in PBS containing 2% BSA. Another three by 10 minutes wash was carried out, before the cells were transferred to the secondary antibody (goat anti mouse Alexa 647, 1:500, Molecular Probes A21236) for 30 minutes at room temperature. Again, the cells were washed three times in PBS for 10 minutes each and mounted for direct stochastic optical reconstruction microscopy (dSTORM) superresolution imaging. At this time the cells were overlaid with STORM blinking buffer: 50mM Tris pH 8.0, 10mM NaCl, 10% Glucose, 100U/ml Glucose Oxidase (Sigma-Aldrich), 40ug/ml Catalase (Sigma-Aldrich).

Image analysis was performed using the open source software, CellProfiler (Carpenter et al., 2006). The signal from the microtubule (MT) cytoskeletal structure was enhanced with the same manual threshold for all images. The binary images generated were then skeletonized using a CellProfiler function called “skelPE”. The resulting skeletonized images were then subjected to branchpoint analysis. The density of the MT was computed by dividing the total skeleton length by the area of the cell. Finally, a MT crossing density was calculated by dividing the number of branchpoints detected by total skeleton length. The angular distribution (angular variance) of the MT network was also analyzed in order to assess whether the network ran in a parallel, or a crossing manner. To achieve this, each pixel of the network was subjected to a rotating morphological filter using a linear structural segment with a length of 11 pixels, and analyzing at which angle we recorded the maximum value.

The value of the angles was computed in steps of 10 degrees from 0 to 170 since at this spacing there is no available information on microtubule polarity. Concomitantly, we also measured the so-called local circular variance at a diameter of 51 pixels; this was carried out using angle doubling which is a commonly used practice for analyzing axial data (Hankin, 2015). If a microtubule in a certain region is parallel to the plane of view it is attributed a value of 1, and has smaller values down to 0 for MTs oriented in a non-parallel manner. We extrapolated this value across the entirety of the cell. Therefore, if the value is 1 (or close to it) this implies that on a scale of 51 pixels the microtubule network is parallel to the viewing plane in orientation.

N.B. **all of the superresolution imaging and computational analysis data were generated by Loredana Iovino and Dr. Christian Tischer respectively at EMBL, Heidelberg, Germany.**

3.1.16 Staining of the dorsal horn of the spinal cord

The whole spinal cord was extracted and fixed for 3 hours in 4% PFA at 4°C. Samples were embedded in 2% agarose and 100μM sections were cut using a vibrotome. Sections were subsequently treated with 50% ethanol for 30 minutes and then incubated with 5 % (normal goat serum) NGS in 0.3% Triton-X in PBS blocking solution for 1 hour. Samples were incubated overnight in primary antibody at 4°C at the following concentrations: CGRP 1:500 (raised in mouse) (Rockland, 200-301-DI5) and IB4 1:100 (Invitrogen, I21414). IB4 labels non-peptidergic nociceptor afferents in laminae I and CGRP labels the afferents of peptidergic nociceptors in laminae I. Following this, sections were washed with PBS and incubated for 1 hour with 1:1000 secondary antibodies (Alexa Fluor 488 and 546, Lifetechnologies) in 5% NGS blocking solution. Samples were then mounted in prolong gold to maintain the fluorescent labelling (Invitrogen, P36930) for EM imaging.

3.1.17 Microtubule axonal transport

DRG were extracted and prepared and the dissociated DRG neurons were then suspended in a 1:1 Matrigel matrix in DRG medium within a two-chamber microfluidic device (Xona Microfluidics,

SD150). The DRGs were allowed to grow for 3-5 days facilitating the growth of their axons across the microchannels connecting the two chambers. The cells were serum starved for 3 hours on the day of the experiment. This was done to increase the rate of uptake of the NGF coupled quantum dots. Subsequently, a solution containing a 1μM mono-biotinylated nerve growth factor (NGF; purified in house from eukaryotic cells), which had been previously coupled to streptavidin conjugated quantum dots 655 (Life Technologies) on ice for 30 minutes, was diluted to 5nM with imaging buffer and added to the axonal chamber of the device. A volume difference of ~25% was maintained between the axonal and cell body chambers of the device in order to prevent backflow between the chambers. Following a 1 hour incubation at 37°C in 5% CO_2, the retrograde transport of the NGF coupled Qdots655 within endosomes was imaged using a confocal Ultraview Vox (Perkin Elmer) with a humidified incubator chamber. The NGF-QD solution was added to the peripheral ends of the axonal outgrowths and, once internalised (with the NGF receptor) via endocytosis, the NGF-QD complex was shuttled retrogradely via the microtubule network towards the soma of the DRG cellImages were acquired at 100 s time lapses with an exposure of 300ms. Images were analyzed using the particle tracking function of the Imaris software.

3.1.18 Fluorescent recovery after photo-bleaching (FRAP) analysis of Piezo2-GFP transfected DRG neurons

FRAP analysis of Piezo2-GFP transfected DRG neurons was undertaken to assess whether differences in the rate of trafficking of this ion channel were evident between the genotypes. DRG neurons were transfected with Piezo2-GFP using a nucleofector device as described previously. The cells were allowed to grow for two days before FRAP analysis was carried out using a Leica SP5 confocal microscope. The imaging procedure was as follows: 10 frames pre-bleach, followed by 10 frames of photo-bleaching (70% laser power) and following from this the cell was imaged once every 1 min for 15 consecutive minutes. Data were analyzed, and graphs generated, using Sigma-Plot.

3.1.19 Immunohistochemical labelling of microtubules in both MEF cells and DRG neurons

DRG neurons previously plated on coverslips (see section 3.1.10) for protocol (DRG neurons or MEFs) were first washed with PBS and then fixed for 15 minutes in cytoskeleton buffer (CB) pH6.3 containing 3% paraformaldehyde, 0.25% triton and 0.2% glutaraldehyde at room temperature. Subsequently, cells were washed three times with PBS-Triton 0.3%. Cells were then blocked with 5% normal goat serum (NGS) in PBS for 1 hour at room temperature. Cells were then stored at 4°C overnight in a 1:1000 solution of PBS containing either anti-α-tubulin (Sigma-Aldrich, T9026) or anti-acetylated-α-tubulin (Sigma-Aldrich, T7451) antibody. Cells were then washed with PBS before labelling with 1:1000 secondary antibody (Alexa Fluor 546 Lifetechnologies) for 1 hour in PBS at room temperature. The coverslips were mounted on glass slides. Images were acquired using a Leica SP5 confocal microscope. Processing of images and generation of surface plots was performed using the surface plot function in ImageJ.

3.1.20 Visualisation of acetylated microtubules in peripheral corneal nerve fibres

Eyes were removed from mice and fixed for 1 hour in 4% PFA at room temperature. The cornea was then separated from each eye and permeabilized with PBS-Triton (0.3%) for 30 minutes. Subsequently, the cornea was immersed in the same permeabilizing solution but this time also containing 1μM SNAP surface 546 (New England Biolabs) for 30 minutes. Following this, the samples were then washed with PBS-Triton 0.3% for 20 minutes and then blocked with 5% NGS in the same solution for 30 minutes. Staining with anti-α-tubulin (1:500) was carried out overnight. Samples were afterwards washed and stained with secondary antibody (Alexa Fluor 488 Lifetechnologies) for 5 hours. Finally, the samples were washed with PBS and stained with DAPI for 10 minutes in order to label cell nuclei. The labelled samples were then mounted on glass slides with 100% glycerol and imaged when dried.

3.1.21 Localisation of acetylated microtubules in the saphenous nerve

In order to assess the localisation of acetylated tubulin within afferents staining was carried out on saphenous nerves extracted from $Atat1^{Control}$ and $Atat1^{cKO}$ mice. Paraffin sections of saphenous nerves were stained after fixation with PFA. After rehydration, antigen retrieval was carried out using 10 mM sodium citrate (pH 6) at boiling temperature for 10 min. Sections were then permeabilized using (0.3% Triton X-100), then blocked with 5% NGS and stained with anti-acetylated-α-tubulin (Sigma-Aldrich, T7451) and anti-myelin basic protein (Chemicon, MAB 386). Samples were imaged using a Leica SP5 confocal microscope.

3.1.22 Atomic Force Microscopy (AFM)

All AFM measurements were performed using the NanoWizard AFM (JPK Instruments, Berlin, Germany) unit which was equipped with a fluid chamber (Biocell; JPK) for analysis of live cells, under an inverted optical microscope (Axiovert 200; Zeiss). DRG neurons taken from $Atat1^{Control}$ and $Atat1^{cKO}$ mice were plated onto glass coverslips which had previously been coated for 1 hour at room temperature with poly-L-Lysine (500µg/ml) and, subsequently, laminin (20µg/ml) for 1 hour at 37°C. The cells were then left to grow in an incubator for at least 15 hour before measurements were made. The neuronal samples were then inserted into the fluid chamber and covered in culture medium. All measurements were recorded at room temperature. The indenters for measuring cellular elasticity consisted of silica microspheres of 4.5µm diameter (Bangs Laboratories Inc.) linked via UV-sensitive glue (Loxeal UV Glue) to tipless V-shaped silicon nitride cantilevers which have spring constants of 0.32N/m or 0.08N/m (NanoWorld, Innovative Technologies). Prior to measurements being made the spring constant of the cantilevers was calibrated using the thermal noise method (Lübbe *et al.*, 2013). Using the optical microscope to visualize the cells, the cantilever with a ‘ball’ shaped tip was brought to bear upon the soma of single DRG neurons to indent the cell. This type of ball shaped tip has a larger indentation area and therefore recruits a larger area of the membrane and sub-membrane cytoskeleton into resisting the applied pressure. The motion of the z-piezo (controlling the downward

motion of the indenter onto the cell) and resulting force were then measured. For each cell, between eight and ten force distance curves were acquired at a force load of 500 pN and a rate of 5µm/sec^{-1} in closed loop feedback mode. By evaluating Young's modulus (a value for elasticity) the cells structural properties could then be assessed. This value was computed by analyzing the approach segment of the Force-Dsiplacement curves using the JPK DP software. This software is capable of converting the approach curve into force-indentation curves by subtracting the value of cantilever bending from the signal height to produce a value for indentation. These force indentation curves were later calibrated for a spherical indenter, used according to the following equation:

$$F = \frac{E}{1-\nu^2}\left[\frac{a^2 + R_s^2}{2}\ln\frac{R_s + a}{R_s - a} - aR_s\right]$$

$$\delta = \frac{a}{2}\ln\frac{R_s + a}{R_s - a}$$

Here, δ corresponds to the indentation depth, a is the constant radius of the indenter, R is the silica bead radius, ν is the Poisson ratio of the sample (set to 0.5 for cell) (Rotsch et al., 1999) and E represents Young's modulus (a measure of elasticity). The fittings were performed at three distinct indentation levels namely, 200, 400 and 600nm respectively.

***N.B.* all AFM data was generated by Dr. Laura Andolfi at SISSA Trieste, Italy.**

3.1.23 Hyperosmotic Shock Cell Shrinking Assays

DRG neurons which had been previously plated on glass coverslips were loaded with 500nM of silicone rhodamine (SiR)-Tubulin2 for 1 hour at 37°C and/or 2µM calcein dye (Invitrogen C3100MP) for 30 minutes at 37ºC in order to facilitate uptake of the fluorecent dye(s). (SiR-Tubulin2 is a microtubule binding fluorogenic dye which is compatible with live cell imaging.) Calcein is a cell permeable dye which has a fluorescence emission in the GFP range. Calcein has the interesting characteristic of self-quenching its own fluorescence when individual molecules interact with one

another. Therefore, when the hyperosmotic shock is applied and reduces cell volume, the intracellular calcein within the cell has less space, meaning that molecules of the dye will interact with one another more frequently. This, in turn, will produce a decrease in fluorescence which is directly proportional to the degree of induced cell shrinkage. Following this the cells were transferred to imaging buffer (10mM Hepes pH 7.4, 140mM NaCl, 4mM KCl, 2mM CaCL2, 1mM MgCl2, 5 mM D-glucose) at 320mOsm. The cells were then given a 5 min acclimatization period before being subjected to a hyperosmotic shock stimulus (440mOsm) for 3 minutes. The hyperosmotic solution used was simply the imaging buffer that had had 120mM of mannitol added to it.

All imaging was carried out using a Leica SP5 resonant scanner. In order to increase the cellular uptake and brightness of the far-red microtubule dye SiR-Tubulin (Lukinavicius et al., 2014) the docetaxel region of SiR-Tubulin was replaced with the more hydrophobic cabazitaxel.

4 Chapter 4: Behavioral Characterisation of Atat^{cKO} Mice

4.1 Results

4.1.1 Assessing animal behavioural response to mechanical, thermal and proprioceptive tests

This series of experiments was designed to assess, behaviorally, the importance of Atat1 for the detection of mechanical low-threshold (innocuous) and high-threshold (noxious) type stimuli, as well as thermal and proprioceptive sensations respectively. This work was vital for establishing the nature of the phenotype, if any. Moreover, previous work carried out on C.elegans was unable to perform such a detailed analysis of both low threshold and high threshold touch stimuli due to the simplicity of this organism.

4.1.2 Atat1^{cKO} mice are insensitive to innocuous mechanical stimuli

Both Atat1^{Control} and Atat1^{cKO} mice were subjected to a series of tests designed to test their response to low-threshold (innocuous) mechanical stimuli on both the hairy and glabrous skin. The first test undertaken was the tape test assay. The results of this assay revealed that Atat1^{cKO} mice showed a significant decrease in the number of attempts to remove the tape (hairy skin) when compared to the Atat1^{Control} group (Student's t-Test, $P<0.05$). (figure 8.0. a). We next investigated the response to an innocuous mechanical stimulus on the glabrous skin by performing a cotton swab assay. Here, our results revealed a significant deficit in recorded responses from the Atat1^{cKO} mice relative to the control group (Student's t-Test, $P<0.05$). (figure 8.0. b). (Tape test n = 8 Atat1^{Control} and 7 Atat1^{cKO}. Cotton swab n = 9 Atat1^{Control} and 9 Atat1^{cKO}.)

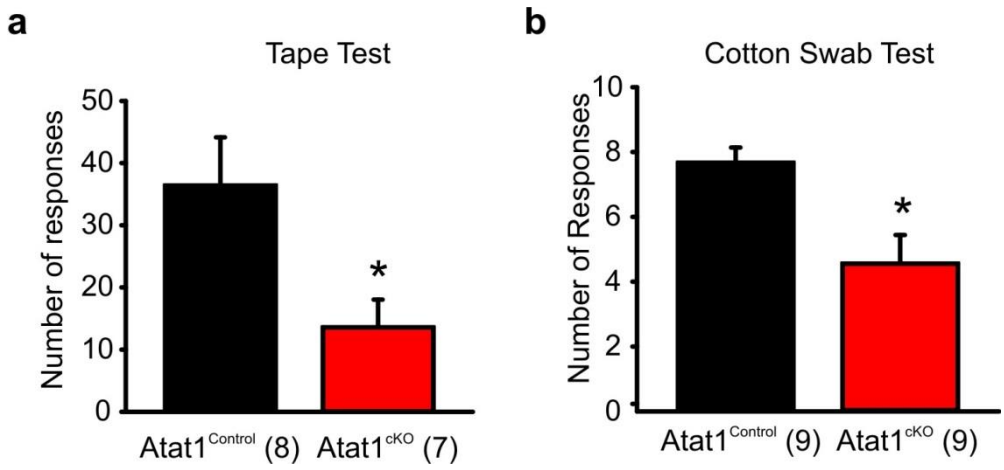


Figure 8.0. **Low-threshold mechanical touch assays carried out on Atat1^{Control} and Atat^{cKO} mice respectively**. **(a),** Tape test assay: the average number of attempts to remove the piece of tape over a 5 minute period was significantly lower in Atat^{cKO} mice compared to controls (Student's t-test, P<0.05). **(b)**, Cotton swab test: a significant decrease in the average number of responses to light brush stoking was observed in Atat^{cKO} mice compared to the Atat^{Control} group (Student's t-test, P< 0.05). Error bars indicate s.e.m. The number of animals used is indicated in parenthesis in the graph.

4.1.3 Atat1^{cKO} mice are insensitive to noxious mechanical stimuli

In order to assess the respective genotypes' response to high threshold (nociceptive) type stimuli we subjected the mice to a pair of behavioural assays designed to evoke punctate painful stimuli. We firstly undertook a von Frey test whereby the animals were given a mechanical prod to their hind-paw from a range of filaments which exert defined forces across a range measured in grams (Bonin, Bories and De Koninck, 2014). The results, shown in figure 8.1. a, revealed that Atat1^{Control} group mice were capable of responding to a stimulus from a filament with an exerted gram force as low as 0.07g, whereas Atat1^{cKO} mice lacked any response at this force. Moreover, across a range of filaments exerting progressively higher gram forces, Atat1^{Control} mice demonstrated a significantly higher frequency of responses (paw flick and or paw licking) than the animals from the Atat1^{cKO} cohort. Indeed, the median force threshold for the control group was significantly lower than that of the knock-out group (median threshold 0.4g for Atat1^{Control} and 1g for Atat1^{cKO} Mann-Whitney test, $P<0.01$). To next assess the animals' response to a strong noxious mechanical stimulus we undertook a tail clip assay. The latency (measured in seconds) required for the Atat1^{cKO} mice to exhibit distress and attempt to remove the clip was significantly longer than that of Atat1^{Control} animals (Student's t-Test, $P<0.05$; figure 8.1. b). Von Frey n = 8 Atat1^{Control} and 8 Atat1^{cKO}. Tail clip assay n = 7 Atat1^{Control} and 7 Atat1^{cKO}.

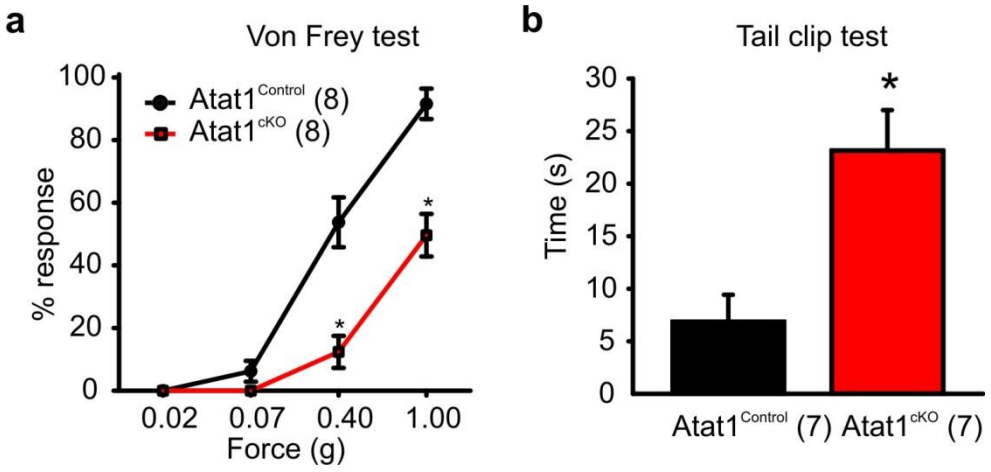


Figure 8.1. **High-threshold mechanical assays carried out on Atat1^{Control} and Atat^{cKO} mice respectively**. **(a),** von Frey assay: significant differences were observed between the groups at 0.4 and 1 gram filament forces respectively (Student's t-test, P <0.05). The percentage response is a value for the number of positive responses recorded from the total number of tests undertaken across all animals. **(b)**, Tail clip test: significant differences in the average time taken (latency to response) to acknowledge the presence of the clip were observed between the groups (Student's t-test, P<0.05). Error bars indicate s.e.m. The number of animals used is indicated in parenthesis in the graph.

4.1.4 Atat1^{cKO} mice showed no difference in thermal sensitivity relative to Atat1^{Control}

Animals from both genetic backgrounds were assessed using a battery of tests designed to assay their sensitivity to both heat and cold. No differences in the latency to response were observed between the groups during hot plate tests conducted using n = 6 animals across a range of temperatures 50, 52.5 and 55˚C respectively (Student's t-Test, $P>0.05$; figure 8.2. a). Nor were any differences exhibited between the Atat1^{Control} and Atat1^{cKO} mice in tail immersion tests that were again conducted using n = 6 animals across a range of temperatures 46, 48 and 50˚C respectively (Student's t-Test, $P>0.05$; figure 8.2. b). Likewise, no significant difference in the scored degree of nocifensive behaviour was apparent during the acetone drop test (figure 8.2. c).

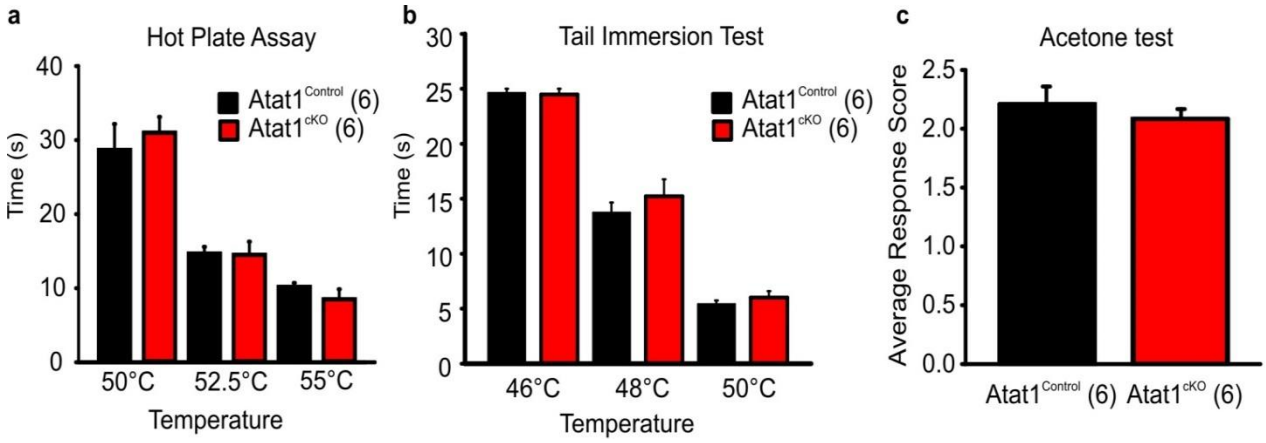


Figure 8.2. **Temperature testing assays carried out on Atat1^{Control} and Atat^{cKO} mice respectively**. **(a)**, Hot plate assay: no significant differences were observed between the groups at 50, 52.5 and 55°C, respectively (Student's t-test, *P*>0.05) in the latency (time in seconds) required for the mice to respond **(b)**, Tail immersion test: no significant differences were observed between the groups at 46, 48 and 50°C respectively (Student's t-test, *P*>0.05) in the latency (time in seconds) required for the mice to respond **(c)**, Acetone test: no significant differences in the average response score were observed between the groups (Student's t-test, *P*>0.05). The scoring method employed assigns a value to the response observed which is dependent on the action observed. Error bars indicate s.e.m. The n numbers are indicated in parenthesis in the graph. The number of animals used is indicated in parenthesis in the graph.

4.1.5 Atat1^{cKO} mice exhibited no deficits in proprioception

During rotarod testing, no deficit in locomotion was revealed between the Atat1^{Control} and Atat1^{cKO} mice across a range of tested speeds (Student's t-Test, $P>0.05$; figure 8.3. a). Concomitantly, we did not observe any significant deficits in fine proprioception between the groups as tested using the grid-walk balance assay (Student's t-Test, $P>0.05$; figure 8.3. b). Rotarod test n = 12 Atat1^{Control} and 9 Atat1^{cKO}. Grid test n = 11 Atat1^{Control} and 10 Atat1^{cKO}.

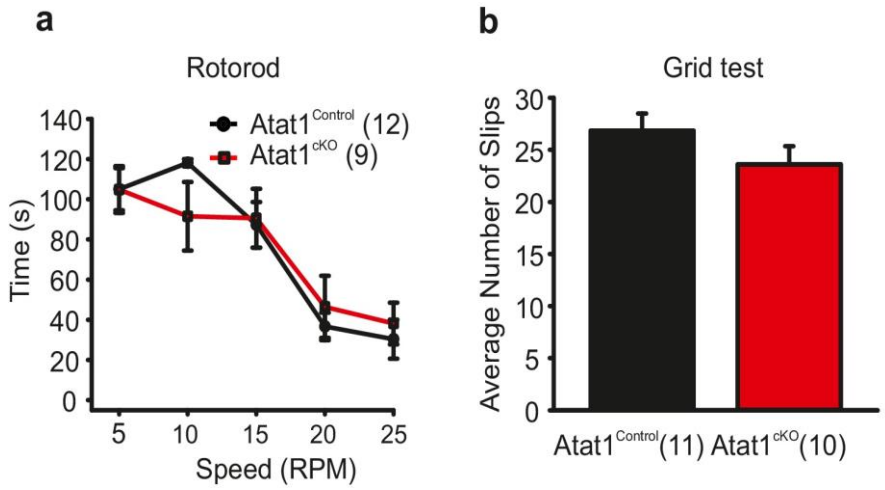


Figure 8.3. Proprioception assays carried out on Atat1^{Control} and Atat^{cKO} mice respectively. (a), Rotarod analysis: there was no significant difference between the groups in the average time that the mice spent on the rotating dowels at either 5, 10, 15, 20 or 25 RPM (Two-Way repeated measures ANOVA, P>0.05). **(b)**, Grip test assay: there was no significant difference between the groups in the average number of slips (foot-faults) that were observed over a 2 minute period (Student's t-test, P>0.05). Error bars indicate s.e.m. The n numbers are indicated in parenthesis in the graph.

4.2 Discussion

4.2.1 Atat1^{cKO} mice are insensitive to low threshold mechanical stimuli

Two tests were utilised to assess the response of Atat1^{Control} and Atat1^{cKO} mice to non-noxious stimuli. These tests are designed to specifically stimulate light touch detecting end organ structures, such as those associated with hair follicles (lanceolate endings) on the hairy skin, and Merkel cells and/or Meissner corpuscles which are located on the glabrous plantar surface of the animal's paws (Ranade *et al.*, 2014). The 'tape test' involved placing a thin strip of adhesive tape along the hairy skin on the lower back of the mice. This tape was positioned so as to be outside the eye line of the mice and therefore its detection depends on their mechanosensory capacity to 'feel' the strip. Over a five-minute recording period, control animals undertook robust and continuous attempts to remove the tape, while Atat1^{cKO} mice were for the most-part unaware to the presence of the material. The results of the tape test seem to depend heavily upon the amount of time that the animals are allowed to habituate to the tape for. In tests where the mice were only given a 5 minute habituation, the number of responses was markedly lower in both genotypes. This could be a result of the animals being more interested in exploring the novel environment, rather than reacting to the innocuous stimulus elicited by the tape. The second assay, the 'cotton swab test', was carried out by lightly mechanically stimulating the glabrous skin on the plantar surface of the animal's hind-paws with a 'puffed out' cotton swab. Once again, the Atat1^{cKO} mice demonstrated a statistically significant drop in response frequency when compared to the control mice. The cotton swab test however also suffers from severe limitations. For example, the amount of force exerted upon the plantar surface of the paw with each brush stroke is impossible to accurately quantify. Moreover, due to the diffuse structure of the cotton, coupled with the almost constant movement of the mice, it is very difficult to direct the stimulus to the same region (area) of the paw plantar surface of different mice. In place of / in conjunction with these tests it would be interesting to carry out air puff (Bai *et al.*, 2015), or a rough / smooth surface discrimination preference type test (Wetzel *et al.*, 2007) to assess whether the Atat1^{cKO} also

demonstrate a drop in responses relative to controls for these low-threshold assays. It is important here to note that despite their insensitivity to low threshold mechanosensation, Atat1^{cKO} mice are not completely oblivious to touch, but rather less sensitive, which is a feature of this phenotype, and which fits well with our proposed mechanism of action, which I will discuss in greater detail later. This lack of complete insensitivity is due to the fact that the efficiency of the Advillin Cre used to drive the deletion of the Atat1 gene from PNS specific tissue has been estimated to be in the region of 75% (Zurborg *et al.*, 2011). This means that approximately 25% of mechanically sensitive peripheral afferents emanate from DRG cells will still harbor the Atat1 protein. It is therefore surprising that the phenotype is as strong as the one observed. Indeed, it is interesting to consider that the insensitivity to touch described in these experiments would likely be even more profound if a more efficient Cre-driver was utilized.

4.2.2 Atat1^{cKO} mice are insensitive to high threshold mechanical stimuli

In this section I shall discuss the results of tests designed to evoke responses to painful stimuli applied to the animals. Painful stimuli which evoke strong behavioural responses are thought to primarily evoke responses which are transmitted by unmyelinated C-fibres, as well as intermediate myelinated A fibre mechanoreceptive (AMs) fibres (Abraira and Ginty, 2013). In our study Atat1^{Control} mice responded to a gram force as low as 0.07g, and their response frequency rose to almost 100% upon stimulus with a 1.0g filament. Strikingly, Atat1^{cKO} mice showed a response frequency of ~50% at this force pressure and their median mechanical threshold was calculated at 1.0g, compared to 0.4g for control mice. The extension of the mechanoinsensitive phenotype into the noxious range was further illustrated in the so-called ‘tail clip test’. Here a crocodile clip, which exerted an approximate gram force of ~400g, was clipped to the base of the tail of free-roaming animals. The clip exerts a progressively painful stimulus when applied to one’s own skin, and therefore we rationalized that, like ourselves, the animals would only tolerate the clips presence until it became too painful. Like the previous test, the Atat1^{cKO} mice showed a remarkable resilience to the presence of the clip, requiring

on average a period of time almost five times longer than that of the control group before behaviourally acknowledging the discomfort. It would also have been interesting to apply the clip test to other regions of the mice. For example, the pinching stimulus could be applied to the hairy skin just below the head of the mice. Moreover, other tests such as the Randall–Selitto test could have been carried out (Ranade *et al.*, 2014) to supplement the other high-threshold assays. Like, the von Frey test, the Randall –Selitto test gives a highly quantitative read-out allowing one to assess the gram force required to elicit a nocifensive response. The results of the von Frey and clip test assays extends the phenotype of our Atat1 knock-out into the nociceptive range and therefore beyond the scope of any previously described mechanosensitive phenotype in a transgenic mouse line. It is important to again here note that this extremely strong phenotype is observed using a genetic knock-out mouse line which still has Atat1 expression in approximately 25% of the DRG (and therefore the afferents) which detect noxious mechanical stimuli (Zurborg *et al.*, 2011).

4.2.3 No differences in thermal sensitivity were observed between the genotypes

We decided to investigate whether or not acetylated microtubules play a role in the detection of noxious hot and cold stimuli. To ascertain the animal's sensitivity to noxious heat we conducted two tests: (1) a hot plate assay and (2) a tail immersion test. In both cases the tests were run across a range of temperatures, all of which were in the noxious range. In both the hot plate and tail immersion assays no clear differences in the latency to response were observed between the $Atat1^{Control}$ and $Atat1^{cKO}$ mice across all temperatures. With regard to these thermal sensitivity tests, it would also have been interesting to carry out a Hargreaves' test which uses an infrared laser to stimulate the plantar surface of the animal's hind-paw(s) and therefore avoids mechanically stimulating the skin.

Our results indicate that the acetylation of microtubules *via* Atat1 is not necessary for the detection of heat-based noxious stimuli. Similarly, in the case of noxious cold, the 'acetone drop test' revealed no differences between the genotypes of mice in their behavioural responses to evaporative cooling. One limitation of the acetone drop test however is that one cannot be sure how much of a stimulus is

being applied to each animal's paw. As the acetone is 'squirted' towards the plantar paw surface the liquid often spreads over a wider area of the mouse's skin, thereby generating a stronger response stimulus. However, like our noxious heat experiments, this result indicates that acetylated microtubules are not required for the detection of noxious cold. We can therefore assume that whatever mechanism is active in allowing temperature sensitive ion channels to function does not require the input of acetylated microtubules.

4.2.4 Proprioceptive testing revealed no differences between the genotypes

If touch or mechanosensation provides an organism with a picture of its external environment, then proprioception can be thought of as mechanosensory modality which gives the organism a picture of its body orientation (or self), within that environment. Interestingly, recent work has shown that the important mechanosensitive ion channel Piezo2 is (Coste *et al.*, 2012) present on proprioceptive end organs associated with sensory muscle afferents in mice (Woo *et al.*, 2015). Moreover, knocking-out Piezo2 from these afferents leads to a severe deficit in locomotion in mice (Woo *et al.*, 2015). In light of these findings, as well as the general interest in Piezo2 in the field of mechanosensory biology, we decided to analyse the proprioceptive capacity of our $Atat1^{Control}$ and $Atat1^{cKO}$ mice. We undertook two assays to assess both the general locomotion (rotarod) and finer proprioceptive capacity (grid test) of the $Atat1^{cKO}$ mice but for both tests we found no statistically significant differences between the two genotypes of mice. In light of these results we concluded that there is no effect on proprioception in mice as a result of knocking-out the Atat1 enzyme in the PNS. For the sake of completeness, it is worth noting that Piezo2-linked deficits in proprioception are associated with visually obvious changes in the movement of mice (Woo *et al.*, 2015). We did not observe such obvious visual deficits in the movement of our $Atat1^{cKO}$ animals, relative to controls. However, previous work by others has shown using promoters which drive Cre expression to knock-out Piezo 2 at different stages of development, that the earlier Piezo2 is knocked-out, the stronger the proprioceptive deficit observed (Woo *et al.*, 2015). As the Advillin promoter only becomes active

around birth (Zurborg *et al.*, 2011), one might assume that another sensory system (such as vision) masks any deficit, as indeed is the case in humans (Chesler *et al.*, 2016). However, experiments (not shown) using the so-called Deleter-Cre germline Atat1^{KO} mice in which Atat1 is removed from all tissues early in their development revealed no deficit in locomotion during the rotarod test relative to control animals (Morley *et al.*, 2016). Thus, it can be confidently asserted that a loss of Atat1 mediated microtubule acetylation does not result in proprioceptive deficiencies.

Note: A detailed electrophysiological evaluation of both the mechanosensory fibres in the skin and the sensitivity of individual DRG neurons to mechanical stimuli was also undertaken. These experiments, which appear in the published version of this work which is located in the appendix of this thesis fully complement the touch insensitivity phenotype observed in these behavioral experiments. Briefly, skin-nerve analysis revealed a touch insensitivity in both low-threshold (paper figure 2a-f) and high-threshold (paper figure 3a-d) mechanically sensitive fibres located in skin samples taken Atat1^{cKO} animals relative to controls. Moreover, single cell electrophysiology experiments demonstrated that individual DRG neurons derived from Atat1^{cKO} animals are less sensitive to mechanical manipulation than their wild-type counterparts (paper figure 5a-d). Finally, it was also demonstrated that a single amino acid substitution in the tubulin protein restored mechanical sensitivity to Atat^{cKO} derived dissociated DRG (paper figure 5f). This so-called 'rescue experiment' was again utilized later in the study and therefore the results are included below, along with a discussion of their meaning.

4.2.5 Mechanosensitivity was restored by genetically mimicking Atat1 activity

We assessed whether or not the reduction in the number of mechanosensitive neurons exhibited by cultured DRG from Atat1^{cKO} mice could be rescued by transfecting cells with exogenous Atat1 cDNA. We first transfected Atat1^{cKO} -derived DRG neurons with an Atat1-YFP construct by electroporation. Transfected Atat1^{cKO} neurons exhibited a full restoration to control levels of mechanical currents (figure 10.2. a). Next, we transfected Atat1^{cKO} DRG neurons with a catalytically

inactive form of Atat1 (Atat1-GGL) (Kalebic *et al.*, 2013). In this case, mechanosensitivity was not restored to transfected DRG when compared to mock transfections using EGFP (figure 10.2. a). Next, we assessed whether the acetylation of Atat1 of the K40 residue of α-tubulin is vital for mechanosensitivity. To achieve this, we transfected Atat1^{cKO} DRG with an α-tubulin construct harbouring a K40Q (lysine – glutamine) point mutation. The K40Q mimics the presence of the acetylated form of lysine and, upon transfection into the Atat1^{cKO} DRG neurons, restores mechanosensation to control levels. Conversely, a tubulin construct harbouring a K40R charge (lysine – arginine) conserving amino acid substitution, elicited no significant changes to the numbers of mechanosensitive DRG neurons when it was transfected into Atat1^{cKO} DRG neurons (figure 10.2. b). Numbers of DRG cells Atat1 transfection n = EGFP (26), Atat1 (20) and Atat1-GGL (19). Tubulin amino acid mimic n = EGFP (26), K40Q (21) and K40R (25).

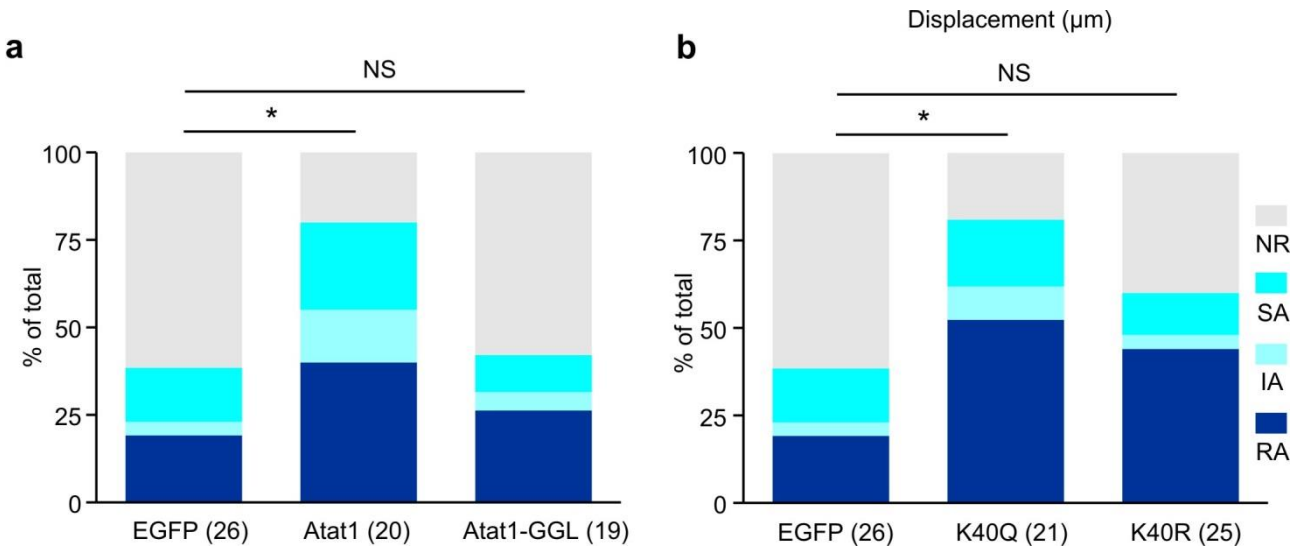


Figure 8.4. Whole cell patch-clamp recording from transfected Atat1^{cKO} DRG to detect restoration of mechanosensation. **(a)**, Stacked histograms showing the proportions of different mechanically-gated currents observed in Atat1^{cKO} DRG neurons transfected with either EGFP, Atat1-YFP or Atat1-GGL-YFP cDNA. Transfection of wild-type Atat1 rescued mechanosensitivity in the Atat1^{cKO} DRG neurons, whilst transfection with the catalytically inactive Atat1 (Atat1-GGL-YFP) failed to do so (χ^2 test, EGFP versus Atat1-YFP, $P<0.05$; EGFP versus Atat1-GGL-YFP, $P>0.05$). **(b)** Stacked histograms showing the proportions of the various mechanically-gated currents observed in Atat1^{cKO} DRG neurons transfected with *EGFP*, α-tubulin^{K40R}-IRES-YFP (*K40R*) or α-tubulin^{K40Q}-IRES-YFP (K40Q) cDNA. Transfection with the acetylated α-tubulin mimic (K40Q), but not the non-acetylatable α-tubulin mutant (K40R), restored mechanically-induced currents in Atat1^{cKO} DRG neurons (χ^2 test, EGFP versus K40Q, $P<0.05$; EGFP versus K40R, $P>0.05$). The number of neurons recorded is indicated in parentheses in each panel. Error bars indicate s.e.m.

4.2.6 Genetically mimicking Atat1 activity restored mechanosensitivity

We undertook experiments in cultured DRG neurons to assess the importance of the Atat1 enzyme, as well as its posttranslational modification of the lysine 40 target residue for mechanosensation. We did this through two separate transfection experiments. The first involved transfecting Atat1^{cKO} DRG neurons with a copy of the Atat1 enzyme labelled with a fluorescent marker. These neurons displayed a complete restoration to control levels of the proportion of DRG neurons capable of generating currents in response to mechanical stimulation. Furthermore, transfected Atat1^{cKO} DRG neurons with the so-called 'Atat1-GGL' copy of the enzyme. This version of Atat1 harbours three amino acid substitutions in the enzyme's active site, thereby rendering it incapable of acetylating the lysine 40 residue. In this instance, we did not see a restoration to control of the numbers of mechanically-sensitive DRG neurons. These experiments indicated that not only is Atat1 required for mechanosensation, but that it is required in the acetylated form, a finding which differs from previously discussed observations in *C. elegans* (Topalidou *et al.*, 2012). The second series of experiments was designed to assess whether or not Atat1's role in post-translationally modifying the lysine 40 residue of α-tubulin, is the critical requirement for normal mechanosensation. Once again, Atat1^{cKO} DRG neurons were transfected, but this time with an α-tubulin construct harbouring a single amino acid substitution glutamine, in the place of the Atat1 target lysine 40 residue (K40Q). Glutamine was chosen for its similarity in size and charge profile to the acetylated form of the lysine amino acid. Indeed, following transfection of this construct into Atat1^{cKO} DRG neurons the proportion of neurons capable of generating mechanically-induced currents was restored to wildtype levels. As a control for this, another α-tubulin construct, this time harbouring an arginine residue in place of the lysine residue (K40R), was also transfected into Atat1^{cKO} DRG neurons. Arginine was chosen due to its different structure, but similar charge, to the acetylated form of the lysine residue. In this case, no significant difference in mechanosensitivity were observed between Atat1^{cKO} and control DRG neurons following transfection with EGFP.

The results of the Atat1 and Atat1-GGL transfections revealed that an active form of the Atat1 enzyme is enough to re-establish normal mechanotransduction in Atat1^{cKO} DRG neurons. Moreover, the transfections with the α-tubulin amino acid mimic K40Q (and the negative control, K40R), revealed that replacing the lysine 40 residue with an amino acid which mimics the structure and charge of the acetylated form of this enzyme is enough to restore mechanosensation to Atat1^{cKO} DRG neurons. Therefore, we concluded that Atat1 is required for effective DRG neuron mechanotransduction and, more specifically, it is this enzyme's acetylation of the lysine 40 residue of α-tubulin which appears to be indispensable for this process.

In conclusion, Atat1^{cKO} mice are profoundly insensitive to mechanical touch and pain, while other peripherally encoded modalities such as thermosensation and proprioception remain unaltered in comparison to control animals. These findings in conjunction with supporting evidence from electrophysiology experiments reveal the broadest ever mechanoinsensitivity phenotype ever described in an animal model harbouring a single gene knock-out. This result points to a central role for acetylated microtubules in the detection of mechanical stimuli. A result which for the first time assigns a function to this PTM other than its previously recognised value as a useful immunohistochemical marker of neuronal tissue. Finally, we have also shown that a single amino acid substitution in the alpha tubulin protein is enough to rescue the Atat1^{cKO} mechanical sensitivity phenotype to control levels. Interestingly suggesting that the very strong Atat^{cKO} phenotype is being mediated by the absence of a post-translational modification to a single lysine amino acid located in the alpha tubulin protein of microtubules.

5 Chapter 5: Examining the structural and functional characteristics of the PNS

5.1 Aims: Examining the structural and functional characteristics of the PNS

In this section I will outline the results of experiments which were undertaken to systematically evaluate the structural and functional characteristics of a number of the various constituent parts of the PNS in Atat1^{Control} and Atat1^{cKO} derived tissues. The aim of these experiments was to ascertain whether any differences in the morphology or function of the various component parts of the PNS were apparent in the Atat1^{cKO} mouse background, thereby explaining the observed mechanoinsensitivite phenotype. For the sake of simplicity, the various experiments are listed in an order starting in the skin, proceeding then inwards towards the nerves, before finally reaching the level of the spinal cord. Furthermore, the methods and results sections are divided into those assays which deal specifically with the morphology / structure of the PNS versus those which measure the function of these structures.

5.2 Results

5.2.1 The structure of the PNS in skin / saphenous nerve was unaltered between genotypes

Using both SNAP-tag technology and EM we visualized the PNS in both skin sections and saphenous nerve tissue extracted from Atat1^{Control} and Atat1^{cKO} mice. There were no quantitative differences in the number or morphology of the mechanosensory end organs observed (outlined in yellow figures 11.0, a) in the skin (figures 11.0. a, b, c and d). Moreover, we did not observe any differences in the number or density of myelinated (yellow arrow figure 11.1 a) and unmyelinated fibres (red arrow figure 11.1b) in extracted saphenous nerve between the genotypes (figures 11.1. a, b, c and d). Number of follicles analysed n = Atat1^{Control} 14 and Atat1^{cKO} 14. Number of saphenous nerve sections analysed n = Atat1^{Control} 30 and Atat1^{cKO} 30.

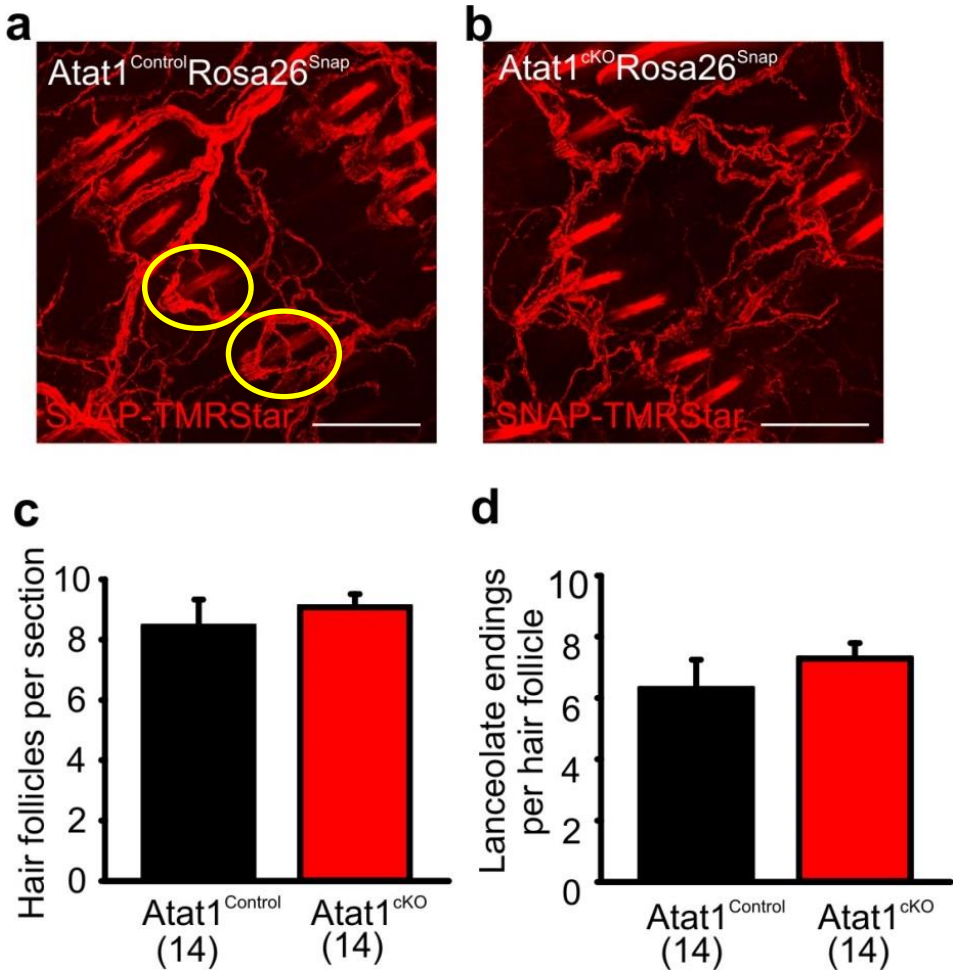


Figure 9.0. Analysis of peripheral nerve afferents / end organs in whole mount skin of Atat1^{Control} and Atat1^{cKO} animals (a and b), Fluorescent images of the peripheral sensory afferents in whole mount skin samples taken from the finger of Atat1^{Control}::SNAP ::CAAX **(a)** and Atat1^{cKO}SNAP::CAAX, lanceolate endings with their accompanying hair follicle are outlined in yellow. **(b)** mice labelled with SNAP-TMR Star (Scale bar 100μm). **(c and d)**, Bar-chart showing the number of innervated hair follicles **(c)** and lanceolate endings per hair follicle **(d)** in skin taken from the digits of Atat1^{Control}::Rosa26^{Snap} and Atat1^{cKO}::Rosa26^{Snap} animals. No significant differences were observed between the genotypes (Student's t-test, P>0.05). The number of skin images analysed is indicated in parentheses in each panel. Error bars indicate s.e.m.

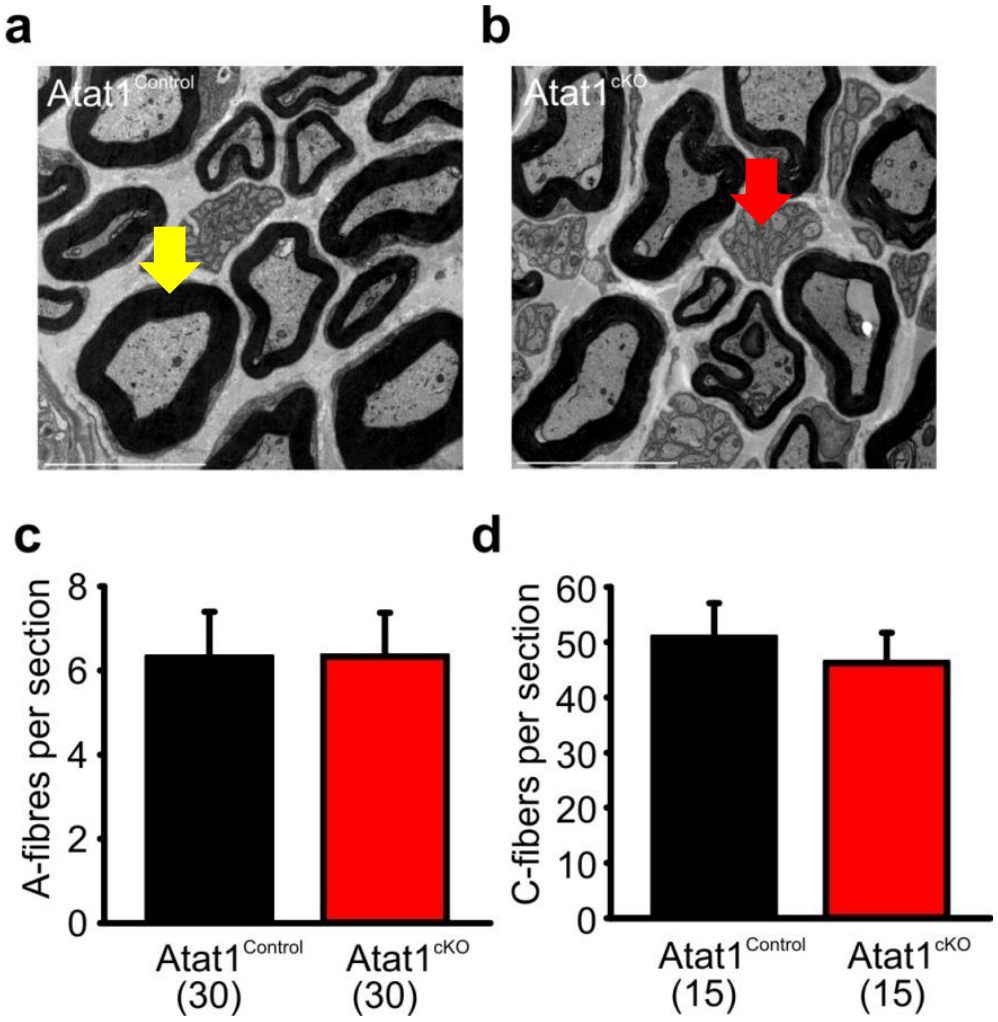


Figure 9.1. Electron microscopy images and analysis of saphenous nerve taken from Atat1^{Control} and Atat^{cKO} mice. **(a and b)**, Electron micrographs of a sectioned saphenous nerve from an Atat1^{Control} **(a)** and Atat1^{cKO} (myelinated fibre highlighted by yellow arrow). **(b)** mouse (Scale bar 5µm) (unmyelinated fibre highlighted by red arrow). **(c and d)**, Graphs showing the number of A type myelinated fibres **(c)** and unmyelinated C fibres **(d)** from saphenous nerve sections. No significant differences were noted between the genotypes of mice (Student's t-test, $P>0.05$). The number of images analysed is indicated in parenthesis in each panel. Error bars indicate s.e.m.

5.2.2 Axonal outgrowth length was unaltered between Atat1^{Control} and Atat1^{cKO} DRG

Wholemount *ex-vivo* DRG explants from Atat1^{Control} and Atat1^{cKO} mice were extracted and grown in DRG medium for one week in a matrigel matrix. To allow the axons time to develop, explants were allowed to grow for one week. The whole mount DRG appear as fluorescently labelled red 'spheres' (yellow arrow figure 11.2 a) at the centre of the image, while the axons appear as long meandering structures emanating from the DRG (blue arrow figure 11.2 a). No difference in axon length was observed between the mice genotypes (figures 11.2. a, b and c). Number of axons analysed n = Atat1^{Control} 127 and Atat1^{cKO} 157.

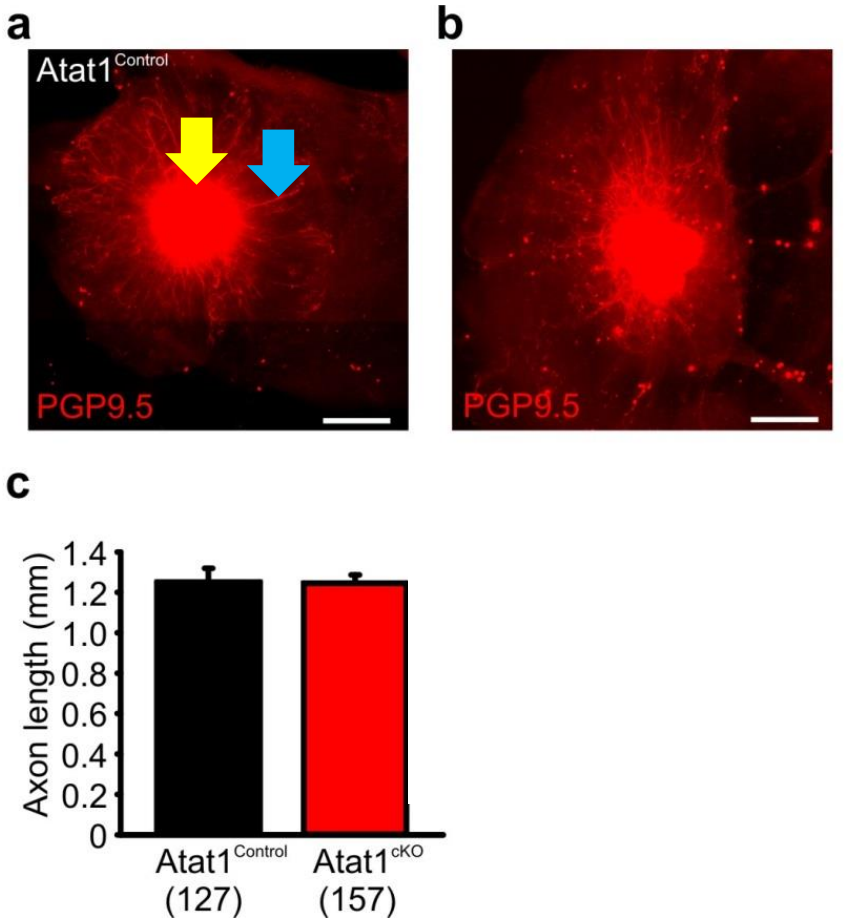


Figure 9.2. Mosaic images and analysis of axon outgrowth from whole mount DRG explants after 7 days in culture. **(a and b)**, Composite mosaic images of PGP9.5 labelled whole mount DRG after 7 days in culture from Atat1^{Control} **(a)** and Atat1^{cKO} (DRG yellow arrow and axonal outgrowth blue arrow) **(b)** mice (Scale bar 500μm). **(c)**, Bar-charts showing the length of axonal outgrowths in both groups after 7 days of culture. No significant difference was observed between the Atat1^{Control} and Atat1^{cKO} DRGs (Student's t-test, P >0.05). The number of axons analysed is indicated in parenthesis within the panel. Error bars indicate s.e.m.

5.2.3 The actin cytoskeleton appeared unaltered in DRG from both genotypes

To assess the general structure of the actin network in cultured DRG neurons we stained neurons with phalloidin. Once again, we did not detect any differences in the structure of the actin network between the genotypes (figures 11.3. a and b). The actin stain had a punctate appearance with no particular localisation bias within the DRG cell. Number of mice n = $Atat1^{Control}$ 2 and $Atat1^{cKO}$ 2.

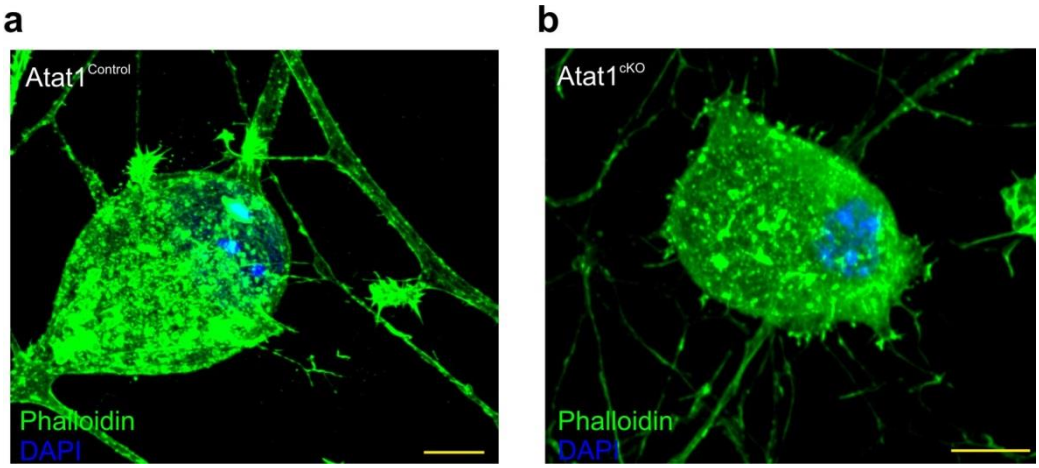


Figure 9.3. Cytoskeletal (actin) organization in DRG neurons derived from Atat1^{Control} and Atat1 ^{cKO} mice. (a), Confocal fluorescent image of a cultured Atat1^{Control} DRG neuron stained with phalloidin (green), which labels actin and Hoechst (blue) labels nuclei (Scale bar 10μm). **(b)**, Confocal fluorescent image of a cultured Atat1^{cKO} DRG neuron stained with phalloidin (green) and Hoechst (blue) (Scale bar 10μm). No differences were observed in the appearance / distribution of actin within DRG neurons between the genotypes.

5.2.4 Superresolution microscopy of α tubulin network in DRG neurons revealed no differences between the groups

To assess the structure of the microtubule architecture we carried out superresolution STORM microscopy of DRG neurons labelled with an anti-α-tubulin fluorophore. Our analysis of these images revealed a complex interwoven network of microtubules spanning the breath of the cell body (figures 11.4. a and b). Using a computational approach, we assessed a number of important tubulin architectural properties, namely, microtubule density, microtubule crossing points and the angular variance of the network. Strikingly, we found no differences between $Atat1^{Control}$ and $Atat1^{cKO}$ cells for any of the parameters analysed (figures 11.4. g, h and i). Number of DRG cells analysed n = $Atat1^{Control}$ 12 and $Atat1^{cKO}$ 11.

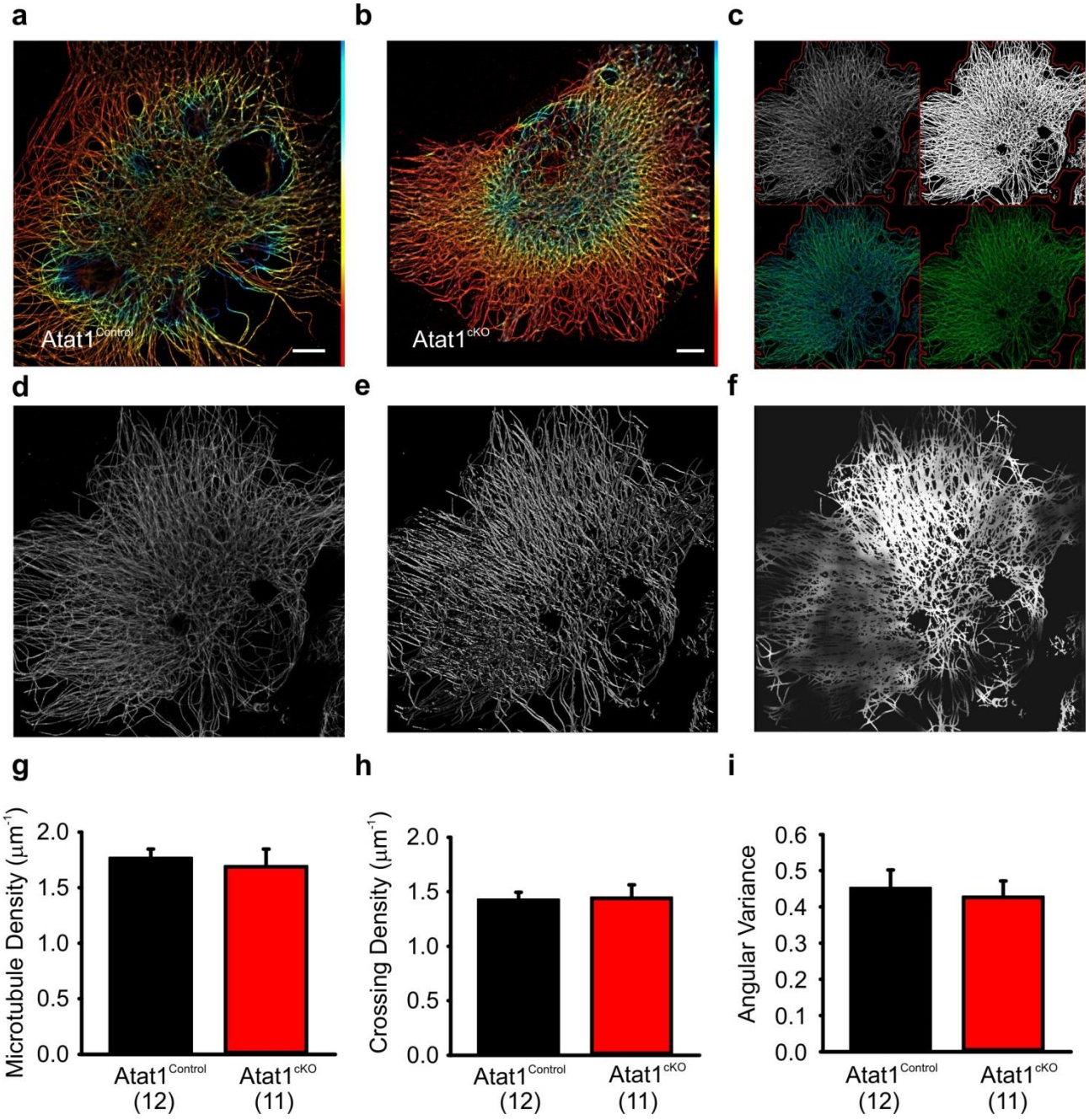


Figure 9.4. Superresolution imaging and analysis of the microtubule network of Atat1^{Control} and Atat^{cKO} –derived DRG neurons. (a and b), Superresolution image of anti α-tubulin staining of Atat1^{Control} (a) and Atat1^{cKO} (b) DRG neurons colour coded by depth (red colour represents nearer to the objective, Scale bar 5µm). (c) Image showing the stages of the automated analyses performed on superresolution images. The top left image shows the original image in grey, the red outline represents the automated area of cell selection. The top right image shows the microtubule image following binarization. The bottom left image shows the detected microtubule skeleton (in blue) overlaid on the microtubule superresolution image (in green); the microtubule skeleton was used to measure network length. The bottom right image is an estimation of the number of branch points present in the microtubule network, with microtubules in green and the

branch points marked in blue. (d-f), A series of images representing the automated analysis of the microtubule network angular variance. (d) Shows the microtubule superresolution image, (e) the automatically determined orientation of the microtubules, (f) the local angular variance of the microtubule orientation, where bright pixels denote a high variance. (g), Graph summarizing the density of the microtubule network within DRG neurons derived from $Atat1^{Control}$ and $Atat1^{cKO}$ mice. (h), Graph showing the density of microtubule crossing points present in the microtubule networks in the two mouse genotypes. (i), Graph summarizing the angular variance of the microtubule cytoskeleton in both $Atat1^{Control}$ and $Atat1^{cKO}$ cultured DRG neurons. No significant differences in any parameter were observed between the two mouse genotypes (Student's t-test, $P > 0.05$). The number of DRG neurons imaged is indicated in parenthesis in each panel. Error bars indicate s.e.m.

5.2.5 Spinal cord morphology was unaltered between the groups

Spinal cord sections from $Atat1^{Control}$ and $Atat1^{cKO}$ animals were stained with IB4 and CGRP respectively. No changes in the general localization of the respective staining was observed for any spinal cord region imaged between the groups. (figures 11.5. a and b). Number of spinal cords sections imaged and stained n = $Atat1^{Control}$ 12 and 12 $Atat1^{cKO}$.

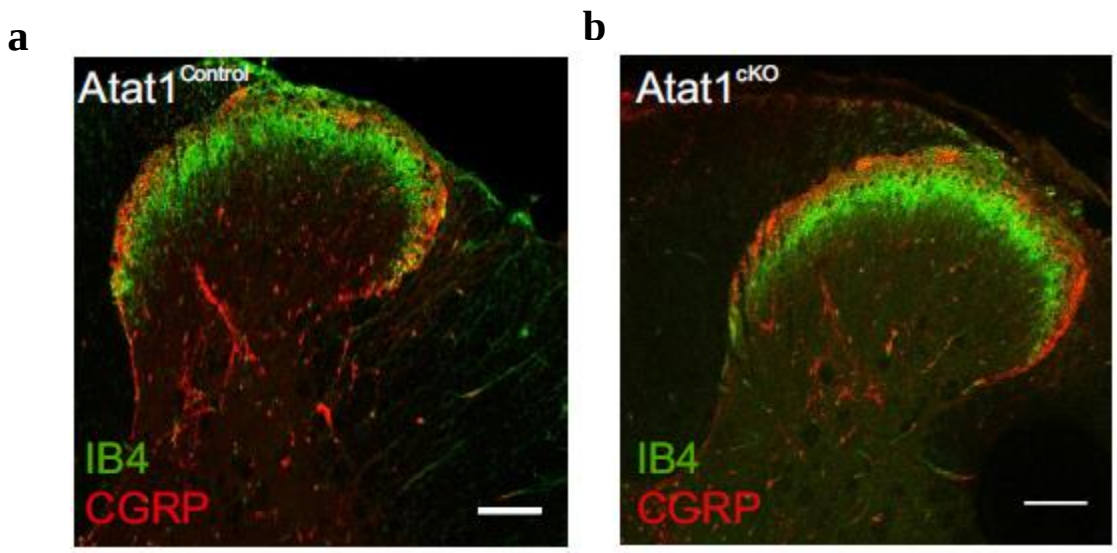


Figure 9.5. Representative images of spinal cord staining from Atat1^{Control} and Atat1^{cKO} mice. (a), Image of Atat1^{Control} sectioned spinal cord stained with IB4 (green) and CGRP (red). **(b)**, Image of Atat1^{cKO} sectioned spinal cord stained with IB4 (green) and CGRP (red). No differences in the distribution of the labelled regions was observed between the two mouse genotypes. n = 2 Atat1^{Control} and 2 Atat1^{cKO}.

5.2.6 Axonal Transport in DRG Neurons was not different between the genotypes

To measure axonal transport, DRG cells were cultured in specialized microfluidic devices which allowed for single particle imaging of retrograde transport using NGF labelled with quantum dots. No significant difference in the rate of retrograde axonal transport was observed between the $Atat1^{cKO}$ and $Atat1^{Control}$ samples respectively (figures 11.6. a, b and c). Number of mice from which DRG were extracted for analysis n = $Atat1^{Control}$ 2 and $Atat1^{cKO}$ 2.

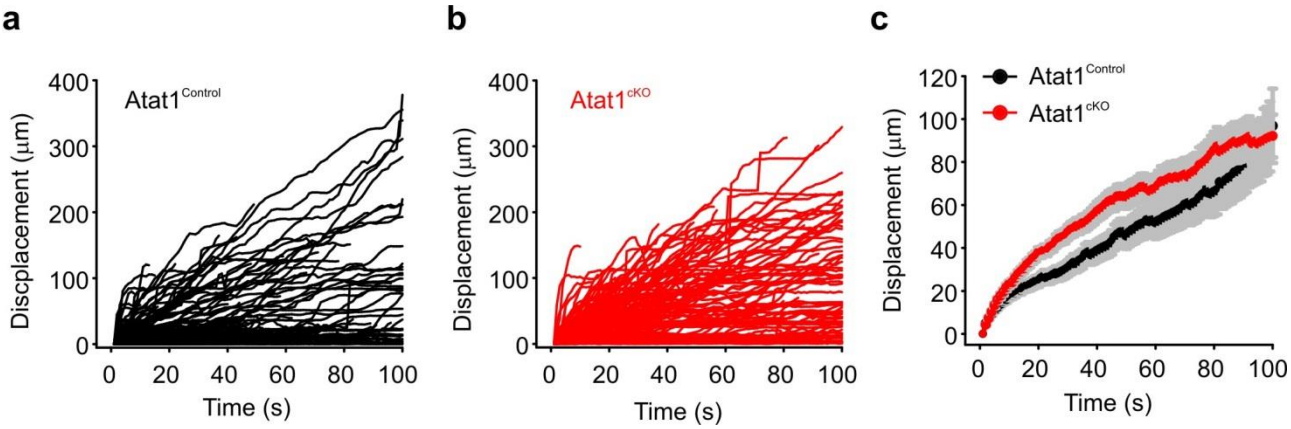


Figure 9.6. Single particle NGF/receptor complex axonal transport in Atat1^{Control} and Atat1^{cKO} DRG cells. (a and b), Graphical representations of single molecule tracking of NGF/receptor complexes along DRG neuronal axons of Atat1^{Control} **(a)** and Atat1^{cKO} mice **(b)** grown in microfluidic devices. **(c)**, Graph summarising the average velocity for NGF/receptor complexes labelled with quantum dots Atat1^{Control} and Atat1^{cKO} DRG. No significant difference in NGF/receptor complex transport was observed between the genotypes (Student's t-test, P >0.05). Error bars indicate s.e.m.

5.2.7 Fluorescence recovery after photobleaching (FRAP) analysis of Piezo2-GFP in transfected DRG neurons revealed no differences in membrane ion channel trafficking

Finally, for this series of experiments, we examined the FRAP dynamics of a Piezo2-GFP fusion protein in the membrane of transfected Atat1^{Control} and Atat1^{cKO} DRG neurons in order to determine the rate of diffusion of the channel into the membrane. Piezo2-GFP was utilized in order to facilitate the visualization of the localisation of the protein. No differences in the rate of recovery of the Piezo2-GFP fusion protein were observed following photobleaching between the transfected Atat1^{Control} and Atat1^{cKO} DRG neurons (figures 11.7 a and b). Number of DRG neurons analysed n = Atat1^{Control} 12 and Atat1^{cKO} 8.

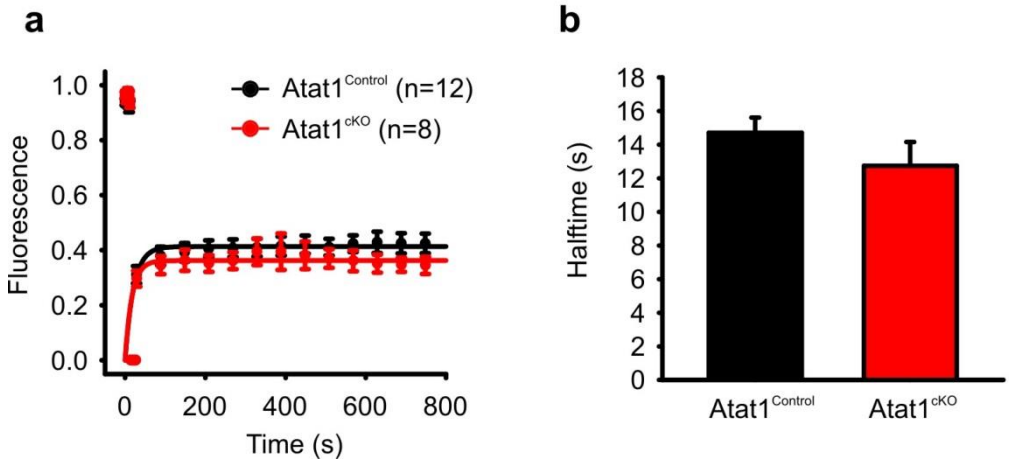


Figure 9.7. FRAP analysis of Piezo2-GFP in transfected Atat1^{Control} and Atat1 ^{cKO} DRG neurons. (a), Graph summarising the return of fluorescence over time of Piezo2-GFP following FRAP in Atat1^{Control} and Atat1^{cKO} DRG neurons. **(b)**, Graph showing the halftime of the return of fluorescence of Piezo2-GFP following FRAP. No differences were observed between the two genotypes (Student's t-test, $P>0.05$). The number of DRG neurons analysed is indicated in parenthesis in the panel. Error bars indicate s.e.m.

5.3 Discussion: Atat1^{cKO} mice show no alterations in gross PNS morphology / function relative to Atat1^{Control}

The reduction in mechanical sensitivity relative to controls observed in our Atat1^{cKO} mice might be due to structural changes in the PNS brought about as a result of knocking-out Atat1. As the skin is the primary surface upon which external mechanical forces are elicited (Lechner and Lewin, 2013), we first assessed the morphology / structure of the nerve fibres and their associated mechanical end organs in the skin. By utilising SNAP-tag technology we were able to fluorescently label the peripheral nerve fibres in whole mount *ex-vivo* hairy skin sections taken from the 'fingers' of Atat1^{Control} and Atat1^{cKO} mice. In both genotypes the analysis revealed a complex mesh of free-nerve fibres, as well as a multitude of afferents associated with distinctive mechanical end organs (specifically lanceolate endings) around hair follicles. However, an assessment of the prevalence and morphology of the distinctive lanceolate endings did not reveal any significant differences in the structure / number of these elements between the two mouse genotypes. Therefore, we concluded that as the gross morphology of the PNS at the level of the skin remains intact in Atat1^{cKO} mice, the reduced mechanical sensitivity of these animals is not due to a lack, or disruption, of these primary sensory appendages.

Following on from this, we assessed, using electron microscopy (EM), the numbers of myelinated and unmyelinated fibres in whole mount saphenous nerves extracted from Atat1^{Control} and Atat1^{cKO} mice. As stated in the Methods, we divided the fibres into myelinated (Aβ and Aδ) and non-myelinated (C-fibres). Taken together, these varying fibre types are responsible for conducting (almost) all of the cutaneous sensory evoked action potentials encoded for by the PNS. Again however, we did not uncover any differences in the numbers of these fibres between the genotypes, suggesting that the 'hardware' involved in carrying electrical signals between the periphery and the cells of the DRG remains intact in Atat1^{cKO} mice.

Having evaluated the other elements of the PNS from the skin inwards we finally arrived at the spinal cord. This complex structure marks the bridging point between the true PNS and the CNS of vertebrates. When cross-sectioned, the structure of the spinal cord can be divided into grey and white matter. The 'butterfly' like appearance of a cross-sectioned spinal cord can be neatly divided into the dorsal and ventral horns. Mechanosensitive afferents synapse with cells mainly located in the dorsal horn region at defined layers or laminae (figure 5). We therefore utilized antibodies which label cells within these laminae in order to comparatively assess the morphology of lumbar spinal cord regions extracted from Atat1 ^{Control} and Atat1^{cKO} mice. In our case we used CGRP and IB4 which mark laminae I and II of the dorsal horn. However, when comparisons of the relative positions and areas labelled by the antibodies between the two mice genotypes we were unable to see any significant differences between them.

To complete our evaluation of the 'structural' characteristics of the PNS we next assessed if the growth rate of axons differed between *ex-vivo* whole mount DRG explants taken from Atat1^{Control} and Atat1^{cKO} mice. Once again however, we did not observe any significant differences in the length of axons between the two mouse genotypes and as such we were able to conclude that the growth rate of axons was not perturbed by knocking-out Atat1 in the PNS.

It is perhaps worth nothing here that a number of the assays we utilised are somewhat redundant, in the sense that they essentially measure the same parameter in a different way. For example, if axon outgrowth were affected one would also expect to see changes in the structure of the PNS in the skin, as well as probable changes in the fibre number as detected by EM imaging of the saphenous nerve. As all of these assays did not reveal any significant differences in morphology between the control and knockout mice, they provide a strong interlinking array of evidence to support our overall conclusion that the mechanoinsensitivity phenotype is not the result of PNS structural deficits in the Atat1^{cKO}. With this in mind, I will now turn my attention to addressing microtubule transport within cultured sensory neurons as a potential explanation for the deficit.

The effect of microtubule PTMs on transport has been discussed in the literature (Nirschl *et al.*, 2016). To assess the potential role of microtubule lysine 40 acetylation on transport we examined trafficking of NGF bound via a biotin-streptavidin linker to a quantum dot (QD), which allows for single particle tracking. This assay was carried out using a microfluidic device, which allowed for precision control over the liquid level and hence the direction of flow of medium within the platform. By tracking the rate of motion of the single brightly fluorescent quantum dots it was possible to assess the rate of microtubule transport in both $Atat1^{Control}$ and $Atat1^{cKO}$ derived DRG neurons. However, as with our other previously discussed assays, we did not witness any significant differences between the two genotypes of microtubule-dependent transport of the NGF-QD complexes. This was perhaps not too surprising given the results of our previous assays such as the whole mount axonal outgrowth measurements, as well as the lack of structural differences in the appearance of the PNS fibres and end-organs in the skin. Nonetheless, given the central role of microtubules in the transport of materials within cells, a role which is essential in the PNS due to the long lengths of the axonal projections emanating from DRG neurons to the skin; it was necessary to explore transport as a potential mechanism / cause of the $Atat1^{cKO}$ phenotype.

Sticking closely with the above assessment of microtubule transport we next assessed the diffusion of Piezo2-GFP into the membrane of DRG neurons following Fluorescence Recovery After Photobleaching (FRAP). By choosing healthy transfected cells and selectively subjecting an area of defined size in their GFP-labelled membranes to a discreet high energy blast of light, we were able to observe a strong 'post bleach' drop in GFP fluorescence in that area. Then, by tracking the return of GFP fluorescence to that region we were able to calculate the 'halftime' value for the re-establishment of fluorescence, thus measuring the diffusion rate of proteins into the membrane of these cells. Again, no differences were observed in the rate of diffusion between the mouse genotypes. The lack of any difference in time taken for this important fluorescently labelled ion channel to return to the membrane indicates that the rate of ion channel turnover is not different, and therefore the

reduced mechnosensitivity of the Atat1^{cKO} mice is unlikely to be due to deficits in membrane trafficking and integration of ion channels in the cell membranes of these mice. However, given the low level of transfection efficiency achieved in this study it would be advantageous to utilize the Piezo-2::GFP mouse line to repeat these experiments (Ranade *et al.*, 2014).

As our search for the potential deficit(s) that underlie the observed phenotype progressed, it was striking that we did not observe any deficits in the gross morphology of the PNS (skin, DRG cell populations, spinal cord morphology and axonal growth), as well as in the rate of microtubule mediated transport / diffusion of materials within DRG neurons of the Atat1^{cKO} mice relative to controls. Because of this we subsequently decided to focus our attention upon the architectural and morphological properties of cytoskeletal components within somatosensory neurons.

Although Atat1 selectively targets microtubules, actin filaments are also a central component of the cytoskeleton of cells. We therefore assessed the morphology of the actin cytoskeleton in Atat1 ^{Control} and Atat1^{cKO} cultured DRG neurons. The images we obtained did not exhibit any differences in the arrangement or distribution of actin between the control and Atat1^{cKO} neurons.

Importantly, very recent work using superresolution microscopy by (D'Este *et al.,* 2016) has demonstrated that all neuronal cells demonstrate a filamentous type network of actin which is laid down within the axons of these cells in a periodically repeating 'ring like' appearance. Unfortunately, we were unable to observe such detail using conventional confocal microscopy. Nevertheless, what we were able to observe did not different between the two mouse genotypes, which suggests to us that deficits in the actin network of Atat1^{cKO}- derived cells are not important / causative with respect to the mechanoinsensitivity phenotype of Atat1^{cKO} mice.

We next turned our attention to the microtubule network within DRG neurons. In this instance, we utilised superresolution dSTORM microscopy to visualise the architecture of this network in great detail. By staining cells with an anti-α tubulin antibody we were able to see the microtubule network

of at the base of each DRG neuron, where the cell membrane contacted the surface of the glass coverslip upon which they were cultured. Despite dSTORM imaging limiting our view of the cytoskeleton to the sub-membrane region of the cell, we reasoned that due to the proximity of the cytoskeleton in this region to the membrane (which after all harbours the mechanosensitive ion channels), that any structural differences observed in the microtubule network here could have a profound influence on mechanosensitive ion channel activity. The images obtained were analysed using a series of computational approaches, owing to the complexity of the network observed. The three parameters evaluated were microtubule density, crossing density and angular variance. For all of the parameters tested no differences were observed between the genotypes. The finding that the microtubule network is not compromised in Atat1^{cKO} relative to controls indicates that the likelihood that any associations which might exist between these proteins and mechanosensitive ion channels and / or the membrane are not affected by knocking-out Atat1.

In conclusion, we found no differences at any level of the PNS that we investigated in terms of both structure and function. This is in contrast with work in the nematode *C. elegans* which had severe structural deficits in nerves associated with the detection of mechanical stimuli (Topalidou *et al.*, 2012). We therefore decided to examine the distribution of acetylated microtubules in DRG neurons to try and identify a mechanism for this phenotype.

6 Chapter 6: Examining the role of Atat1 in regulating the membrane rigidity of DRG neurons

6.1 Aims: Examining the role of Atat1 in regulating the membrane rigidity of DRG neurons

Here I will outline and discuss the results of experiments which aimed to examine the distribution and localisation of acetylated microtubules in DRG neurons and mouse embryonic fibroblast (MEF) cells. This series of experiments was also undertaken to assess the membrane rigidity of Atat1 ^{Control} and Atat1^{cKO} DRG neurons using Atomic Force Microscopy, as well as other biophysical assays.

6.2 Results

6.2.0 Acetylated tubulin has a sub-membrane localization in DRG neurons

The distribution of acetylated microtubules in sensory neurons was investigated by staining cells with an anti-acetylated-α-tubulin antibody. These experiments revealed the presence of a prominent band of acetylated microtubules located just below the membrane in 80±5% of neurons (n = 3 animals) (figure 12.0 a). In contrast, staining cells with the anti-α-tubulin antibody revealed a much more heterogeneous distribution (figure 12.0. b). We did not however observe a similar submembrane localisation of acetylated tubulin in MEFs (n = 2 vials of MEFs), which are non-mechanosensitive cells, whilst the pattern of α-tubulin distribution in the fibroblasts was similar to that seen in the DRG neurons (figure 12.0. c and d)

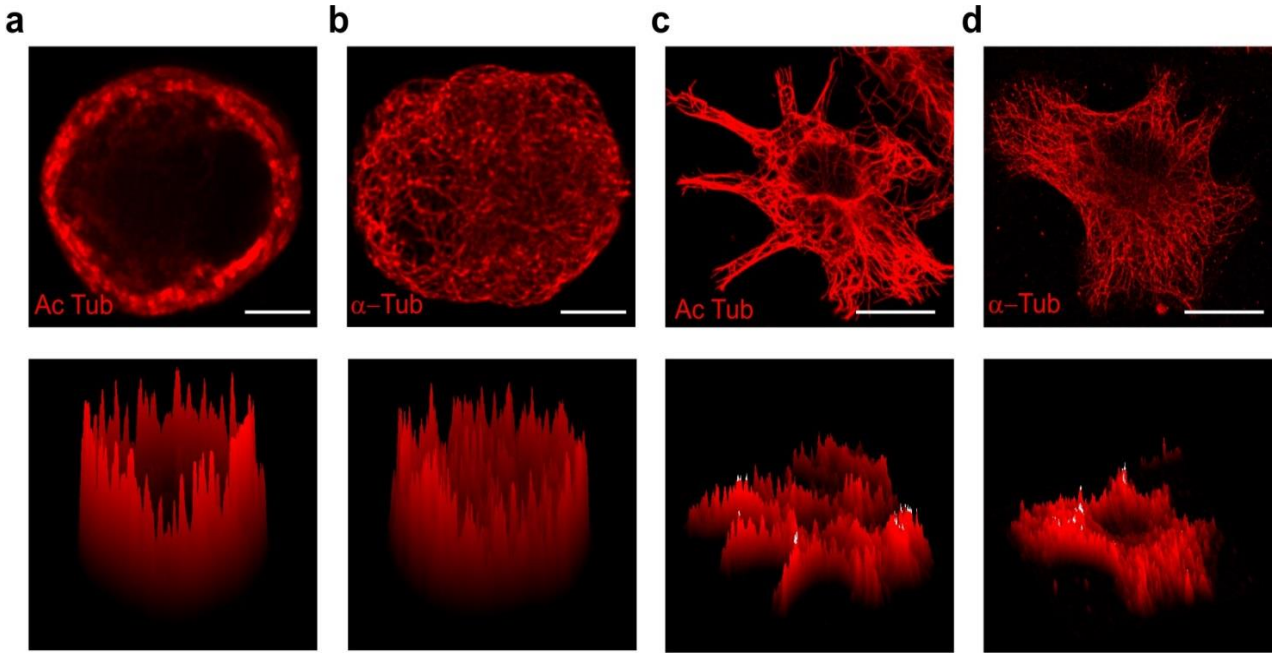


Figure 10.0. Staining and analysis of the distribution of acetylated and non-acetylated α tubulin in Atat1^{Control} DRG neurons and MEFs. (a), Anti-acetylated-α-tubulin staining of Atat1^{Control} cultured DRG neurons (corresponding surface plot below). Note the prominent sub-membrane localisation of acetylated tubulin (Scale bar 5µm). **(b),** Anti α-tubulin staining of Atat1^{Control} cultured DRG neurons (Scale bar 5µm) with the corresponding surface plot below **(c),** Anti-acetylated-α-tubulin staining of Atat1^{Control} MEFs (Scale bar 20µm) with the corresponding surface plot below. Note the even distribution of acetylated tubulin in this cell type relative to the DRG neurons. **(d)** Anti α-tubulin staining of Atat1^{Control} MEFs (Scale bar 20µm) with the respective surface plot below. n = 3 Atat1^{Control} and 2 MEFs stainings with acetylated tubulin and α tubulin.

6.2.1 Acetylated microtubules have a sub-membrane localization in corneal peripheral afferents

We observed a strong localisation of acetylated microtubules at the tips of mechanosensory fibres in the cornea (figure 12.1. a). Corneal tissue was used instead of skin, as the antibodies utilized were not compatible with skin tissue. Note the high level of co-localisation (yellow) between the acetylated microtubule stain in green and the membrane localised SNAP substrate dye in red.

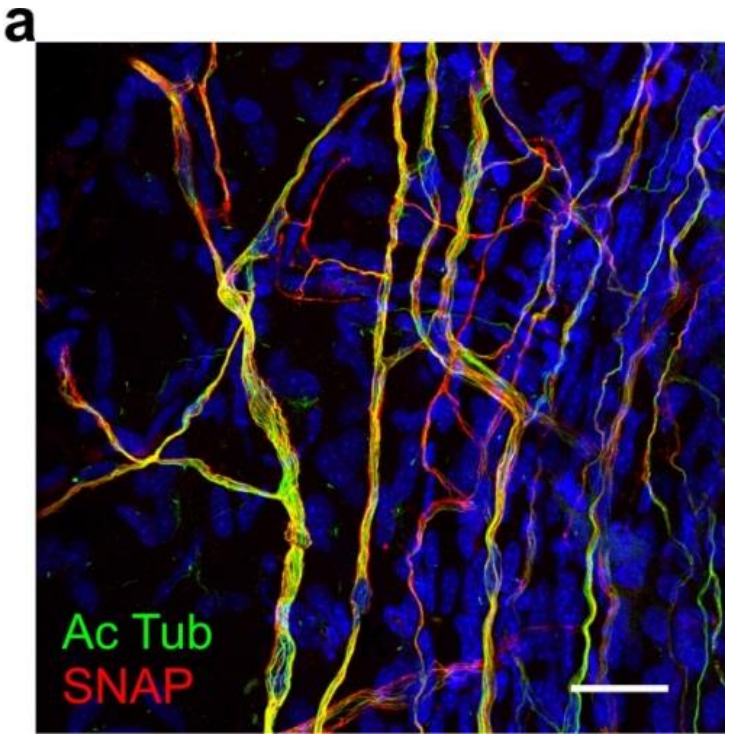


Figure 10.1. **Representative confocal fluorescence image of sensory afferents immunohistochemically labelled for SNAP and acetylated tubulin**. **(a),** Fluorescent image of sensory nerve fibres in a whole mount corneal preparation from an Avil-Cre::SNAP::CAAX mouse. Acetylated tubulin is labelled green and membrane bound SNAP staining is labelled red (Scale bar 30μm). Note the strong co-localisation of signals. n = 2 $Atat1^{Control}$ and 2 $Atat1^{cKO}$.

6.2.2 Acetylated microtubules have a sub-membrane localization in saphenous nerve tissue

Following on from this we looked at the distribution of acetylated microtubules in nerve fibre tissue taken from the PNS. Here, we clearly observed a strong membrane localisation of acetylated microtubules below the myelin sheath of these fibres (figure 12.2. a).

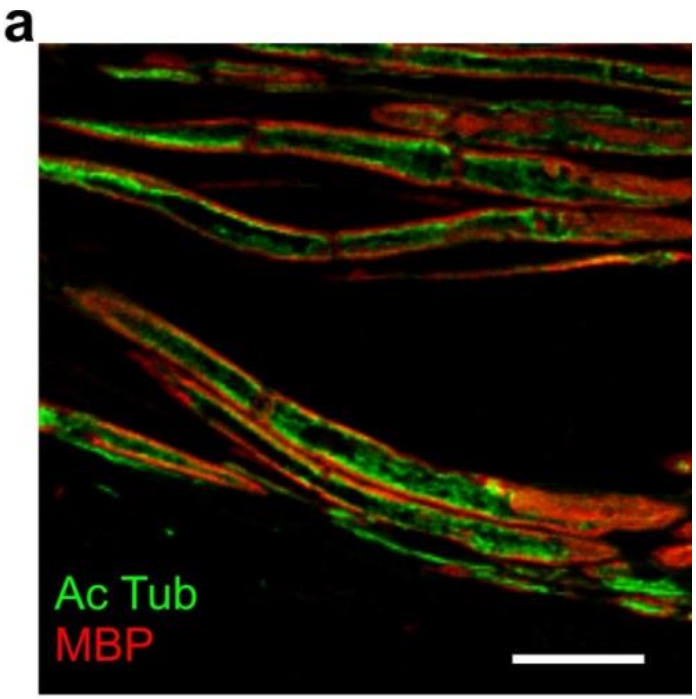


Figure 10.2. **Staining of Atat1 ^{Control} saphenous nerve with anti-acetylated tubulin and myelin basic protein (a)**, Immunohistochemical staining of nerve fibres within the saphenous nerve taken from Atat1^{Control} mice. Anti-acetylated-α-tubulin staining (green) and myelin basic protein (MBP) (red) (Scale bar 10μm). Note the sub-membrane localisation of the anti-acetylated tubulin signal. n = 2 Atat1^{Control} mice.

6.2.3 Atat1^{cKO} DRG neurons have stiffer membranes relative to control cells

Given the submembrane localisation of the acetylated tubulin ring that we found to be present in the vast majority of DRG neurons that we examined, we next assessed whether or not the absence of this structure in Atat1^{cKO} DRG neurons might alter membrane rigidity and thus influence mechanosensitive channel gating. To achieve this, we utilized atomic force microscopy (AFM) to analyse the membrane rigidity of cultured Atat1^{Control} and Atat1^{cKO} - derived DRG neurons. In these studies, we found that the membrane stiffness, which was measured as the force required to indent the membrane, of Atat1^{cKO} neurons was significantly greater than that of control cells across the entire range of different distances tested (i.e. 200, 400 and 600nm) (figure 12.3. a). Number of DRG neurons analysed n = Atat1^{Control} 54 and Atat1^{cKO} 74.

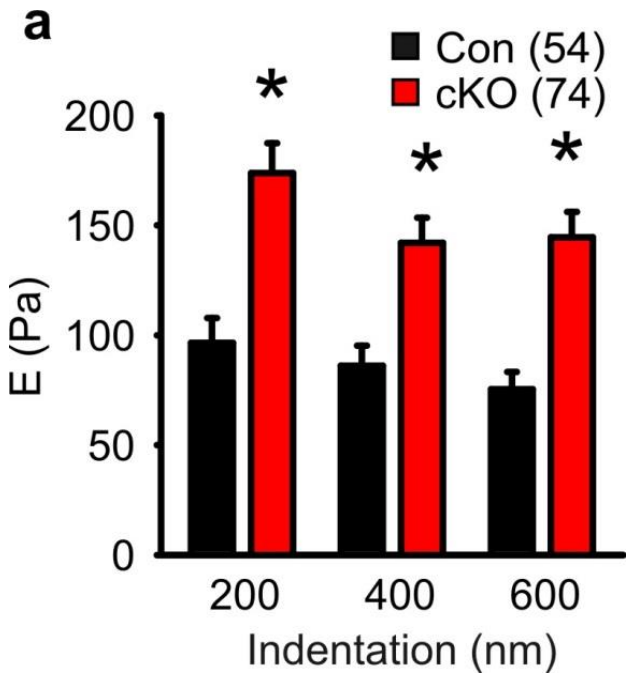


Figure 10.3. Graph summarising AFM results measuring the pressure required to indent the membranes of Atat1^{Control} and Atat1^{cKO} DRG neurons to specific degrees. (a), Quantitative comparison of Young's modulus obtained by fitting force-indentation curves with the Hertz-Sneddon model at different extents of indentations for cultured DRG neurons taken from Atat1^{Control} and Atat1^{cKO} mice. A significantly greater pressure was required to indent the membranes of Atat1^{cKO} neurons relative to that required for Atat1^{Control} –derived DRG neurons (Mann-Whitney test, $P<0.01$). The number of DRG neurons analysed is indicated in parenthesis in the panel. Error bars indicate s.e.m.

6.2.4 Atat1^{cKO} DRG afferents and internal microtubule networks exhibit greater resistence to shrinking than their Atat1^{Control} counterparts

We supplemented these data with a study investigating the effect(s) applying a series of hyperosmotic shocks to cultured DRG neurons. The rationale underlying these assays is that as cellular shrinkage can be induced by applying a hypertonic solution to the outside of cells (due to osmosis), we could determine if the magnitude of shrinkage of DRG neurons differed between those derived from control and transgenic mice. This would thus provide a proxy measure of membrane stiffness.

The axons emanating from Atat1^{cKO} DRG cells showed a stark decrease in shrinkage when compared to Atat1^{Control} cells. This 'increased rigidity' was successfully restored to control levels by transfecting Atat1^{cKO} cells with the aforementioned K40Q mimic (figure 12.4.a). Finally, we assessed the degree of microtubule network compression in live imaging experiments following hyperosmotic shock. When we analysed the fluorescence density of segmented regions of the SIR-Tubulin 2-labelled microtubule network within cells both before and after shrinking (figure 12.4. b), we observed a significant decrease in compression in Atat1^{cKO} neurons with respect to the Atat1^{Control} DRG neurons. Again this drop in compression could be restored to control levels by transfecting cells with the K40Q mimic (figure 12.4. c). Numbers of cells Calcein n = Atat1^{Control} 19, Atat1^{cKO} 17 and K40Q 13. Tubulin amino acid mimic Atat1^{Control} 9, Atat1^{cKO} and K40Q 8.

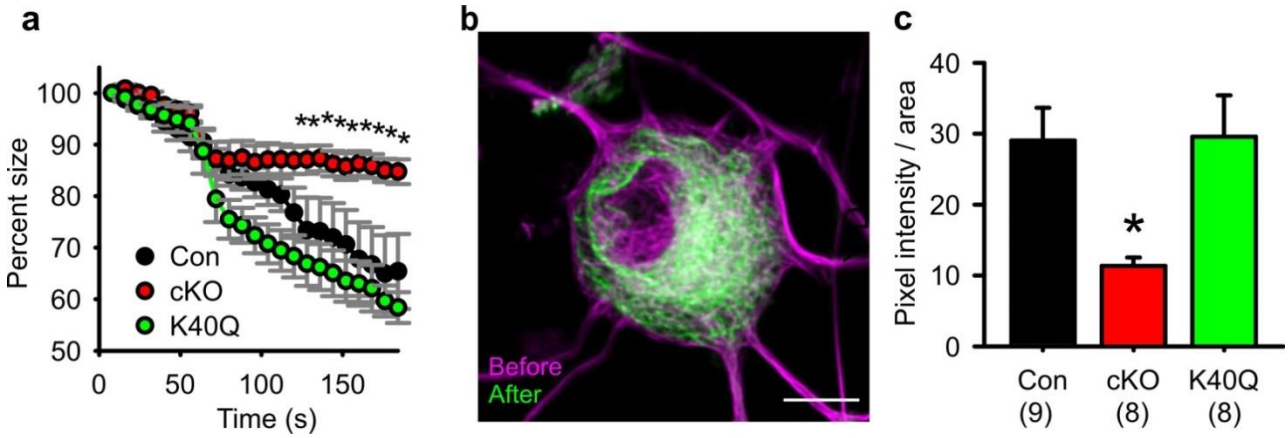


Figure 10.4. **Axonal shrinking / microtubule network density following hyperosmotic shock of Atat1^{Control} , Atat1^{cKO} and Atat1^{cKO} with the K40Q amino acid mimic**. **(a)**, Graph showing the relative shrinkage of axons emanating from Atat1^{Control} and Atat1^{cKO} DRG neurons loaded with calcein (2μM) in response to a hyperosmotic shock stimulus over time. Deletion of Atat1 leads to a significant decrease in the percentage of shrinkage of Atat1^{cKO} axons relative to that seen in control neurons (ANOVA on ranks, multiple comparison Dunn's Method, P<0.05). Note the return to control levels of shrinkage in Atat1^{cKO} DRG neurons following transfection with the K40Q tubulin amino acid mimic **(b)**, Representative image of a cultured DRG neuron showing an overlay of SiR Tubulin2-labelled microtubules before (purple) and after (green) hyperosmotic shock. Note the obvious compression of the microtubule cytoskeleton after shrinking (Scale bar 10μm). **(c)**, Bar-chart summarising osmotically-induced microtubule compression in DRG neurons from Atat1^{Control}, Atat1^{cKO}, and Atat1^{cKO} animals transfected with tubulin-K40Q. There is significantly less compression in Atat1^{cKO} than Atat1^{Control} neurons, which is rescued by transfection of tubulin-K40Q (ANOVA on ranks, multiple comparison Dunn's Method, P<0.05). The number of DRG neurons analysed is indicated in parenthesis in the panel Error bars indicate s.e.m.

6.3 Discussion: Atat1 is essential for regulating the membrane rigidity of DRG and their associated afferents

By using a novel fixation protocol (Prager-Khoutorsky, Khoutorsky and Bourque, 2014) utilising a cytoskeleton buffer in conjunction with an anti-acetylated tubulin antibody we were able to, for first time, visualise the localisation of acetylated microtubules within the soma of cultured DRG neurons. The images that were acquired from $Atat1^{Control}$ cells showed a prominent band of acetylated microtubules in a 'ring' like conformation running beneath the membrane of these cells. Previous experiments using methanol fixation of DRG neurons (Bulinski, Richards and Piperno, 1988) carried out to look at the distribution of acetylated microtubules within DRG neurons had only revealed a blurred distribution within the soma of these neurons without notable localisation to any particular area of the cell. Our fixation protocol also recapitulated the strong axonal staining which had already been described in DRG neurons and other neurons previously (Sudo and Baas, 2010). The use of surface plots to visualise the distribution of fluorescence within the soma of DRG neurons allowed us to confirm via a separate analytical methodology the sub-membrane distribution of the acetylated microtubules. In separate experiments conducted to assess the distribution of non-acetylated α-tubulin within DRG neurons, using the same fixation protocol, a cell wide distribution of the microtubule network was observed and was supported when viewed as a surface plot distribution within DRG neuronal somata. Conversely, in cultured DRG neurons derived from $Atat1^{cKO}$ mice we did not see any evidence of the type of acetylated microtubule 'ring' structure described in the control neurons., whilst still observing the same type of cell wide distribution of a-tubulin we saw in $Atat1^{Control}$ DRG neurons. In order to assess the distribution of both acetylated and non-acetylated α-tubulin in a non-mechanosensitive cell type Mouse Embryonic Fibroblasts (MEFs) derived from $Atat1^{Control}$ mice were stained with the anti-acetylated and anti α-tubulin antibodies. In contrast to DRG neurons the anti-acetylated staining in control MEFs did not reveal a sub-membranous localisation and, instead, showed a cell wide distribution. Likewise, the distribution of the anti α-tubulin stain showed no clear

localisation bias with a cell-wide distribution that was similar to that seen in DRG neurons. Surface plots generated from the immunolabelling of MEFs revealed a wide distribution for both antibodies, highlighting a profound structural difference between DRG neurons and MEFs with respect to the localisation of acetylated microtubules in these two cell types.

Having observed this strong sub-membrane distribution of acetylated microtubules in the soma of Atat1^{Control} DRG neurons we next assessed the arrangement of this form of tubulin in the afferents emanating from DRG neurons.

In saphenous nerve, Myelin Basic Protein (MBP) was used to mark the myelin sheath which coats the exterior of large fibre myelinated afferents. The MBP labelling served as a landmark for the myelin-membrane boundary. A strong staining of acetylated microtubules was also observed just below this point in the tissue.

A similar picture emerged with our labelling of the cornea, which is innervated by unmyelinated C fibres and myelinated Aδ fibres (MacIver and Tanelian, 1993). The genetically-encoded SNAP motif which resides on the inner leaflet of the plasma membrane, was used to mark the membrane of these afferents. Like the results from the saphenous nerve, the afferents of the cornea exhibited a strong staining for acetylated microtubules. However, given that these images were acquired using conventional confocal microscopy, it would be prudent to undertake superresolution microscopy in order to characterise the distribution of the acetylated microtubules within these structures at a higher resolution. That being said, the distribution of the acetylated microtubules just below the membrane of Atat1^{Control} DRG neurons, coupled with the apparent sub-membrane localisation in the afferents emanating from other DRG neurons was convincing enough for us to hypothesise a potential role for these microtubules in mechanosensation with respect to how they may interact with the plasma membrane. This finding in conjunction with recent evidence that microtubules are associated with important mechanosensitive ion channels on the membrane of cells in flies (Zhang *et al.*, 2015) and mice (Prager-Khoutorsky *et al.*, 2014) encouraged us to pursue this hypothesis. Moreover, other work

had shown that PTM's have a role to play in determining the rigidity of cells (Robison *et al.*, 2016). A physical parameter which has a direct impact upon how cells respond to mechanical manipulation.

Therefore, in light of this data and the observed presence of a prominent band of acetylated microtubules located just below the plasma membrane of DRG neurons, along with a recognition of the importance of the properties of the plasma membrane for functional mechanosensory channel activity (Qi *et al.*, 2015; Cox *et al.*, 2016), we decided to investigate whether or not the presence of acetylated microtubules altered the stiffness of the plasma membrane in cultured DRG neurons derived from $Atat1^{Control}$ and $Atat1^{cKO}$ mice. In order to do this we employed AFM which allowed us to precisely measure the pressure required to indent the plasma membrane to a specific extent (measured in nanometers) of DRG neurons. From experiments carried out on cultured DRG neurons from control and knock out animals, we found that there was a statistically significant increase in pressure that was required to indent the membranes of $Atat1^{cKO}$ derived DRG compared to $Atat1^{Control}$ cells. This finding represented the first and only difference in the physiology between the mouse genotypes. Thus, at three separate indentation depths of 200, 400 and 600nm, the amount of pressure required to indent the plasma membrane was significantly greater in $Atat1^{cKO}$ versus $Atat1^{Control}$ neurons. It is worth noting here that a more blunted 'ball' type cantilever tip was employed to indent the membrane, rather than the sharper 'V' shaped tip sometimes used. This blunted tip contacts a greater area of the cell, thereby recruiting a greater surface area of the plasma membrane / underlying cytoskeleton into resisting the applied pressure.

We proposed that the increased pressure required to indent the membrane of $Atat1^{cKO}$ -derived DRG neurons occurred as a result of increased membrane rigidity in the absence of α-tubulin acetylation. As shown when we immunolabelled acetylated α-tubulin in $Atat1^{cKO}$ - derived DRG neurons, these cells lacked the distinctive sub-membrane band of acetylated microtubules. This is in contrast to $Atat1^{Control}$ – derived neurons where acetylated microtubules are localised close to the plasma membrane, a feature which seems to confer added flexibility to the membranes of these neurons (in

comparison to DRG neuronal membranes derived from Atat1^{cKO} mice). For this reason, we hypothesise that microtubule acetylation acts to increase the 'softness' of this type of tubulin, resulting in a more flexible layer of sub-membrane microtubules. In other words, acetylation serves to 'tune' the malleability of microtubules and, owing to their specific location within the DRG neurons, they directly influence the overall rigidity of the plasma membrane itself. In order to test this hypothesis, we carried out a series of experiments to measure the overall malleability of the axonal outgrowths of Atat1 ^{Control} and Atat1^{cKO} DRG neurons as well as the specific rigidity of the microtubule networks within these cells. To assess these parameters we subjected DRG neurons to an acute hyperosmotic shock which induced a sudden decrease in cell size. Although somewhat artificial, this decrease in volume can be viewed as an alternative to applying a localised external pressure force to these cells as both manipulations result in a shrinkage of the plasma membrane and the recruitment of the underlying cytoskeleton into resisting this stimuli. For these osmotic shock experiments we first assessed the percentage change in size of axons emanating from DRG neurons cultured from both genotypes of mice used in the study. In order to visualise the DRG neurons and their outgrowths prior to inducing shrinking we added a fluorescent dye called calcein to the cells. As previously discussed in the methods section calcein has the interesting characteristic of self-quenching its own fluorescence when individual molecules interact with one another.

Utilising this protocol we found that axons of Atat1^{cKO} -derived DRG neurons shrank significantly less than those derived from the wildtype mice. Moreover, by transfecting Atat1^{cKO} DRG neurons with the previously utilised K40Q amino acid mimic, we were able to return the phenotype to that of wildtype DRG neurons. This result strongly suggests that acetylated microtubules play a fundamental role in determining plasma membrane rigidity. Moreover, these data add considerable support to the findings of our earlier AFM experiments and also furthers the biological relevance of those experiments in an important way. Specifically, due to constraints of the technique, the AFM experiments were carried out on the soma of cultured DRG neurons. In contrast, the osmotic shock

experiments involved measuring the shrinkage of axonal outgrowths from the DRG neurons themselves. Therefore, as the initiation of mechanotransduction takes place at the peripheral ends of these axonal structures, the finding that these elements are also more rigid in mice of the $Atat1^{cKO}$ background adds physiological relevance to the same feature appearing in neuronal somata, and also enhances the validity of our hypothesis.

Finally, we wished to assess the rigidity of the microtubule network with the soma of DRG neurons from mice of both genetic backgrounds. Due to the small size of the axons it was impossible to visualise how rigid the microtubules within these structures were using conventional confocal microscopy. Therefore, we settled on the compromise of measuring the rigidity of these elements within neuronal cell bodies, inferring that any differences witnessed in this region were likely to also occur in the peripheral regions of the neurons' projecting afferents. To facilitate this live visualisation of the somatic neuronal microtubule network we used a novel microtubule dye called SIR-tubulin 2. This far red fluorogenic dye selectively binds to microtubules. By using this dye we were able to watch in 'real time' the shrinking of microtubules within the soma of DRG neurons following the hyperosmotic stimulus. By analysing the so called Integrated Density (IntDen) of the fluorescent microtubule network in regions of defined size throughout the cell body before and after shrinking, we revealed a statistically significant decrease in the density of the microtubule network following shrinking in the $Atat1^{cKO}$ DRG neurons compared to controls. This supports our earlier findings as IntDen is a measurement of the density of fluorescence in an area. Therefore, if the fluorescent microtubule network is more flexible then there will be a higher IntDen value for that region following shrinking. Hence, this data supports our hypothesis; in that it indicates that within $Atat1^{cKO}$ DRG neurons the microtubule network is stiffer, and can resist the hyperosmotic stimulus to a greater extent than control cells. Moreover, by once again transfecting $Atat1^{cKO}$- derived DRG neurons with the K40Q amino acid mimic we were able to re-establish the rigidity of the microtubule network to $Atat1^{Control}$ levels.

Taken together, these three separate experimental approaches provide complementary and convincing support for the hypothesis that the acetylation of microtubules within DRG neurons is essential for regulating the properties of membrane rigidity within these somatosensory cells. Up to now, no function for Atat1 had ever been identified. Consequently, the role of microtubule acetylation remained a mystery. Although previous work had demonstrated a touch insensitivity phenotype in *C.elegans* harbouring mutated versions of the acetyltransferase gene, the mechanism by which this insensitivity was brought about was unclear. Moreover, due to the simplicity of these organisms, the range of behavioural assays that can be effectively carried out is limited. Therefore our work not only goes some way toward explaining the mechanism by which mutant Atat1 facilitates a touch insensitivity phenotype, but it also convincingly demonstrated that this phenotype extends into the nociceptive range.

7 Conclusions

The function of acetylated microtubules has long remained a mystery. Even though this PTM of tubulin is conserved across all ciliated organisms, and acetylation has long been considered an important marker of both neuronal axons and cilia themselves (Montagnac *et al.*, 2013), no clear understanding of its role has yet been described. Here we demonstrate that in the absence of the microtubule acetyltransferase, Atat1, mice demonstrate a highly profound and specific deficiency in mechanosensitivity. This phenotype manifests itself as a change in the rigidity of the plasma membrane of somatosensory neurons. This change in membrane rigidity is brought about by a loss of a prominent sub-membrane band of acetylated microtubules, in the absence of Atat1. Our data further illustrate that this touch insensitivity phenotype can be rescued by mimicking the presence of a single acetylated lysine residue, residing on the inner lumen of the α-tubulin subunit of microtubules. Such a profound loss of mechanosensitivity in the absence of a PTM, sheds light on the inherent function and significance of Atat1, and likely the important role of microtubule acetylation in nature.

Our behavioural data, coupled with the skin-nerve electrophysiological data describe the most profound mechanoinsensitivity phenotype described to date. The number of fibre types affected is surprising, and firmly places acetylated microtubules as central components in both innocuous and noxious mechanotransduction. Furthermore, the specificity of this phenotype, which does not influence other PNS sensory modalities such as thermoreception and proprioception, potentially reveals an interesting divergence in the underlying mechanism of how these separate stimuli are detected.

Overall, our finding which demonstrates that a lack of microtubule acetylation leads to an increase in microtubule / plasma membrane rigidity partners well with existing models for mechanotransduction. As previously stated, mechanotransduction is the process of converting physical force into electro /

chemical signals. As also discussed previously, there are two major models that describe how this process may take place. The first involves a direct linkage between mechanosensitive channels (MS-channels) and the underlying microtubule cytoskeleton. Evidence for this model can be found in the Drosophila MS-channel, NOMPC. This channel has been shown to directly link to the microtubule cytoskeleton via intracellular protein motifs called 'ankyrin repeat domains', which project down from the channel into the cytoplasm of the cell (Zhang *et al.*, 2015). In this model, pressure applied to the membrane / channel forces the microtubules to bear this load leading to the opening / activation of the MS channel.

The second idea posits that microtubules are potentially linked either directly or indirectly via an unknown protein intermediary, to the inner leaflet of the plasma membrane. In this model there is no particular relationship between the positioning of the MS channels and these microtubule linkages. Rather, these microtubules 'prop-up' the plasma membrane and, upon application of pressure, these microtubules translate the force, resulting in a stretching of the membrane between the microtubule binding sites. An MS channel located in the membrane between said binding sites will be opened by the stretching of the membrane, thereby facilitating the activation of the channel. It is clear from work on NOMPC that some channels are indeed directly linked to microtubules. Conversely, work on Piezo2 suggests that no such linkages exist, or are indeed required for activation of this channel. Rather based on work with Piezo1 (Cox *et al.*, 2016), Piezo2 is thought to be highly sensitive to membrane stretch / tension. However, if the membrane becomes tenser as a result of being propped-up by stiffer microtubules, the activation of tension-sensitive MSCs will also be affected. Therefore, given the broad effect of both low-threshold and high-threshold stimuli observed on our Atat1^{cKO} mice, whether or not MSC opening is the result of the force being translated to directly-, or indirectly-, linked microtubules, the channels will still be affected by a stiffening of these elements, hence the profundity of our mechanoinsensitivity phenotype.

8 Future directions

Considering the findings of this work there are several potentially interesting avenues of investigation that one could explore in the future.

We have demonstrated using AFM that the membranes of somatosensory DRG neurons are more rigid in the Atat1^{cKO} mice compared to that of control neurons. We also demonstrated that the microtubule network is more rigid in Atat1^{cKO} cells following hyperosmotic shock. However, we have not been able to understand why acetylated microtubules are more rigid, and how this increased rigidity results in a stiffer plasma membrane. Are acetylated microtubules directly linked to the inner leaflet of the membrane? An alternative AFM technique allows for the attachment of a tether to the membrane of cells (Qi *et al.*, 2015). In this assay, rather than pushing on the membrane, the cantilever can pull on it, measuring very accurately the force required to 'drag' the membrane outwards. Carrying out this type of experiment might shed light on whether the acetylated microtubules are in some way directly linked to the membrane, because in their absence (as with Atat1^{cKO} mice) the membrane could pull away more easily from the cytoskeleton, suggesting a disconnect between these elements. This idea could potentially explain the phenotype as if acetylated microtubules are linked to the plasma membrane, they might therefore deform in concert with this structure upon indentation via pressure. Much of this is speculative; but it nevertheless points out some key gaps in the present work.

Another potential methodology that could shed more light on the proposed mechanism would be to image the deformation of sub-membrane microtubules within DRG neurons in real time during prodding with a blunted glass pipette. This assay could also potentially garner information about whether or not the acetylated microtubules are linked to the plasma membrane. If they are indeed linked to the membrane after acetylation, microtubules may 'buckle' differently under pressure. Indeed, as mentioned earlier, live imaging of beating cardiomyocytes has revealed that detyrosination

of tubulin can profoundly affect the buckling of protofilament structures within these cells (Robison *et al.*, 2016). Although in this study this particular PTM led to an altered interaction between microtubules and other cytoskeletal elements, in our case it may be due to a change in microtubule – plasma membrane interactions. To investigate this, one would have to use the novel 'Airyscan' generation of confocal microscopes, which allow for high frame rate / high resolution imaging (Robison *et al.*, 2016) in conjunction with the SIR-tubulin2 dye already described here.

In line with this latter suggestion, another potential mechanism which might explain the difference in the role of acetylated versus non-acetylated microtubules is how they interact with other cytoskeletal elements. We could explore this by examining potential crosslinking between the actin and / or intermediate filament networks using superresolution microscopy. As described previously, we examined and found no differences between the two genotypes of mice studied here in their network architecture of α-tubulin using superresolution microscopy. However, we did not examine the actin or intermediate filament networks in this way. If a difference in crosslinking could be found, it would warrant further study. As mentioned earlier, recent work on detyrosinated microtubules has shown that they interact with desmin intermediate filaments in cardiomyocytes (Robison *et al.*, 2016). An excess of detyrosination results in a greater interaction with desmin, thereby leading to altered contraction of the microtubule protofilaments under mechanical stress. A similar mechanism might account for the change in microtubule rigidity observed in Atat1^{cKO} DRG neurons in our study. In this case live imaging of DRG neurons with fluorescently labelled intermediate filaments and microtubules using an 'Airyscan' confocal would be the best approach for determining if such an effect is present. Using this sensitive method it would even be possible to characterise the nature of microtubule 'buckling' during administration of a mechanical stimulus.

Recent work has highlighted the importance of Piezo2 in the function of proprioceptors (Woo *et al.*, 2015). However, our work did not reveal any deficit in either fine proprioception, or general locomotion in Atat1^{cKO} animals. The other member of the Piezo MS- channels Piezo1 has been shown

to be inherently sensitive to membrane tension, as it functions perfectly well in simplified systems without any cytoskeletal components (Cox *et al.*, 2016). However, as the absence of acetylated microtubules profoundly influences the rigidity of the plasma membrane, it would not be unreasonable to assume that the activity of Piezo2 would be affected by this change, even without any direct link to acetylated microtubules. However, our data suggests this is not the case. Therefore, it would be interesting to examine whether the acetylated rings described in this study are completely absent from the subset of parvalbumin positive proprioceptor DRG neurons. Given, the results of this work it is reasonable to hypothesise that there would not be any co-localisation between either the anti-acetylated tubulin or parvalbumin stains. If this is the case, it therefore is of interest to study the make-up of the mechanotransduction apparatus of proprioceptors which, presumably, is very different from that present in other mechanosensitive cells /afferents.

Given the role of Atat1 in mechanosensation it would be interesting to look at how the absence of this enzyme affects pathological pain states such as neuropathic pain. One symptom of neuropathic pain involves mechanosensory afferents in the skin becoming hypersensitized to low threshold innocuous touch (mechanical allodynia) (Campbell *et al.*, 1988). In this state, previously low-threshold stimuli are perceived as painful. Given the touch insensitivity brought about in the absence of Atat1 shown here, it would be interesting to consider whether pharmacologically targeting this enzyme in the skin of neuropathic pain sufferers might help to alleviate some of the discomfort of this common condition. As a starting point, work in mice to establish if the mechanical threshold of $Atat1^{cKO}$ animals following Spared Nerve Injury (SNI) was higher than that of controls, could reveal a protective value of the knock-out and therefore justify further work.

In this study, we were interested in cutaneous mechanosensation. However, there are other systems within organisms which rely on mechanosensation / mechanotransduction to function correctly. For example, the ear, the Vagus nerve and the bladder are also all innervated by mechanosensitive fibres. It would therefore be interesting to investigate whether hearing, blood pressure and / or rates of

defecation are affected in Atat knock-out mice. To do this one could utilise the Deleter – Cre mouse transgenic line, in which the Cre is expressed in the germline and would therefore remove the Atat1 enzyme from all the cells of the body (Kalebic *et al.*, 2013).

Finally, it is worth noting here that other neuronal cell types, taken from the hippocampus and the cortex also exhibited a sub-membrane distribution of acetylated microtubules, which is in line with what was seen in DRG neurons (data not shown). Given the lack of any sub-membrane localisation of acetylated microtubules in non-mechanosensory cells such as MEFs, one might theorise that perhaps all neuronal cells are evolutionarily-derived from a common proto-neuronal ancestor cell, which was mechanosensitive. Indeed, when the literature is considered this supposition is not so far-fetched, given the widely-held belief that mechanosensation, is, if not the first, then certainly one of the most ancient sensory modalities developed by living things (Martinac and Kloda, 2003). Along these lines, it would be very interesting to carry out immunostaining for acetylated microtubules in the Touch Responsive Neurons (TRNs) of *C. elegans*. Taking into consideration the long evolutionary gap between modern mammals and this simple worm, the presence of a ring of acetylated microtubules below the membrane of these cells would be a strong argument for evolutionary history which leads back to an ancient mechanosensitive proto-neuron. This would perhaps shed light on why neurons located deep in the mammalian brain are, somewhat counterintuitively, equipped with a vital apparatus for sensing mechanical stimuli.

9 References

Abraira, V. and Ginty, D. (2013) 'The sensory neurons of touch', *Neuron*. Elsevier Inc., 79(4), pp. 618–639. doi: 10.1016/j.neuron.2013.07.051.

Abreu-Blanco, M. T., Verboon, J. M. and Parkhurst, S. M. (2011) 'Cell wound repair in Drosophila occurs through three distinct phases of membrane and cytoskeletal remodeling', *Journal of Cell Biology*, 193(3), pp. 455–464. doi: 10.1083/jcb.201011018.

Akay, T. *et al.* (2014) 'Degradation of mouse locomotor pattern in the absence of proprioceptive sensory feedback', *Proceedings of the National Academy of Sciences*. National Academy of Sciences, 111(47), pp. 16877–16882. doi: 10.1073/pnas.1419045111.

Akella, J. S. *et al.* (2010) 'MEC-17 is an a -tubulin acetyltransferase', *Nature*. Nature Publishing Group, a division of Macmillan Publishers Limited. All Rights Reserved., 467(7312), pp. 218–222. doi: 10.1038/nature09324.

Albert, J. T., Nadrowski, B. and Göpfert, M. C. (2007) *Mechanical Signatures of Transducer Gating in the Drosophila Ear*, *Current Biology*. doi: 10.1016/j.cub.2007.05.004.

Aristotle (1994) 'De Anima (On the Soul)', *Book II, Translated by J.A. Smith, written 350 B.C.E.* Available at: http://classics.mit.edu/Aristotle/soul.2.ii.html.

Árnadóttir, J. and Chalfie, M. (2010) 'Eukaryotic Mechanosensitive Channels', *Annual Review of Biophysics*, 39(1), pp. 111–137. doi: 10.1146/annurev.biophys.37.032807.125836.

Assad, J. A., Shepherd, G. M. G. and Corey, D. P. (1991) 'Tip-link integrity and mechanical transduction in vertebrate hair cells', *Neuron*, 7(6), pp. 985–994. doi: 10.1016/0896-6273(91)90343-X.

Bai, L. *et al.* (2015) 'Genetic Identification of an Expansive Mechanoreceptor Sensitive to Skin

Stroking', *Cell*, 163(7), pp. 1783–1795. doi: 10.1016/j.cell.2015.11.060.

Basbaum, A. I. *et al.* (2009) 'Cellular and Molecular Mechanisms of Pain', *Cell*, 139(2), pp. 267–284. doi: 10.1016/j.cell.2009.09.028.

Bell, C. and Shaw, A. (1868) 'Reprint of the "Idea of a New Anatomy of the Brain," with Letters, &c.', *Journal of anatomy and physiology*, 3(Pt 1), pp. 147–82. Available at: http://www.pubmedcentral.nih.gov/articlerender.fcgi?artid=1318665&tool=pmcentrez&rendertype=abstract.

Bell, E. A. *et al.* (2015) 'Potentially biogenic carbon preserved in a 4.1 billion-year-old zircon', *Proceedings of the National Academy of Sciences*, 112(47), pp. 14518–14521. doi: 10.1073/pnas.1517557112.

Bell, J., Bolanowski, S. and Holmes, M. H. (1994) 'The structure and function of pacinian corpuscles: A review', *Progress in Neurobiology*, 42(1), pp. 79–128. doi: 10.1016/0301-0082(94)90022-1.

Bessou, P. and Perl, E. R. (1969) 'Response of cutaneous sensory units with unmyelinated fibers to noxious stimuli.', *Journal of neurophysiology*, 32(6), pp. 1025–1043.

Bewick, G. S. and Banks, R. W. (2014) 'Mechanotransduction in the muscle spindle', *Pflugers Archiv European Journal of Physiology*. Berlin/Heidelberg: Springer Berlin Heidelberg, 467(1), pp. 175–190. doi: 10.1007/s00424-014-1536-9.

Birder, L. A. *et al.* (2002) 'Altered urinary bladder function in mice lacking the vanilloid receptor TRPV1', *Nature Neuroscience*, 5(9), pp. 856–860. doi: 10.1038/nn902.

Bolton, C. F., Winkelmann, R. K. and Dyck, P. J. (1966) 'A quantitative study of Meissner's corpuscles in man', *Neurology*, 16(1), pp. 1–1. doi: 10.1212/WNL.16.1.1.

Bonin, R. P., Bories, C. and De Koninck, Y. (2014) 'A Simplified Up-Down Method (SUDO) for Measuring Mechanical Nociception in Rodents Using von Frey Filaments', *Molecular Pain*. BioMed Central, 10, pp. 1744-8069-10–26. doi: 10.1186/1744-8069-10-26.

Bourque, C. W. (2008) 'Central mechanisms of osmosensation and systemic osmoregulation', *Nature Reviews Neuroscience*. Nature Publishing Group, 9(7), pp. 519–531. doi: 10.1038/nrn2400.

Brown, B. Y. A. G. and Iggo, A. (1967) 'From the Department of Veterinary Physiology , University of Edinburgh', pp. 707–733.

Brunet, T. and Arendt, D. (2016) 'From damage response to action potentials: early evolution of neural and contractile modules in stem eukaryotes.', *Philosophical transactions of the Royal Society of London. Series B, Biological sciences*, 371(1685), p. 20150043-. doi: 10.1098/rstb.2015.0043.

Bulinski, J. C., Richards, J. E. and Piperno, G. (1988) 'Posttranslational modifications of ?? tubulin: Detyrosination and acetylation differentiate populations of interphase microtubules in cultured cells', *Journal of Cell Biology*, 106(4), pp. 1213–1220. doi: 10.1083/jcb.106.4.1213.

Burgess, B. Y. P. R. and Perl, E. R. (1967) 'From the Department of Physiology , University of Utah College', *Journal of Physiology*, 190, pp. 541–562.

Burgess, P. R., Petit, D. and Warren, R. M. (1968) 'Receptor Types in Cat Hairy Supplied Skin by Myelinated', *Journal of Neurophysiology*, 31(6), pp. 833–848. Available at: http://jn.physiology.org/content/31/6/833 (Accessed: 10 December 2016).

Campbell, J. N. *et al.* (1988) 'Myelinated afferents signal the hyperalgesia associated with nerve injury', *Pain*, 32(1), pp. 89–94. doi: 10.1016/0304-3959(88)90027-9.

Cavanaugh, D. J. *et al.* (2009) 'Distinct subsets of unmyelinated primary sensory fibers mediate behavioral responses to noxious thermal and mechanical stimuli', *Proceedings of the National Academy of Sciences of the United States of America*. National Academy of Sciences, 106(22), pp.

9075–9080. doi: 10.1073/pnas.0901507106.

Chalfie, M. (2009) ‘Neurosensory mechanotransduction.’, *Nature reviews. Molecular cell biology*, 10(1), pp. 44–52. doi: 10.1038/nrm2595.

Chalfie, M. and Au, M. (1989) ‘Genetic control of differentiation of the Caenorhabditis elegans touch receptor neurons.’, *Science (New York, N.Y.)*, 243(4894 Pt 1), pp. 1027–33. doi: 10.1126/science.2646709.

Charan, J. and Kantharia, N. D. (2013) ‘How to calculate sample size in animal studies?’, *Journal of Pharmacology & Pharmacotherapeutics*. India: Medknow Publications & Media Pvt Ltd, 4(4), pp. 303–306. doi: 10.4103/0976-500X.119726.

Charras, G. T. (2008) ‘A short history of blebbing.’, *Journal of microscopy*, 231(3), pp. 466–78. doi: 10.1111/j.1365-2818.2008.02059.x.

Charras, G. T. *et al.* (2008) ‘Life and Times of a Cellular Bleb()’, *Biophysical Journal*. The Biophysical Society, 94(5), pp. 1836–1853. doi: 10.1529/biophysj.107.113605.

Chelur, D. S. *et al.* (2002) ‘The mechanosensory protein MEC-6 is a subunit of the C. elegans touch-cell degenerin channel’, *Nature*, 420, pp. 669–673. doi: 10.1038/nature01216.1.

Cheng, L. E. *et al.* (2010) *The Role of the TRP Channel NompC in Drosophila Larval and Adult Locomotion*, *Neuron*. doi: 10.1016/j.neuron.2010.07.004.

Chesler, A. T. *et al.* (2016) ‘The Role of PIEZO2 in Human Mechanosensation’, *New England Journal of Medicine*. Massachusetts Medical Society, 375(14), pp. 1355–1364. doi: 10.1056/NEJMoa1602812.

Clapham, D. E. (2003) ‘TRP channels as cellular sensors’, *Nature*, 426(6966), pp. 517–524. doi: 10.1038/nature02196.

Clapham, D. E. (2007) ‘Calcium Signaling’, *Cell*, 131(6), pp. 1047–1058. doi: 10.1016/j.cell.2007.11.028.

Coombes, C. *et al.* (2016) ‘Mechanism of microtubule lumen entry for the α-tubulin acetyltransferase enzyme αTAT1’, *Proceedings of the National Academy of Sciences* , 113(46), pp. E7176–E7184. doi: 10.1073/pnas.1605397113.

Corey, D. P. and Hudspeth, a J. (1979) ‘Response latency of vertebrate hair cells.’, *Biophysical journal*. Elsevier, 26(3), pp. 499–506. doi: 10.1016/S0006-3495(79)85267-4.

Coste, B. *et al.* (2010) ‘Piezo1 and Piezo2 are essential components of distinct mechanically-activated cation channels’, *Science (New York, N.Y.)*, 330(6000), pp. 55–60. doi: 10.1126/science.1193270.

Coste, B. *et al.* (2012) ‘Piezo proteins are pore-forming subunits of mechanically activated channels’, *Nature*. Nature Publishing Group, a division of Macmillan Publishers Limited. All Rights Reserved., 483(7388), pp. 176–181. Available at: http://dx.doi.org/10.1038/nature10812.

Cox, C. D. *et al.* (2016) ‘Removal of the mechanoprotective influence of the cytoskeleton reveals PIEZO1 is gated by bilayer tension’, *Nature Communications*. Nature Publishing Group, 7, pp. 1–13. doi: 10.1038/ncomms10366.

Cueva, J. G., Hsin, J., Huang, K. C., *et al.* (2012) ‘Post-translational Acetylation of α Tubulin Constrains Protofilament Number in Native Microtubules’, *Current biology : CB*, 22(12), pp. 1066–1074. doi: 10.1016/j.cub.2012.05.012.

Cueva, J. G., Hsin, J., Huang, K. C., *et al.* (2012) ‘Posttranslational acetylation of α-tubulin constrains protofilament number in native microtubules.’, *Current biology : CB*. Elsevier Ltd, 22(12), pp. 1066–74. doi: 10.1016/j.cub.2012.05.012.

D’Este, E. *et al.* (2016) ‘Subcortical cytoskeleton periodicity throughout the nervous system’,

Scientific Reports. The Author(s), 6, p. 22741.

Dallenbach, K. M. (1939) 'Pain: History and Present Status', *The American Journal of Psychology*. University of Illinois Press, 52(3), pp. 331–347. doi: 10.2307/1416740.

Denk, W. *et al.* (1995) 'Calcium imaging of single stereocilia in hair cells: Localization of transduction channels at both ends of tip links', *Neuron*, 15(6), pp. 1311–1321. doi: http://dx.doi.org/10.1016/0896-6273(95)90010-1.

Descartes, R. *et al.* (1664) 'The World and Treatise on Man', *The Philosophical Writings of Descartes*, pp. 79–108. doi: 10.1017/CBO9780511805042.005.

Le Douarin, N. and Kalcheim, C. (1999) *The Neural Crest, Cambridge New York Cambridge University Press*. Available at: http://www.ncbi.nlm.nih.gov/books/NBK10065/.

Drew, L. J. *et al.* (2004) 'Acid-sensing ion channels ASIC2 and ASIC3 do not contribute to mechanically activated currents in mammalian sensory neurones.', *The Journal of physiology*, 556(Pt 3), pp. 691–710. doi: 10.1113/jphysiol.2003.058693.

Edin, B. B. (1992) 'Quantitative analysis of static strain sensitivity in human mechanoreceptors from hairy skin', *J Neurophysiol*, 67(5), pp. 1105–1113. Available at: http://jn.physiology.org/content/67/5/1105 (Accessed: 11 December 2016).

Effertz, T., Wiek, R. and Göpfert, M. C. (2011) 'NompC TRP channel is essential for Drosophila sound receptor function', *Current Biology*, 21(7), pp. 592–597. doi: 10.1016/j.cub.2011.02.048.

Elg, S. *et al.* (2007) 'Cellular subtype distribution and developmental regulation of TRPC channel members in the mouse dorsal root ganglion.', *The Journal of comparative neurology*, 503(1), pp. 35–46. doi: 10.1002/cne.21351.

Ernstrom, G. G. and Chalfie, M. (2002) 'Genetics of sensory mechanotransduction.', *Annual review*

of genetics, 36, pp. 411–53. doi: 10.1146/annurev.genet.36.061802.101708.

Formby, C. *et al.* (1992) 'The role of frequency selectivity in measures of auditory and vibrotactile temporal resolution', *The Journal of the Acoustical Society of America*. Acoustical Society of America, 91(1), pp. 293–305.

Frölich, M. A. *et al.* (2010) 'Temporal Characteristics of Cold Pain Perception', *Neuroscience letters*, 480(1), pp. 12–15. doi: 10.1016/j.neulet.2010.05.045.

Gaertig, J. *et al.* (1995) 'Acetylation of lysine 40 in ??-tubulin is not essential in Tetrahymena thermophila', *Journal of Cell Biology*, 129(5), pp. 1301–1310. doi: 10.1083/jcb.129.5.1301.

Garrison, S. R., Dietrich, a. and Stucky, C. L. (2012) 'TRPC1 contributes to light-touch sensation and mechanical responses in low-threshold cutaneous sensory neurons', *Journal of Neurophysiology*, 107(3), pp. 913–922. doi: 10.1152/jn.00658.2011.

Gaudet, R. (2008) 'A primer on ankyrin repeat function in TRP channels and beyond', *Molecular BioSystems*. The Royal Society of Chemistry, 4(5), pp. 372–379. doi: 10.1039/B801481G.

Ge, J. *et al.* (2015) 'Architecture of the mammalian mechanosensitive Piezo1 channel', *Nature*. Nature Publishing Group, a division of Macmillan Publishers Limited. All Rights Reserved., 527(7576), pp. 64–69. Available at: http://dx.doi.org/10.1038/nature15247.

Gillespie, P. G. and Walker, R. G. (2001) 'Molecular basis of mechanosensory transduction.', *Nature*, 413(6852), pp. 194–202. doi: 10.1038/35093011.

Goodman, M. B. *et al.* (2002) 'MEC-2 regulates C. elegans DEG/ENaC channels needed for mechanosensation.', *Nature*, 415(6875), pp. 1039–1042. doi: 10.1038/nature00853.

Goodwin, a W., Macefield, V. G. and Bisley, J. W. (1997) 'Encoding of object curvature by tactile afferents from human fingers.', *Journal of neurophysiology*, 78(6), pp. 2881–2888.

Goswami, C., Hucho, T. B. and Hucho, F. (2007) ‘Identification and characterisation of novel tubulin-binding motifs located within the C-terminus of TRPV1.’, *Journal of neurochemistry*, 101(1), pp. 250–62. doi: 10.1111/j.1471-4159.2006.04338.x.

Gottlieb, P. *et al.* (2008) ‘Revisiting TRPC1 and TRPC6 mechanosensitivity’, *Pflügers Archiv - European Journal of Physiology*, 455(6), pp. 1097–1103. doi: 10.1007/s00424-007-0359-3.

Hagins, W. a (1972) ‘The visual process: Excitatory mechanisms in the primary receptor cells.’, *Annual review of biophysics and bioengineering 1972. 1:131-158*, 1(ii), pp. 131–58. doi: 10.1146/annurev.bb.01.060172.001023.

Halata, Z. (1977) ‘The ultrastructure of the sensory nerve endings in the articular capsule of the knee joint of the domestic cat (Ruffini corpuscles and Pacinian corpuscles).’, *Journal of Anatomy*, 124(Pt 3), pp. 717–729. Available at: http://www.ncbi.nlm.nih.gov/pmc/articles/PMC1234668/.

Hankin, R. K. S. (2015) ‘Circular Statistics in R’, *Journal of Statistical Software; Vol 1, Book Review 5 (2015)* . doi: 10.18637/jss.v066.b05.

Howard, J. and Bechstedt, S. (2004) ‘Hypothesis: A helix of ankyrin repeats of the NOMPC-TRP ion channel is the gating spring of mechanoreceptors’, *Current Biology*, 14(6), pp. R224–R226. doi: http://dx.doi.org/10.1016/j.cub.2004.02.050.

Huang, M. *et al.* (1995) ‘A stomatin-like protein necessary for mechanosensation in C. elegans’, *Nature*, 378(6554), pp. 292–295. Available at: http://dx.doi.org/10.1038/378292a0.

Idone, V., Tam, C. and Andrews, N. W. (2008) ‘Two-way traffic on the road to plasma membrane repair’, *Trends in Cell Biology*, 18(11), pp. 552–559. doi: http://dx.doi.org/10.1016/j.tcb.2008.09.001.

Iggo, a. and Muir, a. R. (1969) ‘Veterinary Studies, University of’, *Journal of Physiology*, 1882(200), pp. 763–796.

Ikeda, I. *et al.* (1994) ‘Selective phototoxic destruction of rat Merkel cells abolishes responses of slowly adapting type I mechanoreceptor units.’, *The Journal of physiology*, 479 (Pt 2, pp. 247–56. doi: 10.1113/jphysiol.1994.sp020292.

Janig, W., Schmidt, R. F. and Zimmermann, M. (1968) ‘Single unit responses and the total afferent outflow from the cat’s foot pad upon mechanical stimulation’, *Experimental Brain Research*, 6(2), pp. 100–115. doi: 10.1007/BF00239165.

Janke, C. (2014) ‘The tubulin code: Molecular components, readout mechanisms, and functions’, *The Journal of Cell Biology*, 206(4), p. 461 LP-472. Available at: http://jcb.rupress.org/content/206/4/461.abstract.

Janke, C. and Chloë Bulinski, J. (2011) ‘Post-translational regulation of the microtubule cytoskeleton: mechanisms and functions’, *Nat Rev Mol Cell Biol*. Nature Publishing Group, a division of Macmillan Publishers Limited. All Rights Reserved., 12(12), pp. 773–786. Available at: http://dx.doi.org/10.1038/nrm3227.

Jin, X., Touhey, J. and Gaudet, R. (2006) ‘Structure of the N-terminal ankyrin repeat domain of the TRPV2 ion channel.’, *The Journal of biological chemistry*, 281(35), pp. 25006–10. doi: 10.1074/jbc.C600153200.

Johansson, R. S. and Vallbo, A. B. (1979) ‘Detection of tactile stimuli. Thresholds of afferent units related to psychophysical thresholds in the human hand.’, *The Journal of Physiology*, 297, pp. 405–422. Available at: http://www.ncbi.nlm.nih.gov/pmc/articles/PMC1458728/.

Johansson, R. S. and Vallbo, Å. B. (1980) ‘Spatial properties of the population of mechanoreceptive units in the glabrous skin of the human hand’, *Brain Research*, 184(2), pp. 353–366. doi: 10.1016/0006-8993(80)90804-5.

Johnson, K. O. and Lamb, G. D. (1981) ‘Neural mechanisms of spatial tactile discrimination: neural

patterns evoked by braille-like dot patterns in the monkey.', *The Journal of physiology*, 310, pp. 117–44. doi: 10.1113/jphysiol.1981.sp013540.

Kadavath, H. *et al.* (2015) 'Tau stabilizes microtubules by binding at the interface between tubulin heterodimers', *Proceedings of the National Academy of Sciences of the United States of America*. National Academy of Sciences, 112(24), pp. 7501–7506. doi: 10.1073/pnas.1504081112.

Kalebic, N. *et al.* (2013) 'αTAT1 is the major α-tubulin acetyltransferase in mice.', *Nature communications*, 4, p. 1962. doi: 10.1038/ncomms2962.

Kamikouchi, A. *et al.* (2009) 'The neural basis of Drosophila gravity-sensing and hearing', *Nature*. Macmillan Publishers Limited. All rights reserved, 458(7235), pp. 165–171. Available at: http://dx.doi.org/10.1038/nature07810.

Katta, S., Krieg, M. and Goodman, M. B. (2015) 'Feeling Force: Physical and Physiological Principles Enabling Sensory Mechanotransduction', *Annual Review of Cell and Developmental Biology*, 31(1), pp. 347–371. doi: 10.1146/annurev-cellbio-100913-013426.

Konieczny, P. *et al.* (2008) 'Myofiber integrity depends on desmin network targeting to Z-disks and costameres via distinct plectin isoforms', *The Journal of Cell Biology*, 181(4), p. 667 LP-681. Available at: http://jcb.rupress.org/content/181/4/667.abstract.

Krimm, R. F., Davis, B. M. and Albers, K. M. (1999) 'Selectively Restores Sensory Innervation In NT3 Gene Knockout Mice ABSTRACT ':, 3, pp. 40–49.

Kung, C. (2005) 'A possible unifying principle for mechanosensation.', *Nature*, 436(7051), pp. 647–654. doi: 10.1038/nature03896.

L'Hernault, S. W. and Rosenbaum, J. L. (1985) 'Chlamydomonas .alpha.-tubulin is posttranslationally modified by acetylation on the .epsilon.-amino group of a lysine', *Biochemistry*. American Chemical Society, 24(2), pp. 473–478. doi: 10.1021/bi00323a034.

L'Hernault, S. W. and Rosenbaum, J. L. (1983) ‘Chlamydomonas alpha-tubulin is posttranslationally modified in the flagella during flagellar assembly.’, *The Journal of Cell Biology*, 97(1), p. 258 LP-263. Available at: http://jcb.rupress.org/content/97/1/258.abstract.

LaMotte, R. H. and Whitehouse, J. (1986) ‘Tactile detection of a dot on a smooth surface: peripheral neural events’, *Journal of Neurophysiology*, 56(4), p. 1109 LP-1128. Available at: http://jn.physiology.org/content/56/4/1109.abstract.

Lechner, S. G. and Lewin, G. R. (2013) ‘Hairy Sensation’, *Physiology*, 28(3), p. 142 LP-150.

Levina, N. *et al.* (1999) ‘Protection of Escherichia coli cells against extreme turgor by activation of MscS and MscL mechanosensitive channels: identification of genes required for MscS activity.’, *The EMBO journal*, 18(7), pp. 1730–7. doi: 10.1093/emboj/18.7.1730.

Li, L. *et al.* (2011) ‘The functional organization of cutaneous low-threshold mechanosensory neurons’, *Cell*. Elsevier Inc., 147(7), pp. 1615–1627. doi: 10.1016/j.cell.2011.11.027.

Liang, X. *et al.* (2013) ‘A NOMPC-Dependent Membrane-Microtubule Connector Is a Candidate for the Gating Spring in Fly Mechanoreceptors’, *Current Biology*, 23(9), pp. 755–763. doi: http://dx.doi.org/10.1016/j.cub.2013.03.065.

Liao, G. and Gundersen, G. G. (1998) ‘Kinesin Is a Candidate for Cross-bridging Microtubules and’, 273(16), pp. 9797–9803. doi: 10.1074/jbc.273.16.9797.

Lin, S.-H., Sun, W.-H. and Chen, C.-C. (2015) ‘Genetic exploration of the role of acid-sensing ion channels’, *Neuropharmacology*, 94, pp. 99–118. doi: 10.1016/j.neuropharm.2014.12.011.

Löken, L. S. *et al.* (2009) ‘Coding of pleasant touch by unmyelinated afferents in humans.’, *Nature neuroscience*, 12(5), pp. 547–548. doi: 10.1038/nn.2312.

Lübbe, J. *et al.* (2013) ‘Determining cantilever stiffness from thermal noise’, *Beilstein Journal of*

Nanotechnology. Edited by T. Glatzel and U. D. Schwarz. Trakehner Str. 7-9, 60487 Frankfurt am Main, Germany: Beilstein-Institut, 4, pp. 227–233. doi: 10.3762/bjnano.4.23.

MacIver, M. B. and Tanelian, D. L. (1993) 'Structural and functional specialization of A delta and C fiber free nerve endings innervating rabbit corneal epithelium', *The Journal of Neuroscience*, 13(10), p. 4511 LP-4524.

Mannsfeldt, A. G. *et al.* (1999) 'Stomatin, a MEC-2 Like Protein, Is Expressed by Mammalian Sensory Neurons', *Molecular and Cellular Neuroscience*, 13(6), pp. 391–404. doi: http://dx.doi.org/10.1006/mcne.1999.0761.

Maricich, S. M. *et al.* (2009a) 'Merkel cells are essential for light-touch responses.', *Science (New York, N.Y.)*, 324(5934), pp. 1580–1582. doi: 10.1126/science.1172890.

Maricich, S. M. *et al.* (2009b) 'Merkel cells are essential for light-touch responses.', *Science (New York, N.Y.)*, 324(5934), pp. 1580–2. doi: 10.1126/science.1172890.

Maricich, S. M. *et al.* (2012) 'Rodents rely on Merkel cells for texture discrimination tasks.', *J Neurosci*, 32(10), pp. 3296–3300. doi: 10.1523/JNEUROSCI.5307-11.2012.

Marmigère, F. and Ernfors, P. (2007) 'Specification and connectivity of neuronal subtypes in the sensory lineage.', *Nature reviews. Neuroscience*, 8(2), pp. 114–127. doi: 10.1038/nrn2057.

Martinac, B. *et al.* (1987) 'Pressure-sensitive ion channel in Escherichia coli.', *Proceedings of the National Academy of Sciences of the United States of America*, 84(8), pp. 2297–2301. doi: 10.1073/pnas.84.8.2297.

Martinac, B. and Kloda, A. (2003) 'Evolutionary origins of mechanosensitive ion channels', *Progress in Biophysics and Molecular Biology*, 82(1–3), pp. 11–24. doi: 10.1016/S0079-6107(03)00002-6.

Maxwell, D. J. *et al.* (2007) ‘Morphology of inhibitory and excitatory interneurons in superficial laminae of the rat dorsal horn.’, *The Journal of physiology*, 584(D), pp. 521–533. doi: 10.1113/jphysiol.2007.140996.

McGlone, F., Wessberg, J. and Olausson, H. (2014) ‘Discriminative and affective touch: sensing and feeling.’, *Neuron*, 82(4), pp. 737–55. doi: 10.1016/j.neuron.2014.05.001.

Melzack, R. and Wall, P. (1965) ‘Pain Mechanism: A new Theory’, *Science*, pp. 971–979. doi: 10.1126/science.150.3699.971.

Merkel, F. (1875) ‘Tastzellen und Tastkörperchen bei den Hausthieren und beim Menschen’, *Archiv für mikroskopische Anatomie*, 11(1), pp. 636–652. doi: 10.1007/BF02933819.

Mills, L. R. and Diamond, J. (1995) ‘Merkel cells are not the mechanosensory transducers in the touch dome of the rat’, *Journal of Neurocytology*, 24(2), pp. 117–134. doi: 10.1007/BF01181555.

Mitchison, T. and Kirschner, M. (1984) ‘Dynamic instability of microtubule growth’, *Nature*, 312(5991), pp. 237–242. Available at: http://dx.doi.org/10.1038/312237a0.

Moayedi, M. and Davis, K. D. (2013) ‘Theories of pain: from specificity to gate control’, *Journal of Neurophysiology*, 109(1), pp. 5–12. doi: 10.1152/jn.00457.2012.

Moe, P. C., Blount, P. and Kung, C. (1998) ‘Functional and structural conservation in the mechanosensitive channel MscL implicates elements crucial for mechanosensation’, *Molecular Microbiology*, 28(3), pp. 583–592. doi: 10.1046/j.1365-2958.1998.00821.x.

Mogil, J. S. (2012) ‘Sex differences in pain and pain inhibition: multiple explanations of a controversial phenomenon’, *Nat Rev Neurosci*. Nature Publishing Group, a division of Macmillan Publishers Limited. All Rights Reserved., 13(12), pp. 859–866. Available at: http://dx.doi.org/10.1038/nrn3360.

Montagnac, G. *et al.* (2013) '[agr]TAT1 catalyses microtubule acetylation at clathrin-coated pits', *Nature*. Nature Publishing Group, a division of Macmillan Publishers Limited. All Rights Reserved., 502(7472), pp. 567–570. Available at: http://dx.doi.org/10.1038/nature12571.

Montell, C. (2005) 'Drosophila TRP channels', *Pflügers Archiv*, 451(1), pp. 19–28. doi: 10.1007/s00424-005-1426-2.

Morley, S. J. *et al.* (2016) 'Acetylated tubulin is essential for touch sensation in mice', *eLife*, 5, pp. 1–25. doi: 10.7554/eLife.20813.

Munger, B. L., Pubols, L. M. and Pubols, B. H. (1971) 'The Merkel rete papilla - a slowly adapting sensory receptor in mammalian glabrous skin', *Brain Research*, 29(1), pp. 47–61. doi: 10.1016/0006-8993(71)90416-1.

Nirschl, J. J. *et al.* (2016) 'α-tubulin tyrosination and CLIP-170 phosphorylation regulate the initiation of dynein- driven transport in neurons', *Cell reports*, 14(11), pp. 2637–2652. doi: 10.1016/j.celrep.2016.02.046.

Nogales, E. *et al.* (1999) 'High-Resolution Model of the Microtubule', *Cell*, 96(1), pp. 79–88. doi: http://dx.doi.org/10.1016/S0092-8674(00)80961-7.

O'Hagan, R., Chalfie, M. and Goodman, M. B. (2005) 'The MEC-4 DEG/ENaC channel of Caenorhabditis elegans touch receptor neurons transduces mechanical signals', *Nat Neurosci*. Nature Publishing Group, 8(1), pp. 43–50. Available at: http://dx.doi.org/10.1038/nn1362.

Ohtomo, Y. *et al.* (2014) 'Evidence for biogenic graphite in early Archaean Isua metasedimentary rocks', *Nature Geosci*. Nature Publishing Group, 7(1), pp. 25–28. Available at: http://dx.doi.org/10.1038/ngeo2025.

Olausson, H. *et al.* (2002) 'Unmyelinated tactile afferents signal touch and project to insular cortex', *Nature Neuroscience*, 5(9), pp. 900–904. doi: 10.1038/nn896.

Paré, M., Smith, A. M. and Rice, F. L. (2002) ‘Distribution and terminal arborizations of cutaneous mechanoreceptors in the glabrous finger pads of the monkey.’, *The Journal of comparative neurology*, 445(4), pp. 347–59. Available at: http://www.ncbi.nlm.nih.gov/pubmed/11920712 (Accessed: 11 December 2016).

Penn, R. D. and Hagins, W. a (1972) ‘Kinetics of the photocurrent of retinal rods.’, *Biophysical journal*. Elsevier, 12(8), pp. 1073–94. doi: 10.1016/S0006-3495(72)86145-9.

Perozo, E., Cortes, D. M., *et al.* (2002) ‘Open channel structure of MscL and the gating mechanism of mechanosensitive channels’, *Nature*, 418(6901), pp. 942–948. doi: 10.1038/nature00992.

Perozo, E., Kloda, A., *et al.* (2002) ‘Physical principles underlying the transduction of bilayer deformation forces during mechanosensitive channel gating.’, *Nature structural biology*, 9(9), pp. 696–703. doi: 10.1038/nsb827.

Pickles, J. O., Comis, S. D. and Osborne, M. P. (1984) ‘Cross-links between stereocilia in the guinea pig organ of Corti, and their possible relation to sensory transduction’, *Hearing Research*, 15(2), pp. 103–112. doi: http://dx.doi.org/10.1016/0378-5955(84)90041-8.

Piperno, G., LeDizet, M. and Chang, X. J. (1987) ‘Microtubules containing acetylated alpha-tubulin in mammalian cells in culture.’, *Journal of Cell Biology*, 104(2), pp. 289–302. doi: 10.1083/jcb.104.2.289.

Poole, K. *et al.* (2014) ‘Tuning Piezo ion channels to detect molecular-scale movements relevant for fine touch’, *Nature Communications*. The Author(s), 5, p. 3520. Available at: http://dx.doi.org/10.1038/ncomms4520.

Prager-Khoutorsky, M., Khoutorsky, A. and Bourque, C. W. (2014) ‘Unique Interweaved Microtubule Scaffold Mediates Osmosensory Transduction via Physical Interaction with TRPV1’, *Neuron*. Elsevier Inc., 83(4), pp. 866–878. doi: 10.1016/j.neuron.2014.07.023.

Proske, U. and Gandevia, S. C. (2012) 'The Proprioceptive Senses: Their Roles in Signaling Body Shape, Body Position and Movement, and Muscle Force', *Physiological Reviews*, 92(4), p. 1651 LP-1697. Available at: http://physrev.physiology.org/content/92/4/1651.abstract.

Qi, Y. *et al.* (2015) 'Membrane stiffening by STOML3 facilitates mechanosensation in sensory neurons', *Nature Communications*. The Author(s), 6, p. 8512. Available at: http://dx.doi.org/10.1038/ncomms9512.

Rahman, F. *et al.* (2011) *Detection of acid-sensing ion channel 3 (ASIC3) in periodontal Ruffini endings of mouse incisors, Neuroscience Letters*. doi: 10.1016/j.neulet.2010.11.023.

Ranade, S. S. *et al.* (2014) 'Piezo2 is the major transducer of mechanical forces for touch sensation in mice', *Nature*. Nature Publishing Group, a division of Macmillan Publishers Limited. All Rights Reserved., 516(7529), pp. 121–125. Available at: http://dx.doi.org/10.1038/nature13980.

Reddy, A., Caler, E. V. and Andrews, N. W. (2001) 'Plasma membrane repair is mediated by Ca2+-regulated exocytosis of lysosomes', *Cell*, 106(2), pp. 157–169. doi: 10.1016/S0092-8674(01)00421-4.

Rexed, B. (1952) 'The cytoarchitectonic organization of the spinal cord in the cat', *The Journal of Comparative Neurology*, 96(3), pp. 415–495. doi: 10.1002/cne.900960303.

Robison, P. *et al.* (2016) 'Detyrosinated microtubules buckle and bear load in contracting cardiomyocytes', *Science*, 352(6284). Available at: http://science.sciencemag.org/content/352/6284/aaf0659.abstract.

Roll-Mecak, A. and McNally, F. J. (2010) 'Microtubule severing enzymes', *Current opinion in cell biology*, 22(1), p. 96. doi: 10.1016/j.ceb.2009.11.001.

Sharif Naeini, R. *et al.* (2006) 'An N-terminal variant of Trpv1 channel is required for osmosensory transduction', *Nature Neuroscience*, 9(1), pp. 93–98. doi: 10.1038/nn1614.

Shida, T. *et al.* (2010) ‘The major α-tubulin K40 acetyltransferase αTAT1 promotes rapid ciliogenesis and efficient mechanosensation’, *Proceedings of the National Academy of Sciences of the United States of America*. National Academy of Sciences, 107(50), pp. 21517–21522. doi: 10.1073/pnas.1013728107.

Simpson, G. G. (1949) *The meaning of evolution*. New Haven CT: Yale University Press.

Sivilotti, L. and Woolf, C. J. (1994) ‘The contribution of GABAA and glycine receptors to central sensitization: disinhibition and touch-evoked allodynia in the spinal cord’, *Journal of Neurophysiology*, 72(1), p. 169 LP-179. Available at: http://jn.physiology.org/content/72/1/169.abstract.

Steczkiewicz, K. *et al.* (2006) ‘Eukaryotic Domain of Unknown Function DUF738 Belongs to Gcn5-related N-acetyltransferase Superfamily’, *Cell Cycle*. Taylor & Francis, 5(24), pp. 2927–2930. doi: 10.4161/cc.5.24.3572.

Sudo, H. and Baas, P. W. (2010) ‘Acetylation of microtubules influences their sensitivity to severing by katanin in neurons and fibroblasts’, *The Journal of neuroscience : the official journal of the Society for Neuroscience*, 30(21), pp. 7215–7226. doi: 10.1523/JNEUROSCI.0048-10.2010.

Syeda, R. *et al.* (2015) ‘Chemical activation of the mechanotransduction channel Piezo1’, *eLife*, 4(MAY), pp. 1–11. doi: 10.7554/eLife.07369.

Szyk, A. *et al.* (2014) ‘Molecular Basis for Age-Dependent Microtubule Acetylation by Tubulin Acetyltransferase’, *Cell*, 157(6), pp. 1405–1415. doi: http://dx.doi.org/10.1016/j.cell.2014.03.061.

Takahashi-Iwanaga, H. (2000) ‘Three-dimensional microanatomy of longitudinal lanceolate endings in rat vibrissae’, *The Journal of Comparative Neurology*. John Wiley & Sons, Inc., 426(2), pp. 259–269. doi: 10.1002/1096-9861(20001016)426:2<259::AID-CNE7>3.0.CO;2-N.

Talbot, W. H. *et al.* (1968) ‘The sense of flutter-vibration: comparison of the human capacity with

response patterns of mechanoreceptive afferents from the monkey hand.', *Journal of Neurophysiology*, 31(2), p. 301 LP-334. Available at: http://jn.physiology.org/content/31/2/301.abstract.

Todd, A. J. (2010) 'Neuronal circuitry for pain processing in the dorsal horn', *Nat Rev Neurosci*. Nature Publishing Group, a division of Macmillan Publishers Limited. All Rights Reserved., 11(12), pp. 823–836. Available at: http://dx.doi.org/10.1038/nrn2947.

Topalidou, I. *et al.* (2012) 'Enzymatic and non-enzymatic activities of the tubulin acetyltransferase MEC-17 are required for microtubule organization and mechanosensation in C. elegans', *Current Biology*, 22(12), pp. 1057–1065. doi: 10.1016/j.cub.2012.03.066.

Torebjork, H. E., LaMotte, R. H. and Robinson, C. J. (1984) 'Peripheral neural correlates of magnitude of cutaneous pain and hyperalgesia: simultaneous recordings in humans of sensory judgments of pain and evoked responses in nociceptors with C-fibers', *Journal of Neurophysiology*, 51(2), p. 325 LP-339. Available at: http://jn.physiology.org/content/51/2/325.abstract.

Torebjörk, H. E. and Ochoa, J. L. (1980) 'Specific sensations evoked by activity in single identified sensory units in man.', *Acta physiologica Scandinavica*, 110(4), pp. 445–7. doi: 10.1111/j.1748-1716.1980.tb06695.x.

Tsubouchi, A., Caldwell, J. C. and Tracey, W. D. (2012) 'Dendritic Filopodia, Ripped Pocket, NOMPC, and NMDARs Contribute to the Sense of Touch in Drosophila Larvae', *Current Biology*, 22(22), pp. 2124–2134. doi: 10.1016/j.cub.2012.09.019.

Usoskin, D. *et al.* (2015) 'Unbiased classification of sensory neuron types by large-scale single-cell RNA sequencing', *Nat Neurosci*. Nature Publishing Group, a division of Macmillan Publishers Limited. All Rights Reserved., 18(1), pp. 145–153. Available at: http://dx.doi.org/10.1038/nn.3881.

Vásquez, V. (2009) 'A Structural Mechanism for MscS', 1210. doi: 10.1126/science.1159674.

Vriens, J., Nilius, B. and Voets, T. (2014) ‘Peripheral thermosensation in mammals’, *Nature Reviews Neuroscience*. Nature Publishing Group, 15(9), pp. 573–589. doi: 10.1038/nrn3784.

Walker, R. G., Willingham, A. T. and Zuker, C. S. (2000) ‘A Drosophila Mechanosensory Transduction Channel’, *Science*, 287(5461), p. 2229 LP-2234. Available at: http://science.sciencemag.org/content/287/5461/2229.abstract.

Wang, W. *et al.* (2008) ‘The Structure of an Open Form of an’, *Seven*, 1179(2008), pp. 1179–83. doi: 10.1126/science.1159262.

Wellnitz, S. A. *et al.* (2010) ‘The Regularity of Sustained Firing Reveals Two Populations of Slowly Adapting Touch Receptors in Mouse Hairy Skin’, *Journal of Neurophysiology*. Bethesda, MD: American Physiological Society, 103(6), pp. 3378–3388. doi: 10.1152/jn.00810.2009.

Westermann, S. and Weber, K. (2003) ‘Post-translational modifications regulate microtubule function’, *Nat Rev Mol Cell Biol*. Nature Publishing Group, 4(12), pp. 938–948. Available at: http://dx.doi.org/10.1038/nrm1260.

Wetzel, C. *et al.* (2007) ‘A stomatin-domain protein essential for touch sensation in the mouse’, *Nature*, 445(7124), pp. 206–209. Available at: http://dx.doi.org/10.1038/nature05394.

Woo, S.-H. *et al.* (2014) ‘Piezo2 is required for Merkel-cell mechanotransduction’, *Nature*. Nature Publishing Group, a division of Macmillan Publishers Limited. All Rights Reserved., 509(7502), pp. 622–626. Available at: http://dx.doi.org/10.1038/nature13251.

Woo, S.-H. *et al.* (2015) ‘Piezo2 is the principal mechanotransduction channel for proprioception’, *Nat Neurosci*. Nature Publishing Group, a division of Macmillan Publishers Limited. All Rights Reserved., 18(12), pp. 1756–1762. Available at: http://dx.doi.org/10.1038/nn.4162.

Woodbury, C. J. and Koerber, H. R. (2003) ‘Widespread projections from myelinated nociceptors throughout the substantia gelatinosa provide novel insights into neonatal hypersensitivity.’, *The*

Journal of neuroscience : the official journal of the Society for Neuroscience, 23(2), pp. 601–10. doi: 23/2/601 [pii].

Woodbury, C. J. and Koerber, H. R. (2007) 'Central and peripheral anatomy of slowly adapting type I low-threshold mechanoreceptors innervating trunk skin of neonatal mice.', *The Journal of comparative neurology*, 505(5), pp. 547–61. doi: 10.1002/cne.21517.

Wu, H., Williams, J. and Nathans, J. (2012) 'Morphologic diversity of cutaneous sensory afferents revealed by genetically directed sparse labeling', *eLife*, 2012(1), pp. 1–20. doi: 10.7554/eLife.00181.

Yan, Z. *et al.* (2013) 'Drosophila NOMPC is a mechanotransduction channel subunit for gentle-touch sensation', *Nature*. Nature Publishing Group, a division of Macmillan Publishers Limited. All Rights Reserved., 493(7431), pp. 221–225. Available at: http://dx.doi.org/10.1038/nature11685.

Yang, G. *et al.* (2015) 'Genetic targeting of chemical indicators in vivo', *Nat Meth*. Nature Publishing Group, a division of Macmillan Publishers Limited. All Rights Reserved., 12(2), pp. 137–139. Available at: http://dx.doi.org/10.1038/nmeth.3207.

Yasaka, T. *et al.* (2007) 'Cell-type-specific excitatory and inhibitory circuits involving primary afferents in the substantia gelatinosa of the rat spinal dorsal horn in vitro.', *J Physiol*, 581(Pt 2), pp. 603–618. doi: 10.1113/jphysiol.2006.123919.

Zelle, K. M. *et al.* (2013) 'The Genetic Architecture of Degenerin/Epithelial Sodium Channels in Drosophila', *G3: Genes|Genomes|Genetics*. Genetics Society of America, 3(3), pp. 441–450. doi: 10.1534/g3.112.005272.

Zhang, W. *et al.* (2013) 'Sound response mediated by the TRP channels NOMPC, NANCHUNG, and INACTIVE in chordotonal organs of Drosophila larvae', *Proceedings of the National Academy of Sciences of the United States of America*. National Academy of Sciences, 110(33), pp. 13612–

13617. doi: 10.1073/pnas.1312477110.

Zhang, W. *et al.* (2015) ‘Ankyrin Repeats Convey Force to Gate the NOMPC Mechanotransduction Channel.’, *Cell*, 162(6), pp. 1391–403. doi: 10.1016/j.cell.2015.08.024.

Zhang, Y. *et al.* (2002) ‘Identification of genes expressed in C. elegans touch receptor neurons’, *Nature*. Macmillian Magazines Ltd., 418(6895), pp. 331–335. Available at: http://dx.doi.org/10.1038/nature00891.

Zimmermann, K. *et al.* (2009) ‘Phenotyping sensory nerve endings in vitro in the mouse’, *Nature protocols*, 4(2), pp. 174–196. doi: 10.1038/nprot.2008.223.

Zotterman, Y. (1939) ‘Touch, pain and tickling: an electro-physiological investigation on cutaneous sensory nerves’, *The Journal of Physiology*, 95(1), pp. 1–28. Available at: http://www.ncbi.nlm.nih.gov/pmc/articles/PMC1393960/.

Zurborg, S. *et al.* (2011) ‘Generation and characterization of an Advillin-Cre driver mouse line’, *Molecular Pain*. BioMed Central, 7, p. 66. doi: 10.1186/1744-8069-7-66.

Zylka, M. J., Rice, F. L. and Anderson, D. J. (2005) ‘Topographically Distinct Epidermal Nociceptive Circuits Revealed by Axonal Tracers Targeted to Mrgprd’, *Neuron*, 45(1), pp. 17–25. doi: http://dx.doi.org/10.1016/j.neuron.2004.12.015.

10 **Appendix**

Publication arising from research.

1. Shane J Morley, Yanmei Qi, Loredana Iovino, Laura Andolfi, Da Guo, Nereo Kalebic, Laura Castaldi, Christian Tischer, Carla Portulano, Giulia Bolasco, Kalyanee Shirlekar, Claudia M Fusco, Antonino Asaro, Federica Fermani, Mayya Sundukova, Ulf Matti, Luc Reymond, Adele De Ninno, Luca Businaro, Kai Johnsson, Marco Lazzarino, Jonas Ries, Yannick Schwab, Jing Hu, Paul A Heppenstall. **Acetylated tubulin is essential for touch sensation in mice**. *eLife*, 2016; 5 DOI: 10.7554/eLife.20813

eLIFE elifesciences.org

RESEARCH ARTICLE

Acetylated tubulin is essential for touch sensation in mice

Shane J Morley[1,2†], Yanmei Qi[3†], Loredana Iovino[1,2], Laura Andolfi[4], Da Guo[3], Nereo Kalebic[1,5], Laura Castaldi[1], Christian Tischer[6], Carla Portulano[1], Giulia Bolasco[1], Kalyanee Shirlekar[1], Claudia M Fusco[1], Antonino Asaro[1], Federica Fermani[1], Mayya Sundukova[1], Ulf Matti[6], Luc Reymond[7], Adele De Ninno[8], Luca Businaro[8], Kai Johnsson[7], Marco Lazzarino[4], Jonas Ries[6], Yannick Schwab[6], Jing Hu[3*], Paul A Heppenstall[1,2*]

[1]EMBL Mouse Biology Unit, Monterotondo, Italy; [2]Molecular Medicine Partnership Unit (MMPU), Heidelberg, Germany; [3]Centre for Integrative Neuroscience, Tuebingen, Germany; [4]Istituto Officina dei Materiali-CNR, Trieste, Italy; [5]Max Planck Institute of Molecular Cell Biology and Genetics, Dresden, Germany; [6]European Molecular Biology Laboratory, Heidelberg, Germany; [7]Ecole Polytechnique Federale de Lausanne, Lausanne, Switzerland; [8]Consiglio Nazionale delle Ricerche, Rome, Italy

Abstract At its most fundamental level, touch sensation requires the translation of mechanical energy into mechanosensitive ion channel opening, thereby generating electro-chemical signals. Our understanding of this process, especially how the cytoskeleton influences it, remains unknown. Here we demonstrate that mice lacking the α-tubulin acetyltransferase Atat1 in sensory neurons display profound deficits in their ability to detect mechanical stimuli. We show that all cutaneous afferent subtypes, including nociceptors have strongly reduced mechanosensitivity upon Atat1 deletion, and that consequently, mice are largely insensitive to mechanical touch and pain. We establish that this broad loss of mechanosensitivity is dependent upon the acetyltransferase activity of Atat1, which when absent leads to a decrease in cellular elasticity. By mimicking α-tubulin acetylation genetically, we show both cellular rigidity and mechanosensitivity can be restored in Atat1 deficient sensory neurons. Hence, our results indicate that by influencing cellular stiffness, α-tubulin acetylation sets the force required for touch.
DOI: 10.7554/eLife.20813.001

***For correspondence:** jing.hu@cin.uni-tuebingen.de (JH); paul.heppenstall@embl.it (PAH)

[†]These authors contributed equally to this work

Competing interests: The authors declare that no competing interests exist.

Funding: See page 23

Received: 20 August 2016
Accepted: 29 November 2016
Published: 13 December 2016

Reviewing editor: Matthias Kneussel, Germany

© Copyright Morley et al. This article is distributed under the terms of the Creative Commons Attribution License, which permits unrestricted use and redistribution provided that the original author and source are credited.

Introduction

Mechanical forces acting upon cells or tissues are propagated into the opening of mechanically gated ion channels such as Piezo2 as the first step in the sense of touch (***Abraira and Ginty, 2013***; ***Maksimovic et al., 2014***; ***Ranade et al., 2014***; ***Woo et al., 2014***). In many cases this process occurs through direct interplay of ion channels with the lipid bilayer. For example, the bacterial mechano-transduction channel MscS (***Sukharev, 2002***) and eukaryotic two-pore-domain potassium channels TRAAK and TREK1 (***Brohawn et al., 2014a***, ***2012***, ***2014b***; ***Lolicato et al., 2014***) are fully activated by mechanical stimuli when reconstituted in reduced membrane systems, and the mechanosensitive ion channel Piezo1 is also likely to be gated by force exerted via lipids due to its exceptional sensitivity to membrane tension (***Cox et al., 2016***; ***Lewis and Grandl, 2015***). However, in-vivo, membrane ion channels are not isolated from the cytoplasm and extracellular matrix, and mechanical sensitivity may depend on further interaction with other cellular components such as the underlying cytoskeleton to modify and redistribute membrane tension (***Delmas et al., 2011***; ***Krieg et al., 2015***; ***Qi et al., 2015***). Indeed, in *Drosophila*, NompC ion channels were shown to be linked between the

plasma membrane and microtubules by a tether protein domain in the N-terminus of the channel, and this linkage is essential for mechanosensitivity of the channel (**Zhang et al., 2015**). Moreover, in *C. elegans* touch sensitivity of specialized touch receptor neurons is dependent on both the actin binding protein β spectrin (**Krieg et al., 2014**) and the microtubule cytoskeleton (**Bounoutas et al., 2009**).

A feature of *C. elegans* touch receptor neurons is that their axons are filled with specialized cross-linked bundles of heavily acetylated 15-protofilament microtubules (**Chalfie and Thomson, 1982**). Disruption of the molecular components of these microtubules, MEC7 β-tubulin and MEC12 α-tubulin leads to a loss of mechanical sensitivity (**Bounoutas et al., 2009**; **Fukushige et al., 1999**). Moreover, mutation of MEC17, the major tubulin acetyltransferase (**Akella et al., 2010**; **Shida et al., 2010**) also reduces touch sensitivity in *C. elegans* (**Cueva et al., 2012**; **Topalidou et al., 2012**; **Zhang et al., 2002**). Of note, it is not clear whether this loss of touch sensitivity stems from the absence of tubulin acetylation in MEC17 mutants (**Shida et al., 2010**) or from other unknown actions of MEC17 (**Akella et al., 2010**; **Davenport et al., 2014**; **Fukushige et al., 1999**; **Topalidou et al., 2012**).

MEC17 functions to transfer an acetyl group to the lysine 40 (K40) residue on the luminal side of microtubules (**Szyk et al., 2014**), and this post-translation modification is remarkably well conserved in organisms that have cells with cilia (**Shida et al., 2010**). Intriguingly, Atat1, the mammalian orthologue of MEC17, is expressed ubiquitously in all mouse peripheral sensory neurons (**Kalebic et al., 2013a**), and these neurons have amongst the highest level of α-tubulin acetylation in the mouse (**Kalebic et al., 2013b**). This raises the question as to whether acetylated microtubules also have an essential function in mouse sensory neurons, and if yes, how, mechanistically they influence mechanosensation.

In this study, we investigated the contribution of microtubule acetylation to mammalian mechanosensation by conditionally deleting Atat1 from mouse peripheral sensory neurons. We found that Atat1^{cKO} mice display a profound loss of mechanical sensitivity to both light touch and painful stimuli with no impact on other sensory modalities. We demonstrate that this arises from a reduction in mechanosensitivity of all cutaneous afferent subtypes, including nociceptors, and adecreased mechanically activated currents in sensory neurons upon Atat1 deletion. We further establish that this broad loss of mechanosensitivity is dependent upon the acetyltransferase activity of Atat1, and that by mimicking α-tubulin acetylation genetically, mechanosensitivity can be restored in Atat1 deficient sensory neurons. Finally we show that acetylated microtubules localize to a prominent band under the membrane of sensory neuron cell bodies and axons, and in the absence of Atat1 and acetylated α-tubulin, cultured sensory neurons display significant reductions in their cell elasticity. Our results indicate that the microtubule cytoskeleton is an essential component of the mammalian mechanotransduction complex and that by influencing cellular stiffness, α-tubulin acetylation can tune mechanical sensitivity across the full range of mechanoreceptor subtypes.

Results

Atat1^{cKO} mice display reduced sensitivity to innocuous touch and pain

To investigate cell autonomous effects of Atat1 disruption in sensory neurons we took a conditional gene deletion strategy. *Atat1*$^{fl/+}$ mice (**Kalebic et al., 2013b**) were crossed with a sensory neuron specific Cre driver line *Avil*-Cre (**Zurborg et al., 2011**) to generate *Avil*-Cre::*Atat1*$^{fl/fl}$ (referred to as Atat1^{cKO}) and control *Avil*-Cre::*Atat1*$^{fl/+}$ mice (referred to as Atat1^{Control}). Mice were then subjected to a series of behavioural assays. We first tested their ability to detect an innocuous mechanical stimulus applied to the hairy skin. Adhesive tape was fixed gently to the backs of animals and the number of responses counted over a 5 min observation period. While control mice made regular attempts to remove the tape, Atat1^{cKO} mice effectively ignored the tape for much of the time, and the total number of responses was significantly lower ($p<0.05$) (**Figure 1a**, **Video 1**). We next investigated the sensitivity of mice to innocuous mechanical stimuli applied to the glabrous skin by lightly stroking the underside of the paw with a diffuse cotton swab. Again, Atat1^{cKO} mice responded significantly less ($p<0.01$) to this stimulus than Atat1^{Control} mice (**Figure 1b**). We also examined whether mechanical sensitivity to punctate stimuli was altered in Atat1^{cKO} mice by applying von Frey filaments of calibrated forces to the hindpaw of mice. Control animals responded to

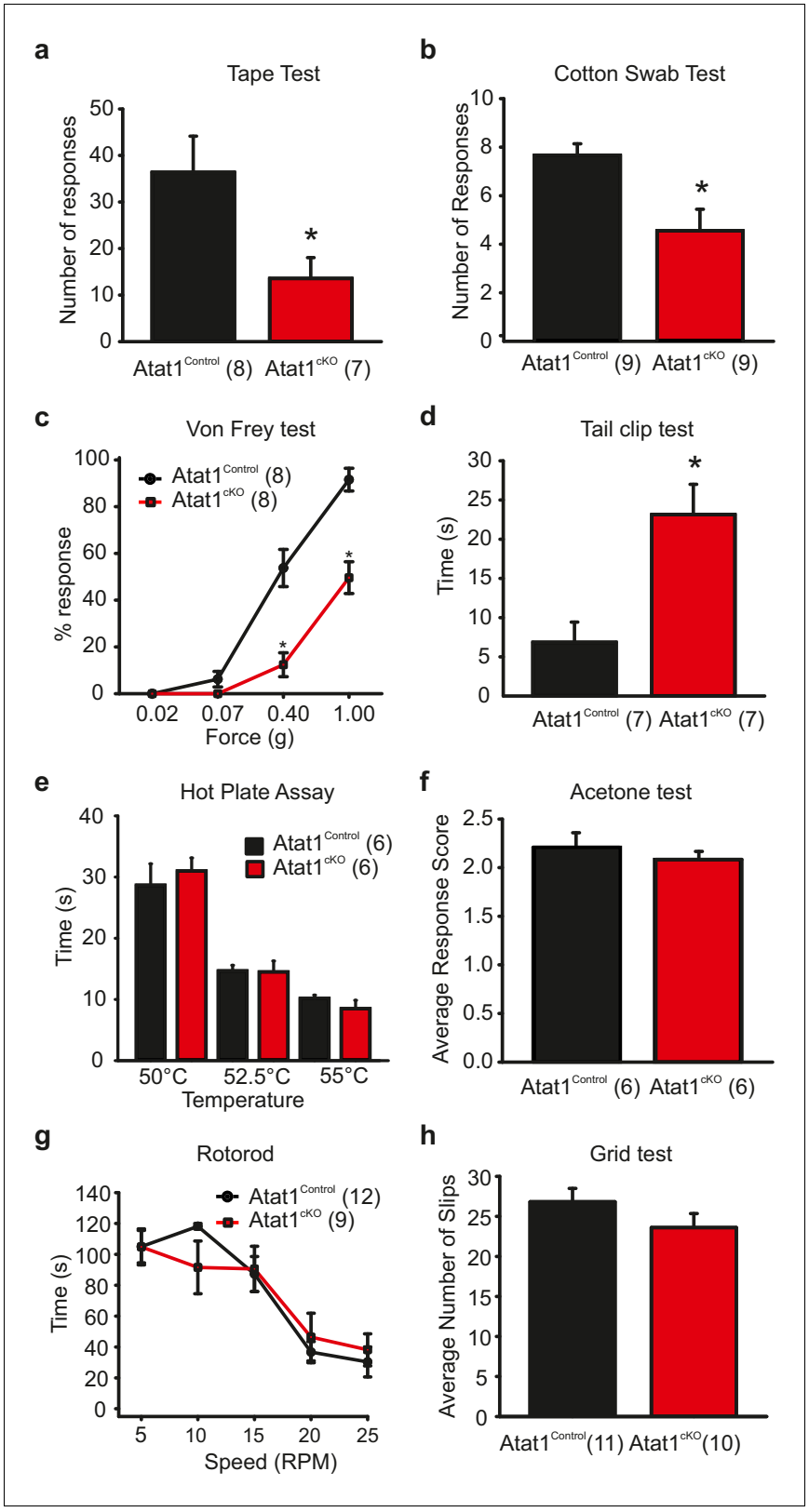


Figure 1. Behavioural analysis of Atat1^{cKO}mice. (**a**) Bar-chart summarising the results of a tape test to assay low threshold mechanosensation. Atat1^{cKO} mice demonstrated significantly less response events over the 5 min counting period (t-Test, $p<0.05$). (**b**) Results from the cotton swab analysis assaying low threshold mechanosensation. Atat1^{cKO} mice demonstrated significantly less response events then Atat1^{Control} counterparts

Figure 1 continued on next page

Figure 1 continued

(t-Test, $p<0.01$). (**c**) Graph of von Frey thresholds showing the significantly lower response frequency in $Atat1^{cKO}$ animals (Two-way RM ANOVA, Holm-Sidak method, $p<0.001$). (**d**) Bar-chart showing latency to a clip attached to the base of the tail. $Atat1^{cKO}$ animals take significantly longer to respond to the stimulus (t-Test, $p<0.01$). (**e**) No significant differences in the responses recorded to noxious heat between $Atat1^{cKO}$ and $Atat1^{Control}$ animals (t-Test, $p>0.05$). (**f**) No significant difference in cold response was observed using the acetone drop assay (t-Test, $p>0.05$) (**g**), No significant difference in motor performance as assayed using the Rotarod test (Two-Way RM ANOVA, Holm-Sidak method, $p>0.05$) and (**h**), No significant difference was observed in the average number of slips between the genotypes during the grid test (t-Test, $p>0.05$). Error bars indicate s.e.m.

DOI: 10.7554/eLife.20813.002

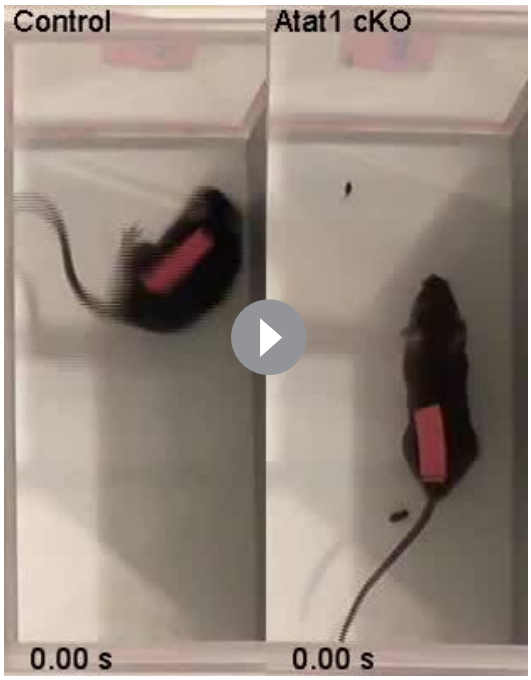
The following figure supplement is available for figure 1:

Figure supplement 1. Behavioral analysis of $Atat1^{cKO}$ mice.

DOI: 10.7554/eLife.20813.003

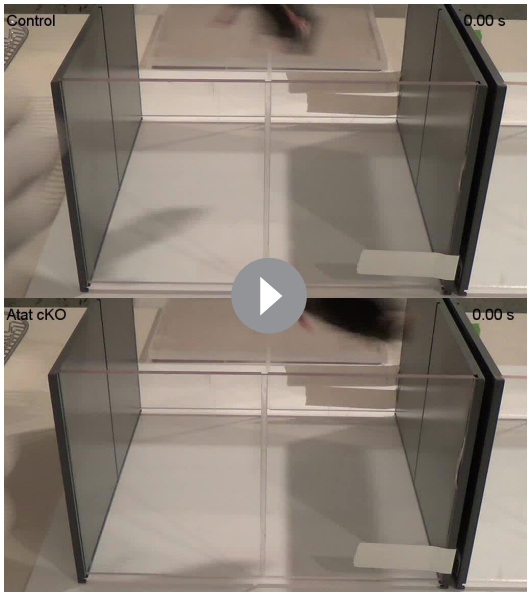
forces as low as 0.07g with an increase in detection into the noxious range. However, $Atat1^{cKO}$ mice required significantly higher forces to evoke a response throughout the range of von-Frey filaments (median threshold 0.4g for $Atat1^{Control}$ and 1g for $Atat1^{cKO}$ $p=0.003$, Mann-Whitney test) (***Figure 1c***). To investigate noxious mechanical sensitivity in more detail, we analysed responses to a clip applied to the base of the tail. $Atat1^{cKO}$ mice displayed substantially longer response latencies to the clip compared to $Atat1^{Control}$ mice and again, essentially ignored this noxious stimulus ($p<0.01$) (***Figure 1d***, ***Video 2***). We further tested whether thermal detection was effected by Atat1 deletion by measuring responses to noxious heat or to evaporative cooling. We observed no difference in withdrawal latencies to a range of temperatures in the hotplate test between $Atat1^{cKO}$ and $Atat1^{Control}$ mice (***Figure 1e***) or to tail immersion in a hot water bath (***Figure 1—figure supplement 1***). Similarly, sensitivity to cooling of the paw with acetone was comparable in $Atat1^{cKO}$ and $Atat1^{Control}$ mice (***Figure 1f***). Finally we assessed the motor coordination and of $Atat1^{cKO}$ mice by evaluating their performance on a rotarod device or on a raised metal grid. $Atat1^{cKO}$ and $Atat1^{Control}$ mice displayed similar latencies to fall from the rotating drum across all speeds tested (***Figure 1g***) and a similar number of slips from the grid (***Figure 1h***). Thus, Atat1 is required for the detection of innocuous and noxious mechanical touch but not for noxious heat or proprioceptive coordination.

We further assessed the efficiency of Cre mediated recombination of the floxed *Atat1* allele in sensory neurons, and the suitability of using heterozygote *Avil*-Cre::$Atat1^{fl/+}$ mice as controls, by examining behavioural sensitivity to innocuous and noxious mechanical stimuli in full *Atat1* knockout mice ($Atat1^{-/-}$) and wildype mice. In both the tape test and tail clip test, $Atat1^{cKO}$ mice performed similarly to $Atat1^{-/-}$ mice, and $Atat1^{Control}$ mice behaved comparably to wild-type (***Figure 1—figure supplement 1***). Thus in line with previous reports Avil-Cre mediated deletion is efficient and Cre expression has no apparent effect on sensory driven behaviour (***Zurborg et al., 2011***).



Video 1. Tape test assay. Video recording of mice showing attempts to remove a piece of tape by $Atat1^{Control}$ (left) and $Atat1^{cKO}$ (right), over a 5 min period.

DOI: 10.7554/eLife.20813.004



Video 2. Tail clip assay. Video of Atat1^{Control} (top) and Atat1^{cKO} (bottom) mice to measure the time taken until the first response of the animals to the clip.
DOI: 10.7554/eLife.20813.005

Atat1^{cKO} mice display reduced mechanosensitivity across all mechanoreceptor subtypes innervating the skin

Sensory neuron axons terminate in the skin and form a diverse range of functionally distinct mechanoreceptors that underlie the sense of touch (***Abraira and Ginty, 2013***). They can be classified by their conduction velocity (into Aβ, Aδ and C fibres), their adaptation properties (into rapidly adapting or slowly adapting) and by their mechanical thresholds (into mechanoreceptors and mechanonociceptors). To determine whether the profound loss of mechanical sensitivity to both light touch and painful stimuli is due to the deficit in of each of these populations, we utilized an ex vivo skin-nerve preparation to record from single cutaneous sensory neurons in the saphenous nerve.

We first considered low threshold Aβ and Aδ fibres, separating them into slowly adapting (SAM) and rapidly adapting (RAM) Aβ mechanoreceptors, and Aδ D-hairs. We observed a striking reduction in the mechanical sensitivity of SAM fibres that was apparent as a reduced number of action potentials per stimulus indentation (***Figure 2a and b***, ***Figure 2—figure supplement 1***) and a ~10-fold increase in the latency of the response (***Figure 2—figure supplement 1***) in Atat1^{cKO} mice. Reductions in firing frequencies were evident during both the ramp phase (***Figure 2a***) of the mechanical stimulus and during the static phase (***Figure 2b***). RAM fibres displayed a similar reduction in their stimulus response function (***Figure 2c***, and ***Figure 2—figure supplement 2***) and an increased latency to the highest displacement stimulus (***Figure 2—figure supplement 2***). A characteristic of these fibres is that they display higher firing frequencies with increasing stimulus speed (***Milenkovic et al., 2008***), a feature which was also reduced in Atat1^{cKO} mice (***Figure 2d*** and ***Figure 2—figure supplement 2***). D-hairs also displayed significant reductions in their stimulus response function (***Figure 2e*** and ***Figure 2—figure supplement 3***), as well as longer latencies for mechanical activation (***Figure 2—figure supplement 3***), and decreased sensitivity to dynamic stimuli (***Figure 2f*** and ***Figure 2—figure supplement 3***) in Atat1^{cKO} mice. Electrical thresholds and conduction velocities were unchanged in low threshold Aβ and Aδ fibres in the absence of Atat1 (***Figure 2—figure supplements 1–3***).

We next examined high threshold nociceptive fibres which can be classified by their conduction velocities into Aδ-mechanonociceptors (AM) and C-fibre mechanonociceptors. Similar to low threshold fibres, both populations of nociceptor exhibited a reduced number of action potentials evoked by indentation (AM units: ***Figure 3a and b***, ***Figure 3—figure supplements 1*** and ***2***), longer latencies for mechanical activation (***Figure 3—figure supplements 1*** and ***2***) and no change in electrical thresholds and conduction velocities in the absence of Atat1 (***Figure 3—figure supplements 1*** and ***2***). Mechanical thresholds to von Frey stimuli were also elevated in C-fibre nociceptors (***Figure 3—figure supplement 2***) highlighting the strength of the phenotype in this population. Finally, we analysed heat responsiveness of C-fibre nociceptors in Atat1^{Control} and Atat1^{cKO} mice. We observed no difference between genotypes in the proportion of C-fibres responding to heat, or in their activation thresholds and firing rate in response to a heat stimulus (***Figure 3—figure supplement 3***). Thus collectively, these data indicate that Atat1 is specifically required for mechanical sensitivity across all major fibre types innervating the skin.

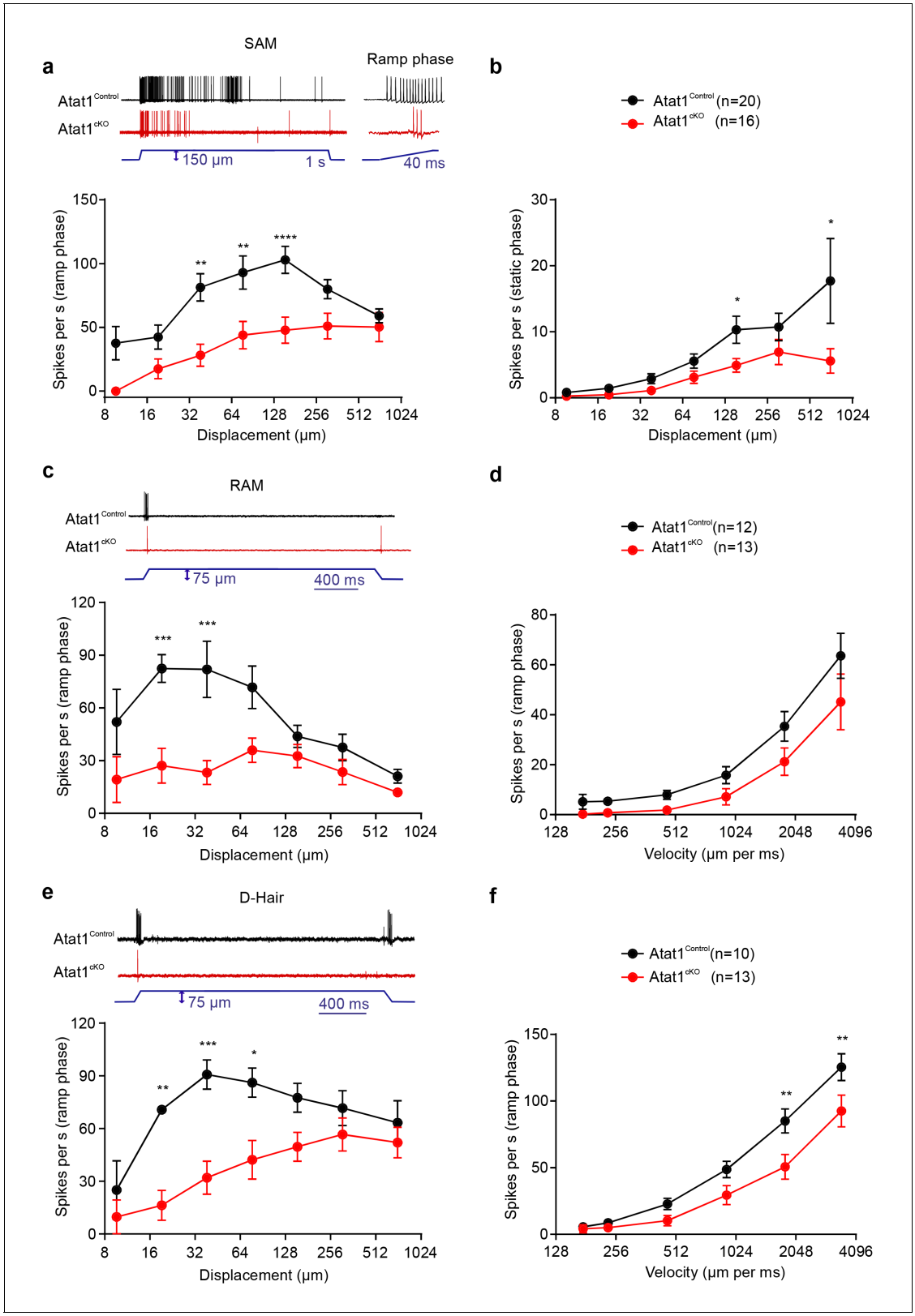


Figure 2. αTAT1 is required for mechanosensitivity of low threshold mechanoreceptors. Slowly adapting mechanoreceptor fibers (SAM): Typical responses (top) and stimulus-response functions (bottom) to increasing displacement for the ramp (**a**) and static (**b**) phase (two-way ANOVA with *post-hoc* Bonferroni's test, ramp phase: $p<0.0001$; static phase: $p<0.001$). Rapidly adapting mechanoreceptor fibers (RAM): Typical responses (top) and stimulus-response functions (bottom) to increasing displacement (**c**) and velocity (**d**) (two-way ANOVA with *post-hoc* Bonferroni's test, displacement:

Figure 2 continued on next page

Figure 2 continued

p<0.0001; velocity: p<0.001). D-hair afferents: Typical responses (top) and stimulus-response functions (bottom) to increasing displacement (**e**) and velocity (**f**) (two-way ANOVA with *post-hoc* Bonferroni's test, displacement: p<0.0001; velocity: p<0.0001). The number of fibres recorded is indicated in parentheses in each panel. *p<0.05; **p<0.01; ***p<0.001; ****p<0.0001. Error bars indicate s.e.m.

DOI: 10.7554/eLife.20813.006

The following figure supplements are available for figure 2:

Figure supplement 1. Electrical excitability and stimulus response properties of SAM fibres in Atat1^{Control} and Atat1^{cKO} mice.

DOI: 10.7554/eLife.20813.007

Figure supplement 2. Electrical excitability and stimulus response properties of RAM fibres in Atat1^{Control} and Atat1^{cKO} mice.

DOI: 10.7554/eLife.20813.008

Figure supplement 3. Electrical excitability and stimulus response properties of D-hair fibres in Atat1^{Control} and Atat1^{cKO} mice.

DOI: 10.7554/eLife.20813.009

Morphological analysis of the peripheral nervous system in Atat1^{cKO} mice

The absence of Atat1 could potentially have wide-ranging effects on the development, morphology and structure of peripheral sensory neurons, each of which could contribute to a loss of mechanosensitivity. We thus performed a systematic analysis of the organization of the peripheral nervous system upon deletion of Atat1. We first tested whether the number of sensory neurons and their innervation of the skin and spinal cord were affected by deletion of Atat1. We observed no change in the number of myelinated and unmyelinated fibres in the saphenous nerve (***Figure 4a–d***), in the number, density, or organization of terminal endings in the skin (***Figure 4e–h***), or in the innervation of the spinal cord by CGRP, IB4 and NF200 positive sensory neurons (***Figure 4m–p*** and ***Figure 4—figure supplement 1***). We next examined axonal outgrowth and neurotrophin/receptor transport in sensory neurons. In whole mount DRG explants supported in the presence of NGF we detected no difference in the growth rate or length of axons in DRG from Atat1^{Control} and Atat1^{cKO} mice (***Figure 4i–k***). Moreover, single molecule imaging of NGF/receptor transport in a microfluidic device revealed that the displacement and velocity of quantum dot labelled NGF molecules (***Sung et al., 2011***), was not altered in the absence of Atat1 (***Figure 4l***, ***Figure 3—figure supplement 2*** and ***Video 3***). Taken together with electrophysiological analysis, these data indicate that the loss of mechanosensitivity is not due to generalized effects on neuronal function but rather arises from defects in the ability of sensory neurons to transduce mechanical forces into electrical signals.

Deficits in mechanically activated currents in DRG neurons from Atat1^{cKO} mice

To determine how deletion of Atat1 influences mechanotransduction in sensory neurons we recorded mechanosensitive currents from cultured DRG neurons indented with a blunt glass probe. Such a stimulus can evoke mechanically gated currents in ~90% of DRG neurons that are further classified as rapidly adapting (RA), intermediate-adapting (IA) and slowly adapting (SA) responses (***Hu and Lewin, 2006***). In the absence of Atat1, we observed a marked loss in the number of mechanically sensitive neurons evoked by cell prodding that was evident across each subtype of current (***Figure 5a***). Furthermore, the small proportion of neurons which still displayed mechanosensitive currents in Atat1^{cKO} mice exhibited significantly reduced current amplitudes and higher thresholds (***Figure 5b–d***, ***Figure 5—figure supplement 1***), but no difference in their activation kinetics (***Figure 5—figure supplement 1***). Other functional parameters such as voltage gated channel activity, resting membrane potential, action potential threshold, and sensitivity to capsaicin or pH were indistinguishable between Atat1^{Control} and Atat1^{cKO} mice (***Figure 5—figure supplements 2*** and ***3***). We also examined perimembrane dynamics of the mechanosensitive ion channel Piezo2 in the absence of Atat1, and observed no difference in Fluorescence Recovery After Bleaching (FRAP) of a Piezo2-GFP fusion construct transfected into dissociated neurons (***Figure 5—figure supplement 4***). Thus the reduced mechanical sensitivity of DRG neurons in Atat1^{cKO} mice does not arise from compromised membrane properties in these cells or defects in mechanosensitive ion channel trafficking.

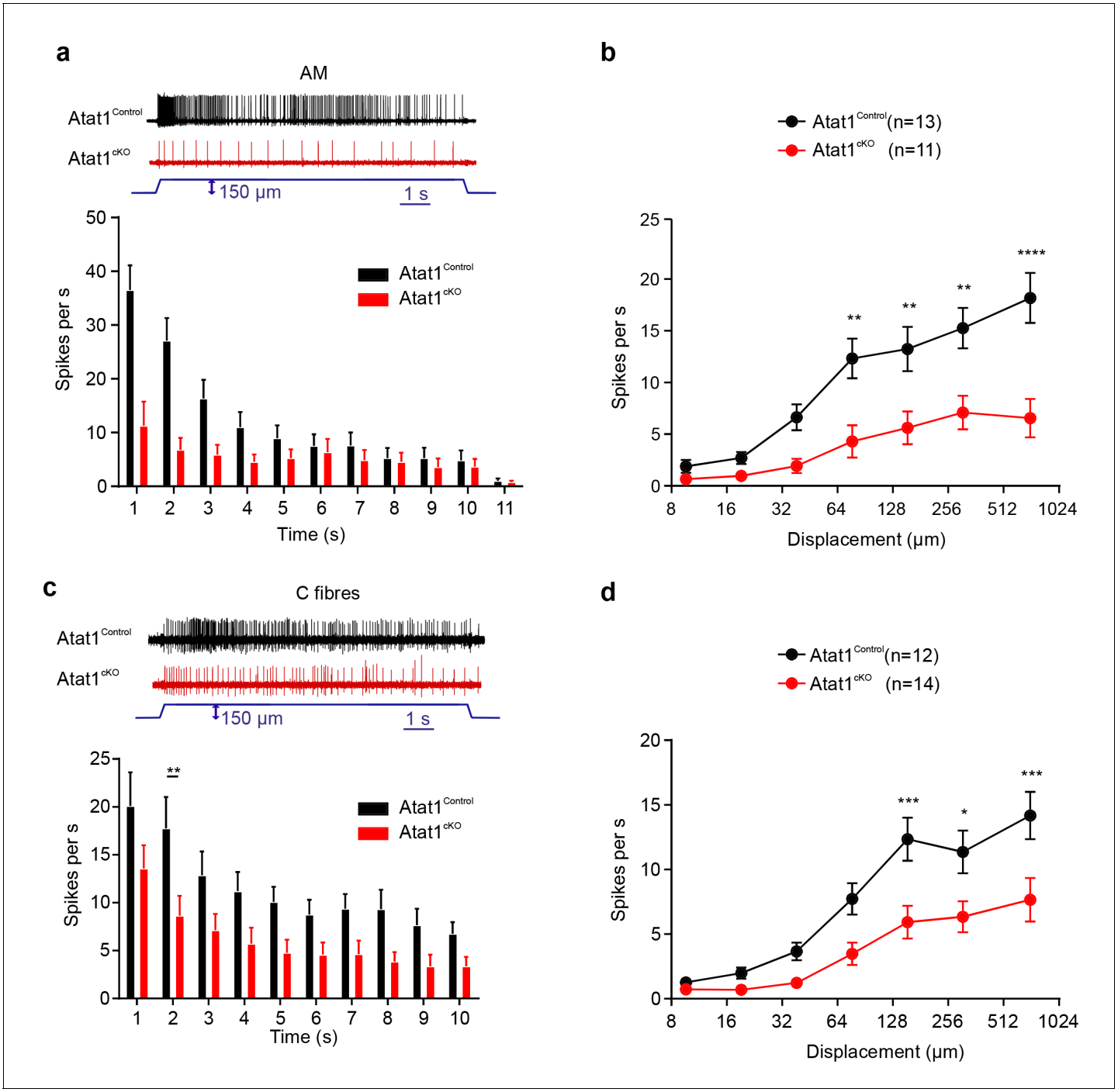


Figure 3. αTAT1 is required for mechanosensitivity of nociceptors. Typical responses (top) and mean discharge rates (1 s bins) during 10 s 150 µm stimulus of Aδ-mechanonociceptors (AM) (**a**) and C-fibre nociceptors (**c**) from $\alpha TAT1^{control}$ and $\alpha TAT1^{cko}$ mice (two-way ANOVA with *post-hoc* Bonferroni's test, AM: p<0.05; C-fibre: p<0.0001). (**b**) Stimulus-response functions (bottom) to increasing displacement for AM (**b**) and C-fibre nociceptors (**d**) (two-way ANOVA with *post-hoc* Bonferroni's test, AM: p<0.0001; C-fibre: p<0.0001). The number of fibres recorded is indicated in parentheses in each panel. *p<0.05; **p<0.01; ***p<0.001; ****p<0.0001. Error bars indicate s.e.m.

DOI: 10.7554/eLife.20813.010

The following figure supplements are available for figure 3:

Figure supplement 1. Electrical excitability and stimulus response properties of AM fibres in $Atat1^{Control}$ and $Atat1^{cKO}$ mice.

DOI: 10.7554/eLife.20813.011

Figure supplement 2. Electrical excitability and stimulus response properties of C fibres in $Atat1^{Control}$ and $Atat1^{cKO}$ mice.

DOI: 10.7554/eLife.20813.012

Figure 3 continued on next page

Figure 3 continued

Figure supplement 3. Heat response of C fibers in Atat1^{Control} and Atat1^{cKO} mice.
DOI: 10.7554/eLife.20813.013

Genetically mimicking α-tubulin acetylation restores mechanosensitivity of Atat1^{cKO} sensory neurons

We next asked whether the reduction in mechanosensitivity observed in Atat1^{cKO} mice is dependent upon the α-tubulin acetyltransferase activity of Atat1 by testing if mechanically activated current properties could be re-established to control levels by expression of exogenous cDNAs. As a positive control we determined that transfection of an Atat1-YFP construct rescued mechanosensitivity in Atat1^{cKO} cultures and that the proportion of RA, IA and SA responses across the DRG returned to control levels (***Figure 5e***). We subsequently transfected a catalytically inactive form of Atat1 (termed Atat1-GGL) that has no acetyltransferase activity but remains functional (***Kalebic et al., 2013a***). Expression of Atat1-GGL did not restore mechanosensitivity in Atat1^{cKO} neurons, and we observed no difference in the proportion of different types of mechanically activated current compared to mock EGFP transfection (***Figure 5e***). Thus the acetyltransferase activity of Atat1 is required for normal mechanical sensitivity of DRG neurons.

Atat1 has also been demonstrated to acetylate other substrates in addition to α-tubulin (***Castro-Castro et al., 2012***). Therefore, to determine whether α-tubulin acetylation underlies the mechanosensory phenotype in Atat1^{cKO} mice, we transfected a K40Q point mutant of α-tubulin that genetically mimics α-tubulin lysine 40 acetylation. Expression of K40Q α-tubulin rescued mechanosensitivity of Atat1^{cKO} DRG neurons to Atat1^{Control} levels, while a charge conserving control mutation (K40R) had no significant effect (***Figure 5f***). Collectively these data strongly indicate that the acetyltransferase activity of Atat1 modulates mechanosensitivity and that acetylated α-tubulin is the likely effector.

Cytoskeletal organization in sensory neurons from Atat1^{cKO} mice

A recent study has demonstrated that the mechanosensitivity of hypothalamic osmosensory neurons is dependent upon a unique interweaved organization of microtubules in these cells (***Prager-Khoutorsky et al., 2014***). We therefore asked whether a similar structure is also evident in peripheral sensory neurons and whether it is dependent upon the presence of acetylated α-tubulin. We performed superresolution dSTORM (direct stochastic optical reconstruction microscopy)(microscopy on DRG neurons stained with α-tubulin antibodies, and indeed observed that microtubules form an interweaved network in all neurons examined, especially towards the centre of the cell (***Figure 6a and b***). However, we were unable to detect clearly visible differences in organization between Atat1^{Control} and Atat1^{cKO} sensory neurons (***Figure 6a and b***). To assay this more quantitatively we subjected superresolution images to an unbiased automated analysis (***Figure 6c–f***). We observed no difference in microtubule density (***Figure 6g***), the number of microtubule crossing points (***Figure 6h***), or the angular variance of the microtubule cytoskeleton (***Figure 6i***) in any neuron between Atat1^{Control} and Atat1^{cKO} mice indicating that acetylation does not influence the gross organization of the microtubule network. To investigate whether the absence of microtubule acetylation could indirectly impact upon the actin cytoskeleton, we also performed phalloidin staining on DRG neurons. Again we did not detect any difference in the organization of the actin network upon deletion of Atat1 (***Figure 6—figure supplement 1***).

Acetylated tubulin localizes to a prominent submembrane band in peripheral sensory neurons

We next investigated the contribution of acetylated tubulin to mechanosensitivity by examining the distribution of acetylated microtubules in sensory neurons. Strikingly, we observed that acetylated α-tubulin was concentrated in a band directly under the plasma membrane in cultured DRG neurons that was evident in 80 ± 5% of neurons (***Figure 7a*** and ***Figure 6—figure supplement 1***), while total α-tubulin was distributed evenly across the cytoplasm of all cells (***Figure 7b***). Importantly, this band was not present in non-mechanosensory cells such as serum-starved fibroblasts where acetylated α-

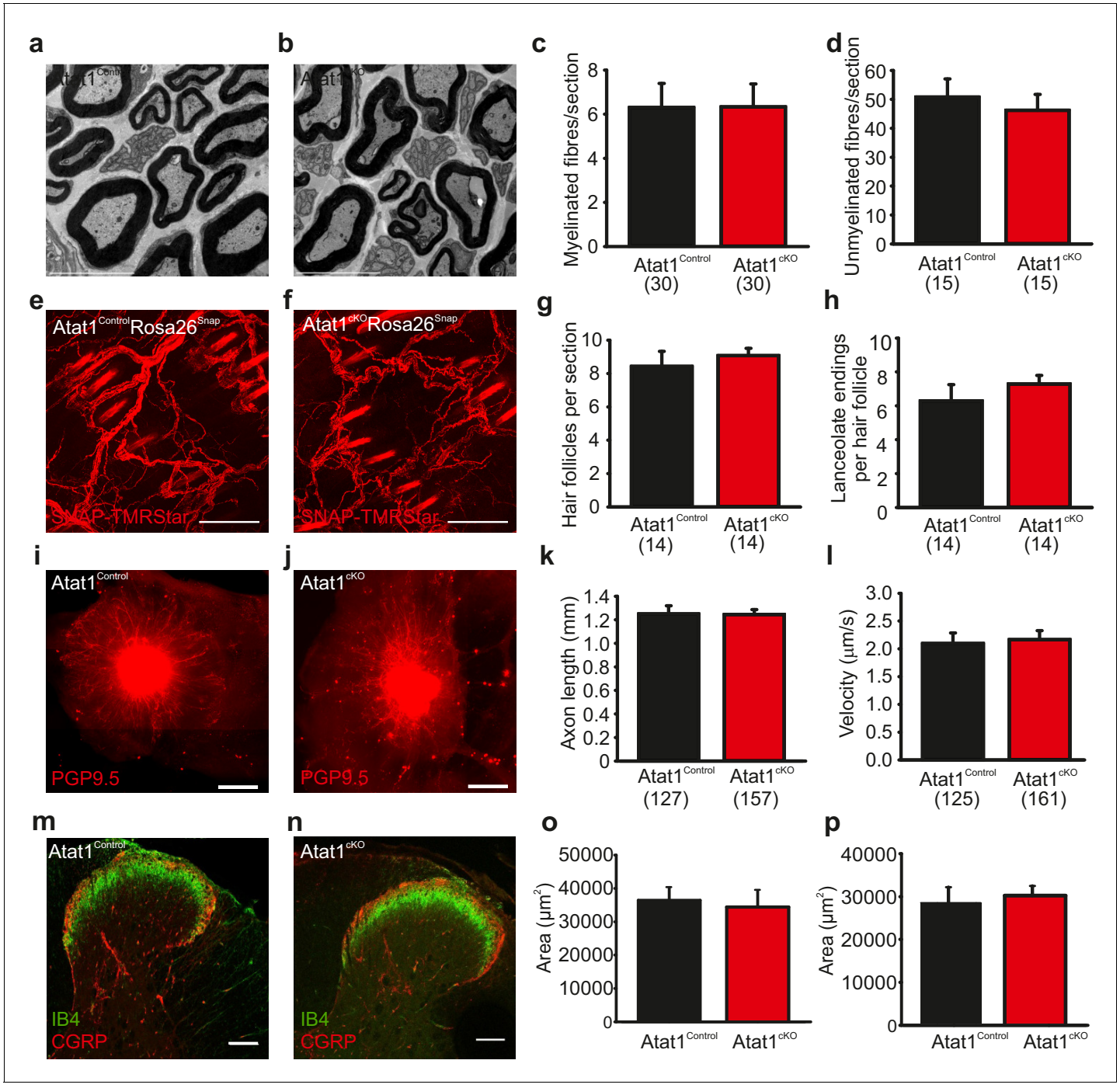


Figure 4. Morphological analysis of the peripheral nervous system in Atat1^{cKO} mice. (**a** and **b**) Electron micrographs of a sectioned saphenous nerve from an Atat1^{Control} (**a**) and Atat1^{cKO} (**b**) mouse (Scale bar 5 µm). (**c** and **d**) Graph summarizing the number of myelinated fibres (**c**) and unmyelinated fibres (**d**) from saphenous nerve sections. No significant difference was noted between the samples (t-Test, p>0.05). (**e** and **f**) Fluorescent image of skin taken from the finger of an Atat1^{Control}::Rosa26^{Snap} mouse (**e**) and Atat1^{cKO}::Rosa26^{Snap} mouse (**f**) labelled with SNAP-TMR Star (Scale bar 100 µm). (**g** and **h**) Bar-chart showing the number of innervated hair follicles (**g**) and lanceolate endings per hair follicle (**h**) in skin taken from the digits of Atat1^{Control}::Rosa26^{Snap} and Atat1^{cKO}::Rosa26^{Snap} animals. No significant difference was observed between the genotypes (t-Test, p>0.05). (**i** and **j**) Mosaic image of PGP9.5 stained whole mount DRG after seven days in culture from Atat1^{Control} (**i**) and Atat1^{cKO} (**j**) mice (Scale bar 500 µm). (**k**) Bar-chart showing the length of axonal outgrowths after 7 days of culture. No significant difference was observed in Atat1^{Control} and Atat1^{cKO} DRG (t-Test, p>0.05). (**l**) Single molecule tracking of NGF molecules in neurites from Atat1^{Control} and Atat1^{cKO} DRG grown in microfluidic devices. Graph showing the average instantaneous velocity for NGF coupled quantum dots. No significant difference in NGF transport was observed between the genotypes (t-Test, p>0.05). (**m** and **n**) Confocal images of sectioned spinal cord dorsal horn from Atat1^{Control} (**m**) and Atat1^{cKO} (**n**) stained with IB4 (green) and CGRP

Figure 4 continued on next page

Figure 4 continued

(red) antibody respectively (Scale bar 100 μm). (**o**) Bar-chart showing the size of the area stained with IB4. No significant difference was observed in the size of the area between Atat1^{Control} and Atat1^{cKO} spinal cord (t-Test, p>0.05). (**p**) Bar-chart showing the size of the area stained with a CGRP antibody. No significant difference was observed in the size of the area between Atat1^{Control} and Atat1^{cKO} spinal cord (t-Test, p>0.05). Error bars indicate s.e.m.

DOI: 10.7554/eLife.20813.014

The following figure supplements are available for figure 4:

Figure supplement 1. Spinal cord staining in Atat1^{Control} and Atat1^{cKO} mice.

DOI: 10.7554/eLife.20813.015

Figure supplement 2. Axonal transport in DRG neurons from Atat1^{cKO} mice.

DOI: 10.7554/eLife.20813.016

tubulin was found throughout the microtubule network (***Figure 7c and d***). We further examined the distribution of acetylated α-tubulin in intact preparations of the peripheral nervous system.Acetylation was enriched under the membrane of axons in the saphenous nerve (as determined from staining with a Myelin Basic Protein antibody) (***Figure 7—figure supplement 1***) and also apparently at sensory neuron terminal endings in the cornea where mechanotransduction takes place (***Figure 7—figure supplement 1***, ***Video 4***).

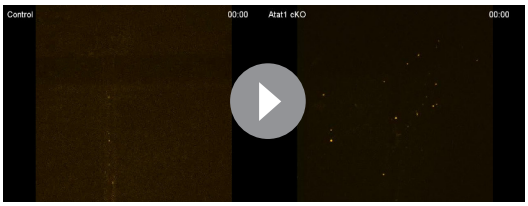
Increased rigidity of DRG neurons from Atat1^{cKO} mice

What then is the function of the acetylated α-tubulin band, and how does it impact upon mechanosensitivity across the range of mechanoreceptors in the skin? One possibility is that it sets the rigidity of cells thereby influencing the amount of force required to displace the plasma membrane and activate mechanosensitive channels. We explored this by directly measuring cell elasticity using atomic force microscopy. In DRG neurons from Atat1^{cKO} mice we observed that cellular stiffness was significantly higher across a range of indentations extending from displacements of 200 nm to 600 nm ($p<0.01$) (***Figure 7e*** and ***Figure 7—figure supplement 2***). Thus higher forces are required to indent sensory neurons from Atat1^{cKO} mice than Atat1^{Control} mice.

We confirmed this further by assaying the shrinkage of sensory neurons induced by a hyperosmotic stimulus. In the absence of Atat1, sensory neuron axons displayed less shrinkage than their control counterparts, an effect that could be rescued by expression of the acetylation mimicking mutation α-tubulin K40Q ($p<0.05$) (***Figure 7f***). Finally we examined how the microtubule cytoskeleton responds to compression induced by osmotic pressure. Using a novel tubulin labelling fluorescent dye we were able to resolve individual microtubule bundles in live imaging experiments. Strikingly, in DRG neurons from Atat1^{cKO} mice we observed significantly reduced microtubule displacement upon application of hyperosmotic solutions compared to control and K40Q expressing cells ($p<0.05$) (***Figure 7g*** to m), again supporting the premise that in the absence of α-tubulin acetylation sensory neurons are more resistant to mechanical deformation.

Discussion

Here we establish that deletion of the α-tubulin acetyltransferase Atat1 from mouse peripheral sensory neurons results in a profound and remarkably selective loss of cutaneous mechanical sensation. We demonstrate that this impacts strongly upon both light touch and pain, and that all mechanoreceptor subtypes which innervate the skin are less responsive in the absence of Atat1. This phenotype arises from reduction of the amplitude of mechanically activated currents in sensory neurons, and we propose that it is mediated by the loss of a sub-membrane band of acetylated α-tubulin in Atat1^{cKO} mice that sets mechanical rigidity of these cells. Our data thus



Video 3. Microfluidics. Movement of NGF labelled quantum dots along the neurites of cultured DRG. Atat1^{Control} (left) and Atat1^{cKO} (right).

DOI: 10.7554/eLife.20813.017

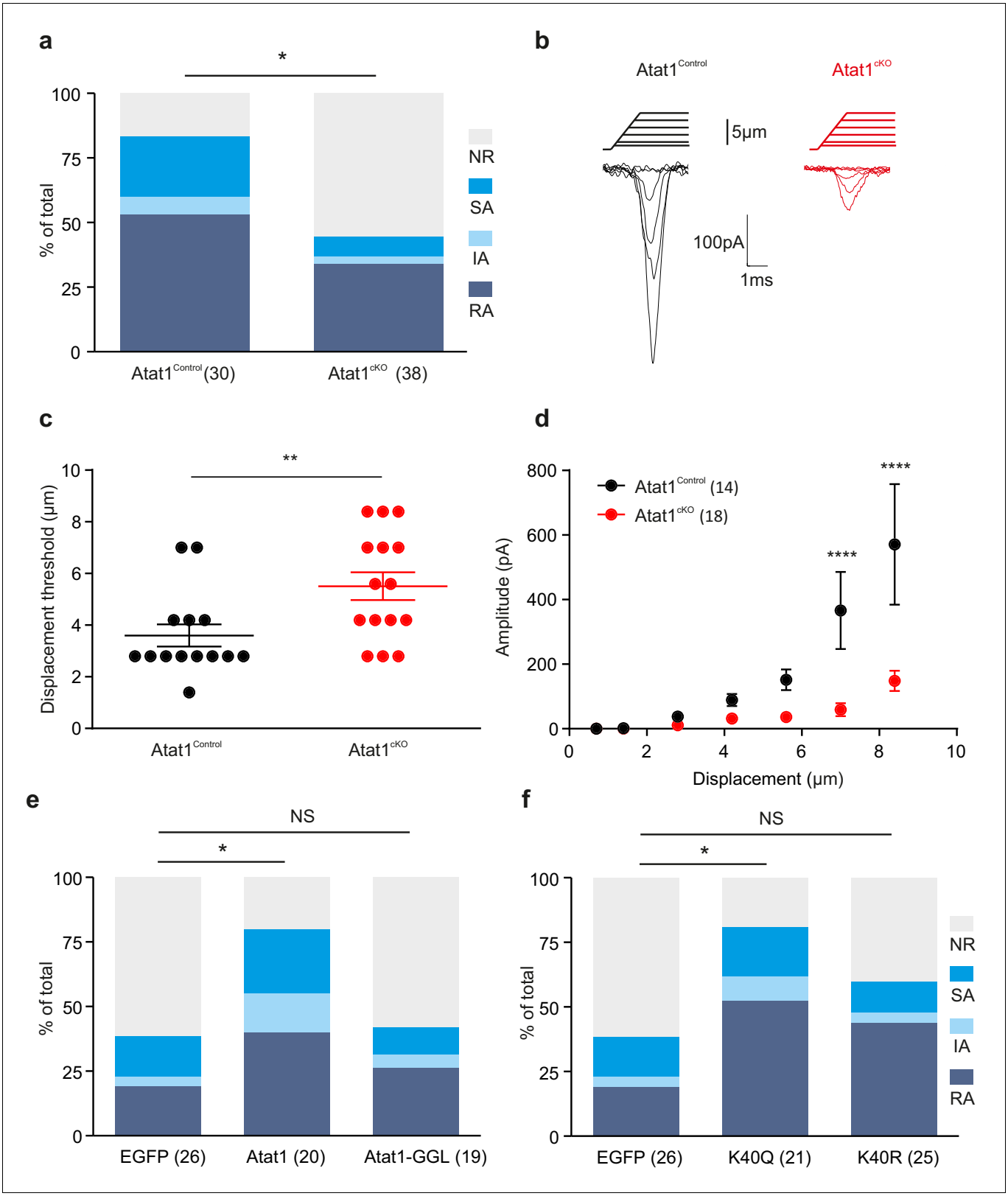


Figure 5. Atat1-mediated acetylated microtubules regulate mechanosensitivity in sensory neurons. (**a**) Stacked histograms showing the proportion of different mechano-gated currents activated by neurite indentation in sensory neurons from control Atat1^{Control} and Atat1^{cKO} mice (χ^2 test, $p<0.05$). NR, non-responsive to given displacement 512 nm. (**b**) Representative traces of RA currents elicited by increasing probe displacement on soma of Atat1^{Control} and Atat1^{cKO} sensory neurons. (**c**) Threshold of activation of RA currents was determined as mechanical stimulus that elicited a current $\geq$ 20

Figure 5 continued on next page

Figure 5 continued

pA. Closed circles indicate individual recorded cells. Note the marked increase in the displacement threshold in Atat1^{cKO} sensory neurons (Mann-Whitney test, p<0.01). (**d**) Stimulus-response curve of RA currents evoked by increasing probe displacement. Genetic depletion of aTAT1 in sensory neuron significantly reduced RA-currents amplitude (two-way ANOVA with *post-hoc* Bonferroni's test, p<0.0001). (**e**) Stacked histograms showing the proportions of different mechano-gated currents from stimulation of the neurites observed in Atat1^{cKO} sensory neurons transfected with EGFP, Atat1-YFP or Atat1-GGL-YFP cDNA. Transfection of wild-type Atat1 rescued the loss of mechanosensitivity, while transfection of catalytically inactive Atat1 (Atat1-GGL-YFP) failed to restore it in Atat1^{cKO} sensory neurons (χ^2 test, EGFP versus Atat1-YFP, p<0.05; EGFP versus Atat1-GGL-YFP, p>0.05). (**f**) Stacked histograms showing the proportions of different mechano-gated currents from stimulation of the neurites observed in Atat1^{cKO} sensory neurons transfected with *EGFP*, α-tubulin^{K40R}-IRES-YFP (*K40R*) or α-tubulin^{K40Q}-IRES-YFP (K40Q) cDNA. Transfection of acetylated α-tubulin mimics (K40Q) but not non-acetylatable α-tubulin mutant (K40R) restored mechanosensitivity in Atat1^{cKO} sensory neurons (χ^2 test, EGFP versus K40Q, p<0.05; EGFP versus K40R, p>0.05). The number of neurons recorded is indicated in parentheses in each panel. **p<0.01; ****p<0.0001; Error bars indicate s.e.m.

DOI: 10.7554/eLife.20813.018

The following figure supplements are available for figure 5:

Figure supplement 1. Absence of Atat1 in sensory neurons does not alter kinetic properties of RA currents.

DOI: 10.7554/eLife.20813.019

Figure supplement 2. Absence of Atat1 in sensory neurons does not alter membrane electrophysiological properties and proton activated currents.

DOI: 10.7554/eLife.20813.020

Figure supplement 3. Capsaicin response of DRG neurons in Atat1^{Control} and Atat1^{cKO} mice.

DOI: 10.7554/eLife.20813.021

Figure supplement 4. FRAP analysis of Piezo2 in transfected DRG from Atat1^{Control} and Atat1^{cKO} mice.

DOI: 10.7554/eLife.20813.022

describe a model whereby cellular stiffness regulates mechanical sensitivity by setting the force required to indent the plasma membrane and activate mechanosensitive ion channels.

In addition to its well characterized role as an α-tubulin acetyltransferase, Atat1 has been shown to have functions beyond its acetyltransferase activity at α-tubulin (***Castro-Castro et al., 2012***; ***Kalebic et al., 2013a***). Indeed in C. elegans, several reports indicate that acetylated tubulin is not required for touch sensitivity (***Akella et al., 2010***; ***Davenport et al., 2014***; ***Fukushige et al., 1999***; ***Topalidou et al., 2012***) and as such it is unknown as to how MEC17 (the C. elegans orthologue of Atat1) regulates mechanosensation in nematodes. It was therefore important to determine whether α-tubulin acetylation does indeed underlie the loss of mechanosensation in Atat1^{cKO} mice. We addressed this through genetic rescue experiments where we attempted to restore mechanosensitivity of Atat1^{cKO} sensory neurons by exogenous expression of Atat1 and α-tubulin point mutants. Importantly, we found that an acetyltransferase deficient form of Atat1 had no effect on mechanically activated current amplitude, while genetically mimicking tubulin acetylation with an α-tubulin K40Q mutation did restore mechanosensitivity. Thus acetylated microtubules are likely the effector for the loss of mechanosensation in Atat1^{cKO} mice, suggesting that mammals and nematodes may utilize Atat1 differentially in controlling touch sensation.

Given the multitude of cellular processes that depend on microtubules, especially in cells with elongated axons such as peripheral sensory neurons, one possible mechanism by which Atat1 might be affecting mechanosensitivity is via altered structure of the peripheral nervous system, perhaps as a result of aberrant axonal transport in the absence of acetylated microtubules (***Reed et al., 2006***). We performed a thorough analysis of the organization of the peripheral sensory system and observed no differences in rates of neurotrophin/receptor transport and axon outgrowth in vitro, or in the ultrastructure of peripheral nerves and their innervation of the skin and spinal cord in vivo. Moreover, deletion of Atat1 was remarkably selective in that it impacted only on cutaneous mechanosensation and had no effect on thermal responses, or on electrical or other functional properties of sensory neurons such as their sensitivity to capsaicin and pH. We have previously reported that STOML3, another critical mediator of mechanotransduction, associates with microtubules in a specialized vesicle where it interacts with acid-sensing (proton-gated) ion channel (ASIC) subunits (***Lapatsina et al., 2012***). Uncoupling of vesicles from microtubules leads to incorporation of STOML3 into the plasma membrane and increased acid-gated currents. Acetylation status of microtubules could conceivably influence the transport of these vesicles and contribute to the phenotype in

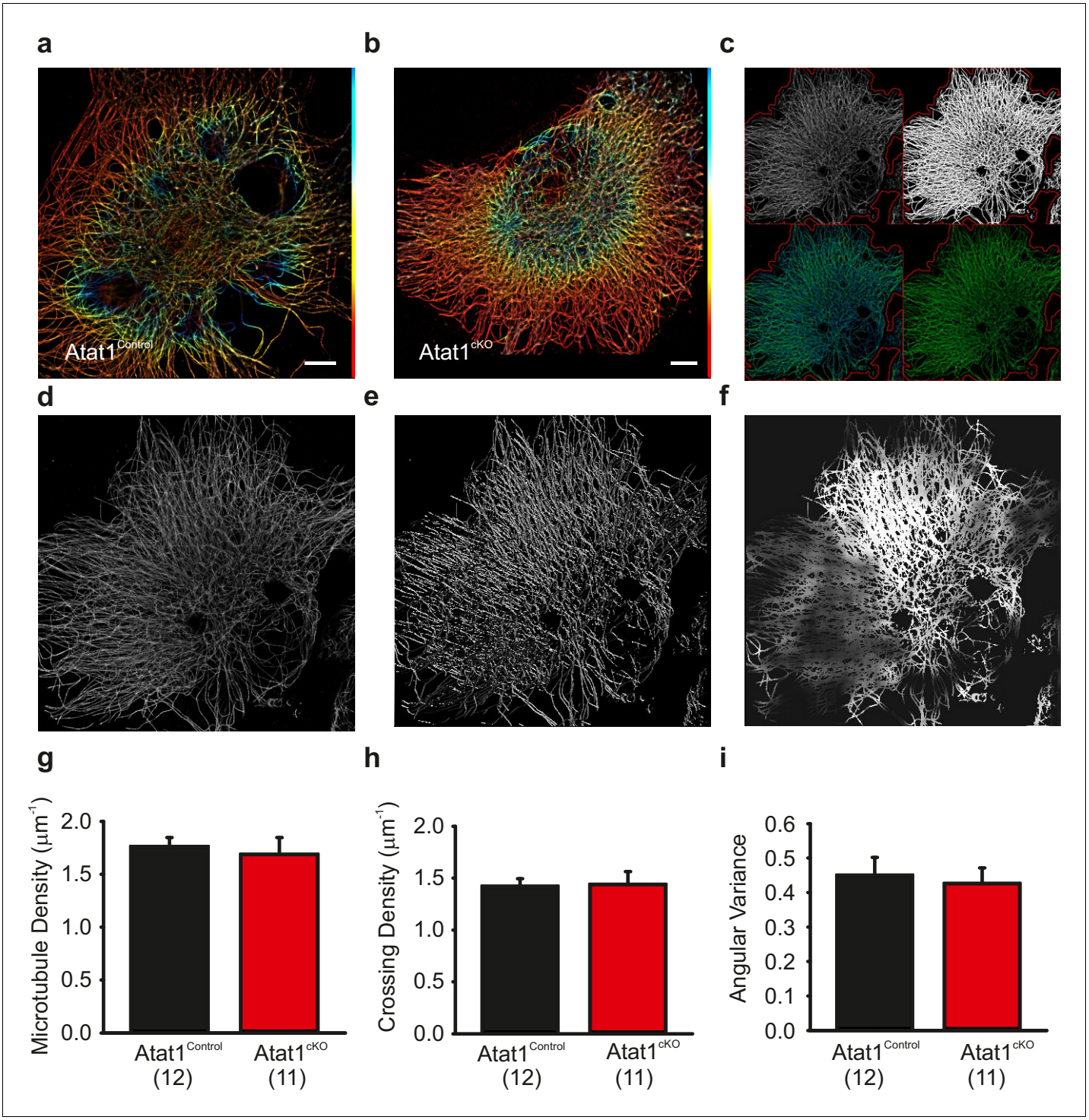


Figure 6. Superresolution imaging of microtubules in DRG from Atat1^{Control} and Atat1^{cKO} mice. (**a** and **b**) Superresolution image of anti α-tubulin staining of Atat1^{Control} (**a**) and Atat1^{cKO} (**b**) DRG colour coded by depth (red close to objective, Scale bar 5 µm). (**c**) Graphical representation of automated analyses performed on superresolution images. The top left image shows the original image in grey and the automated selection of the imaged cell area as a red outline. The top right image shows the microtubule image after binarization. The bottom left image shows the detected microtubule skeleton (in blue) overlaid on the microtubule superresolution image (in green); the microtubule skeleton was used to measure network length. The bottom right image is an estimation of the number of branch points present in the microtubule network, with microtubules in green and the branch points marked in blue. (**d–f**) Graphical representation of the automated analysis of the microtubule network angular variance. (**d**) Shows the microtubule superresolution image, (**e**) the automatically determined orientation of the microtubules, (**f**) the local angular variance of the microtubule orientation, where bright pixels denote a high variance and vice versa. (**g**) Graph summarizing the microtubule density in DRG taken from Atat1^{Control}

Figure 6 continued on next page

Figure 6 continued

and Atat1^{cKO} mice. (**h**) Graph showing the density of microtubule crossings present in the microtubule networks in the two genotypes. (**i**) Graph summarizing the angular variance of the microtubule cytoskeleton in both Atat1Control and Atat1cKO cultured DRG.. No significant difference in any parameter was observed between the genotypes (t-Test, p>0.05).Error bars indicate s.e.m.

DOI: 10.7554/eLife.20813.023

The following figure supplement is available for figure 6:

Figure supplement 1. Actin cytoskeletal organization in DRG from Atat1^{cKO} mice.

DOI: 10.7554/eLife.20813.024

Atat1^{cKO} mice. However, since we observed no alteration in proton gated currents, it is unlikely that the reduction of mechanosensitivity is due to the altered transport of STOML3 in Atat1^{cKO} mice.

Despite the profound loss of cutaneous mechanosensation, we observed no deficits in proprioception in Atat1^{cKO} mice. This is in contrast to Piezo2 knockout mice which display severe proprioceptive defects (***Woo et al., 2015***). The lack of proprioceptive phenotype in Atat1^{cKO} mice does not stem from incomplete recombination by the Avil-Cre driver in proprioceptive neurons because we previously observed that full Atat1 knockout mice also display no alterations in proprioception (***Kalebic et al., 2013b***). Rather it may arise either from developmental compensation of a partial reduction in mechanosensitivity in these neurons, or from mechanistic differences in mechanotransduction in proprioceptors and cutaneous afferents. Similarly, we did not observe here, or in ubiquitous knockout mice (***Kalebic et al., 2013b***), any apparent change in other aspects of mechanosensation, such as whisker function and exploration, or in developmental consequences of reduced touch sensitivity such as nursing or growth. This may reflect a lack of sensitivity of the tests we performed, or again, developmental compensation arising from residual responsiveness. The use of more selective conditional Cre lines would circumvent this problem and also allow for further studies on the role of Atat1 in specific touch sensations such as those arising from C-low threshold mechanoreceptors or from visceral mechanical nociceptors, which were not considered here.

We found that acetylated microtubules localize to a prominent band under the membrane of sensory neuron cell bodies. Furthermore our AFM measurements showed that in the absence of Atat1 and acetylated α-tubulin, the stiffness of sensory neurons was significantly elevated across a range of indentation stimuli in Atat1^{cKO} mice, and cells were more resistant to osmotically induced shrinkage. We also monitored the movement of microtubules during shrinking using live imaging, and again observed reduced compression of the microtubule network upon Atat1 deletion. Importantly this defect could be rescued by introduction of the α-tubulin acetylation mimic into neurons. Thus our data point towards a role for acetylated tubulin in setting neuronal elasticity, and imply that in its absence, cells are stiffer which ultimately changes the force distribution to the neuronal membrane, requiring more force to indent the membrane and activate mechanosensitive channels. This is consistent with the phenotype in Atat1^{cKO} mice in that all mechanoreceptor subtypes, regardless of the type of mechanosensitive currents/channels, are less responsive in the absence of Atat1. It also suggests that a residual response may be evident across patch clamping, skin-nerve electrophysiology and behavioural experiments, in that at higher forces, neuronal membranes in Atat1^{cKO} mice would eventually be displaced, leading to mechanosensitive ion channel activation. Whether this is the case could be directly addressed using new technology based upon pillar arrays that displace neurons in the nanometer range allowing for quantitative analysis of mechanoelectrical transduction (***Poole et al., 2014***). Similarly, another approach which has been used previously (***Ranade et al., 2014***; ***Wetzel et al., 2007***), would be to determine whether any afferents lose their mechanosensitivity completely in the ex vivo skin nerve preparation, which we did not investigate here.

While our data shows that there is a correlation between reduced mechanical sensitivity and neuronal elasticity in the absence of Atat1, there are some caveats to this interpretation. For example, we performed AFM measurements at the neuronal soma whereas in vivo, mechanotransduction occurs at sensory neuron endings. In future work it would therefore be informative to assess cell stiffness along neurites which are much more sensitive to mechanical displacement than the cell body (***Hu and Lewin, 2006***; ***Poole et al., 2014***). Moreover, we detected acetylated tubulin enriched under the membrane of axons which are not in themselves mechanosensitive, and while we show that acetylated tubulin is expressed at neuronal endings in the cornea, superresolution microscopy would be required to demonstrate conclusively that it is indeed submembrane localized. In this light

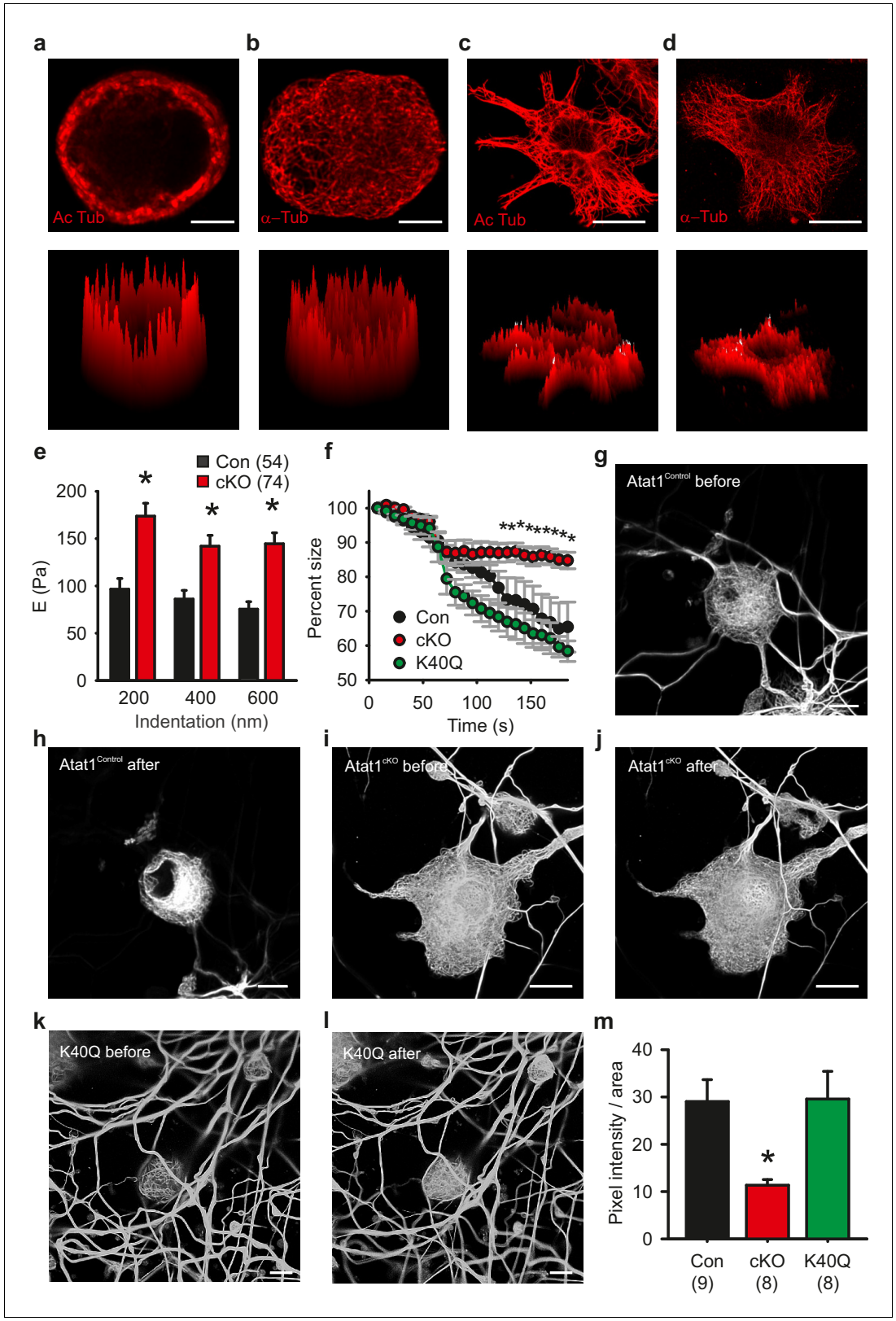


Figure 7. Microtubule organization in peripheral sensory neurons. (**a**) Anti-acetylated-α-tubulin staining of Atat1^{Control} cultured DRG cells (corresponding surface plot below). Note the prominent sub-membrane localisation of acetylated tubulin (Scale bar 5 μm). (**b**) Anti α-tubulin staining of Atat1^{Control} cultured DRG cells (Scale bar 5 μm) (**c**) Anti-acetylated-α-tubulin staining of serum-starved Atat1^{Control} MEFs (Scale bar 20 μm). Note the even distribution of acetylated tubulin in this cell type. (**d**) Anti α-tubulin staining of serum-starved Atat1^{Control} MEFs (Scale bar 20 μm). (**e**) Quantitative

Figure 7 continued on next page

Figure 7 continued

comparison of Young's modulus obtained by fitting force-indentation curves with the Hertz-Sneddon model at different indentations for cultured DRG taken from Atat1^{Control} and Atat1^{cKO} mice. A significantly higher pressure is required to indent the membranes of Atat1^{cKO} neurons over Atat1^{Control} cells (Mann-Whitney test, $p<0.01$). (**f**) Graph showing the relative shrinkage of axonal outgrowths from Atat1^{Control} and Atat1^{cKO} DRG loaded with calcein (2 µM) in response to a hyperosmotic shock over time. Deletion of Atat1 leads to a significant decrease in the percentage shrinking of Atat1^{cKO} axons relative to control samples (ANOVA on ranks, multiple comparison Dunn's Method, $p<0.05$). (**g–l**) Live imaging of microtubules labelled with SiR Tubulin two and subjected to hyperosmotic shock (scale bars 10 µm) (**g**, **h**) Atat1^{Control} DRG before and after hyperosmotic shock. (**I**, **j**) Atat1^{cKO} DRG before and hyperosmotic shock. (**k**, **l**) Atat1^{cKO} DRG transfected with the tubulin K40Q amino acid mimic before and hyperosmotic shock. (**m**) Bar-chart summarising osmotically induced microtubule compression in DRG neurons from Atat1^{Control}, Atat1^{cKO}, and Atat1^{cKO} neurons transfected with tubulin-K40Q. There is significantly less compression in Atat1^{cKO} than Atat1^{Control} neurons, which is rescued by transfection of tubulin-K40Q (ANOVA on ranks, multiple comparison Dunn's Method, $p<0.05$). Error bars indicate s.e.m.

DOI: 10.7554/eLife.20813.025

The following figure supplements are available for figure 7:

Figure supplement 1. Acetylated microtubule distribution in sensory neurons from Atat1^{cKO} mice.

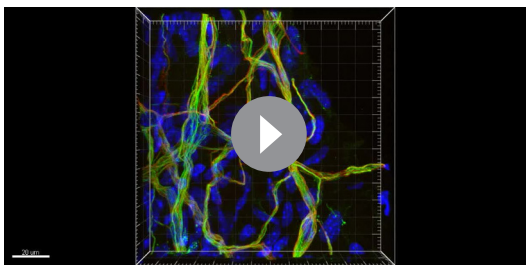
DOI: 10.7554/eLife.20813.026

Figure supplement 2. Atomic Force Microscopy of DRG from Atat1^{cKO} mice.

DOI: 10.7554/eLife.20813.027

there are also other models of mechanosensation that would accord with our data. For example, microtubules have been implicated in sensory mechanotransduction in *Drosophila* larval dendritic arborisation neurons (***Zhang et al., 2015***), *C. elegans* touch receptor neurons (***Bounoutas et al., 2009***; ***Fukushige et al., 1999***) and mammalian osmosensory neurons (***Prager-Khoutorsky et al., 2014***). Their role has mainly been explored from the perspective of an anchoring function that serves to tether mechanosensitive ion channels in the membrane. Further support for a tethered mechanotransduction complex comes from observations in sensory neurons where a physical tether has been described that may link mechanosensitive ion channels to the extracellular matrix (***Chiang et al., 2011***; ***Hu et al., 2010***). It is possible that acetylated tubulin serves as a coordination point for these tethers in the mechanotransduction complex, and that in its absence misorganization of the microtubule network leads to reduced force transfer from the extracellular matrix to ion channels. Finally, another critical component of the complex, STOML3 has been demonstrated to change the force distribution in neuronal membrane via binding cholesterol. However, while a specific reduction of stiffness in sensory neuron membranes is observed in STOML3 knockout mice (***Qi et al., 2015***), cellular stiffness is increased upon deletion of Atat1, yet both STOML3 knockout mice and Atat1^{cKO} mice exhibit deficits in mechanosensation. One explanation for this difference is that disruption of α-tubulin acetylation increases the overall neuronal stiffness, rendering sensory neurons more resistant to mechanical deformation, and thereby impeding the transmission of force to other mechanical transducing elements, including STOML3, the cytoskeleton, extracellular matrix and plasma membrane. In contrast, STOML3 distributes the force directly within the membrane to ion channels, and a stiffened membrane facilitates this process. It is also possible that membrane stiffness is set at an optimal range to distribute force among the membrane, cytoskeleton and extracellular matrix and thus tune the sensitivity of mechanosensitive ion channels.

In light of the increased stiffness of Atat1^{cKO} sensory neurons we also examined the gross organization of the cytoskeleton in these cells. Similar to osmosensory neurons in the hypothalamus (***Prager-Khoutorsky et al., 2014***) we observed that microtubules formed a lattice like structure in DRG neurons; however this was not altered in the absence of Atat1. Similarly, we detected no difference in phalloidin staining in Atat1^{cKO} mice suggesting that mechanosensory defects do not arise from interaction with the actin cytoskeleton. How α-tubulin acetylation sets



Video 4. Acetylated tubulin distribution in cornea. 3D rendering of a whole mount cornea preparation showing membrane bound SNAP labeling in red and acetylated tubulin in green.

DOI: 10.7554/eLife.20813.028

cellular stiffness is therefore not immediately apparent, and a key question will be to investigate whether this occurs by directly altering the rigidity of individual microtubules or through interaction with other membrane and cytoskeletal elements. Intriguingly, it has recently been shown that another tubulin posttranslation modification, detyrosination, stiffens cardiomyocytes and promotes microtubule buckling in these cells (**Robison et al., 2016**). Desmin intermediate filaments were identified as a physical link between detyrosinated microtubules and the sarcomere, opening up the possibility that analogous mechanisms may function in sensory neurons, and that other microtubule posttranslational modifications may also influence sensory mechanotransduction. Further work using electron microscopy for example to examine the structure of microtubules and their modifications at the ultrastructural level, particularly under the membrane, may give insight into this process. What is clear however is that the mechanism appears to be broadly applicable since the lack of mechanosensitivity of Atat1^{cKO} mice extends beyond phenotypes observed when other mechanotransduction complex proteins such as Piezo2 (**Ranade et al., 2014**) and STOML3 (**Wetzel et al., 2007**) are deleted. The convergence of multiple mechanisms onto a single posttranslational modification of α-tubulin, and its remarkable selectivity, indicates that microtubule acetylation represents a fundamental component of the mechanosensory apparatus, as well as an attractive target for novel therapeutic strategies to treat mechanical pain.

Materials and methods

Mouse lines

The generation and genotyping of all mouse lines used has been described previously (**Kalebic et al., 2013b**; **Yang et al., 2015**; **Zurborg et al., 2011**).

Behavioural testing

The tape test (**Ranade et al., 2014**), cotton swab (**Ranade et al., 2014**), von Frey (**Kwan et al., 2006**), tail clip (**Ranade et al., 2014**), hot plate (**Kwan et al., 2006**), tail immersion test (**Elhabazi et al., 2014**), acetone drop (**Choi et al., 1994**) and rotarod assay (**Hamm et al., 1994**) respectively, were all performed as described previously. The grid test was performed by counting the number of steps versus slips over 2 min from a free roaming mouse placed atop a metal grid.

Electrophysiological recordings

The skin nerve preparation was used essentially as previously described (**Wetzel et al., 2007**). Mice were sacrificed using CO2 inhalation, and the saphenous nerve together with the skin of the hind limb was dissected free and placed in an organ bath. The chamber was perfused with a synthetic interstitial fluid (SIF buffer) consisting of (in mM): NaCl, 123; KCl, 3.5; MgSO4, 0.7; NaH2PO4, 1.7; CaCl2, 2.0; sodium gluconate, 9.5; glucose, 5.5; sucrose, 7.5; and HEPES, 10 at a pH of 7.4.) The skin was placed with the corium side up, and the nerve was placed in an adjacent chamber for fiber teasing and single-unit recording. Single units were isolated with a mechanical search stimulus applied with a glass rod and classified by conduction velocity, von Frey hair thresholds and adaptation properties to suprathreshold stimuli. A computer-controlled nanomotor (Kleindiek Nanotechnik) was used to apply mechanical ramp-and-hold stimuli of known amplitude and velocity. Standardized displacement stimuli of 2 s or 10 s duration were applied to the receptive field at regular intervals (interstimulus period, 30 s). The probe was a stainless steel metal rod with a flat circular contact area of 0.8 mm. For thermal sensitivity, C fibers were tested with a thermal contact stimulator based on the Peltier principle (Thermal Stimulator, Yale University School of Medicine). Standard ramp-and hold heating stimulus (ramp 3°C per s, 32°C to 56°C, hold 5 s) was applied to the receptive field. The signal driving the movement of the linear motor and raw electrophysiological data were collected with a Powerlab 4.0 system and Labchart 7.1 software (AD instruments), Spikes were discriminated off-line with the spike histogram extension of the software.

Patch clamping

DRG neurons were collected from mice and dissociated as described (**Wetzel et al., 2007**). Transfections were carried out using the Nucleofector system (Lonza AG) in 20 µl of Mouse Neuron Nucleofector solution from the SCN nucleofector kit (Lonza AG) and a total 4–5 µg of plasmid DNA at

room temperature using the preinstalled program SCN Basic Neuro program 6. After electroporation, the cell suspension was transferred to 500 µl of RPMI 1640 medium (Gibco) for 10 min at 37˚C. This suspension, supplemented with 10% horse serum, was used to plate the cells onto glass coverslips for recording. The RPMI medium supplemented with 100 ng/ml nerve growth factor (NGF), 50 ng/ml BDNF was replaced with the standard DRG medium 3–4 hr later. Electrophysiology experiments began 12 hr after plating and only transfected cells (as determined by fluorescence) were selected for patch clamping. As a negative control, cells were transfected with an eGFP plasmid alone.

Whole-cell recordings from isolated DRG neurons were made as previously described (***Hu and Lewin, 2006***). Recordings were made from DRG neurons using fire-polished glass electrodes with a resistance of 3–7 MΩ. Extracellular solution contained (mM): NaCl 140, MgCl2 1, CaCl2 2, KCl 4, glucose four and HEPES 10 (pH 7.4), and electrodes were filled with a solution containing (mM): KCl 130, NaCl 10, MgCl2 1, EGTA one and HEPES 10 (pH 7.3). Cells were perfused with drug-containing solutions by moving an array of outlets in front of the patched cells (WAS02; Ditel, Prague). Observations were made with an Observer A1 inverted microscope (Zeiss) equipped with a CCD camera and the imaging software AxioVision. Membrane current and voltage were amplified and acquired using EPC-10 amplifier sampled at 40 kHz; acquired traces were analyzed using Patchmaster and Fitmaster software (HEKA). Pipette and membrane capacitance were compensated using the auto function of Pulse. For most of the experiments, to minimize the voltage error, 70% of the series resistance was compensated and the membrane voltage was held at −60 mV with the voltage-clamp circuit. After establishing whole-cell configuration, voltage-gated currents were measured using a standard series of voltage commands. Briefly, the neurons were pre-pulsed to −120 mV for 150 ms and depolarized from −65 to +55 mV in increments of 5 mV (40 ms test pulse duration). Next the amplifier was switched to current-clamp mode and current injection was used to evoke action potentials. If the membrane capacitance and resistance changed more than 20% after the mechanical stimulus, the cell was regarded as membrane damaged and the data discarded. Mechanical stimuli were applied using a heat-polished glass pipette (tip diameter 3–5 µm), driven by a MM3A Micromanipulator system (Kleindiek), and positioned at an angle of 45 degrees to the surface of the dish. For soma indentation, the probe was typically positioned so that a 1.4 µm movement did not visibly contact the cell but that a 2.8 µm stimulus produced an observable membrane deflection under the microscope. So a 2.8 µm probe movement was defined as a 1.4 µm mechanical stimulation, and a series of mechanical steps in 0.7 µm increment were applied at 5 s intervals. The displacement threshold was determined as mechanical stimulus that elicited a current ≥20 pA. For analysis of the kinetic properties of mechanically activated current, traces were fit with single exponential functions using the Fitmaster software (HEKA).

Calcium imaging

Calcium imaging was performed as previously described (***Chen et al., 2014***). Fluorescence microscopy was done on an Observer A1 inverted microscope (Zeiss, Germany) using a 25 × 0.8 numerical aperture water immersion objective and a 175W Xenon lamp as a light source. Before imaging, DRG neurons were incubated with 4 mM Fura-2 at 37˚C for 40 min and washed with extracellular solution at 37˚C for another 30 min. Excitation light was passed either through a 340 BP 30 filter or a 387 BP 16 filter. Two filters were switched by an ultra-high speed wavelength switcher Lambda DG-4 (Sutter, Novato, CA). Emissions elicited from both excitation wavelengths were passed through a 510 BP 90 filter and collected by a charge-coupled device camera (Zeiss). Different solutions were applied by multi barrel perfusion system (WAS02, DITEL, Prague). AxioVision software (Zeiss) was used to record image data. After background (B_{340}, B_{380}) subtraction in each channel (F_{340}, F_{380}), the ratio (R) of fluorescence elicited by two excitation light was calculated: $R=(F_{340} - B_{340}) / (F_{380} - B_{380})$. Data was analyzed in AxioVision, Matlab (MathWorks, Natick, Massachusetts), and GraphPad prism (GraphPad Software Inc., San Diego, CA).

DRG neurons culture and transfection

DRG neurons from adult male mice were prepared as previously described (***Hu and Lewin, 2006***). Briefly, DRGs were dissected and collected in a 1.0 ml tube of phosphate-buffered saline (PBS) on ice. Ganglia were cleaned, enzymatically treated and mechanically dispersed. Before plating on

poly-l-lysine–laminin coated coverslips, cells were transfected using the Nucleofector system (Lonza AG). In brief, neurons were suspended in 20 µl of Mouse Neuron Nucleofector solution from SCN nucleofector kit (Lonza AG) and a total 4–5 µg of plasmid DNA at room temperature. The mixture was transferred to a cuvette and electroporated with the preinstalled program SCN Basic Neuro program 6. After electroporation, the cell suspension was transferred to 500 µl of RPMI 1640 medium (Gibco) for 10 min at 37˚C. This suspension, supplemented with 10% horse serum, was used to plate the cells onto glass coverslips for recording. The RPMI medium supplemented with 100 ng/ml nerve growth factor (NGF), 50 ng/ml BDNF was replaced with the standard DRG medium 3–4 hr later. Electrophysiology experiments began 12 hr after plating.

Immunofluorescence and staining

For microtubule staining in DRG cultures, cells were washed once with PBS, and then fixed for 15 min in cytoskeleton buffer (CB) pH 6.3 containing 3% paraformaldehyde, 0.25% triton and 0.2% glutaraldehyde at room temperature. Cells were then washed three times with PBST (0.3% triton). Samples were then subsequently blocked with 5% normal goat serum (NGS) in PBS for 1 hr at room temperature. Cells were then placed overnight at 4˚C with primary anti α-tubulin (1:1000) (Sigma-Aldrich, T9026) or anti-acetylated-α-tubulin (1:1000) (Sigma-Aldrich, T7451) in PBS. Cells were then washed with PBS and incubated for 1 hr with fluorescently labelled secondary antibodies (1:1000) (Alexa Fluor 546 Lifetechnologies) for 1 hr at room temperature. All images were acquired using a 40 X objective on a Leica SP5 confocal microscope. Processing of images and generation of surface plots were performed using ImageJ. Images were deconvoluted using Huygens software.

Actin filaments were stained with phalloidin using the protocol outlined (***Cramer and Mitchison, 1995***). Briefly, actin filaments in DRG primary cultures were stained with Alexa488-phalloidin at 0.5 µg/ml (Lifetechnologies).Cells were fixed with fresh 4% PFA (EM grade, TAAB) in cytoskeleton buffer (10 mM MES, 138 mM KCl, 3 mM MgCl, 2 mM EGTA) freshly added supplemented of 0.3 M sucrose, permeabilized in 0.25% Triton-X-100 (Sigma-Aldrich), and blocked in 2% BSA (Sigma-Aldrich).

Immunostaining of saphenous nerves was performed on paraffin sections after fixation with PFA. Following rehydration, antigen retrieval was performed with 10 mM sodium citrate (pH 6) at boiling temperature for 10 min. Subsequently, sections were permeabilized (0.3% Triton X-100), blocked (5% goat serum) and stained with anti-acetylated-α-tubulin (Sigma-Aldrich, T7451) and anti-myelin basic protein (Chemicon, MAB386).

For cornea staining, the eyes were removed and fixed for 1 hr in 4% PFA at room temperature. The cornea was then dissected and permeabilized with PBS-Triton 0.03% for 30 min. Following this, the cornea was immersed in PBS-Triton 0.03% containing 1 µM SNAP surface 546 (New England Biolabs) for 30 min. The samples were then washed with PBS-Triton 0.03% for 20 min and subsequently blocked with 5% normal goat serum in PBS-Triton 0.03% for 30 min. The tissue was then stained with anti-acetylated-α-tubulin (1:500) overnight. Samples were then washed with PBS and a secondary antibody (Alexa Fluor 488 Lifetechnologies) was added for 5 hr. The samples were again washed with PBS and stained with DAPI 10 min. The cornea was then mounted on glass with 100% glycerol and imaged.

Axon outgrowth assay

For whole mount axon outgrowth assays, individual DRG were extracted from mice and grown in Matrigel (Corning) for seven days. Preparations were fixed with 4% PFA for 5 min and labelled with the primary antibody PGP9.5 (1:200) overnight at 4˚C. The samples were then labelled with secondary antibodies (1:1000) Alexa Fluor 546 Lifetechnologies) for 1 hr at room temperature. All images were acquired using a Leica LMD 7000.

SNAP-tag skin labelling

SNAP-tag labelling was carried out by intradermal injection of the finger in anaesthetized mice of 2 µM BG TMRstar substrate as described previously (***Yang et al., 2015***). After five hours the animals were sacrificed and the samples were mounted in 80% glycerol for imaging.

Electron microscopy of saphenous nerve

Saphenous nerves were postfixed for 24 hr with 4% PFA, 2.5% glutaraldehyde (TAAB) in 0.1 M phosphate buffer at 4C. Then incubated for 2 hr with 1% osmium tetraoxide with 1.5% potassium ferrocyanide, then dehydrated in ethanol and embedded in Epon for ultrathin sectioning and TEM imaging.

Spinal cord staining of the dorsal horn

Spinal cord was extracted and fixed for 3 hr in 4% PFA at 4°C. Samples were embedded in 2% agarose and 100 µM sections were cut. The sections were treated with 50% ethanol 30 min and subsequently incubated with a 5% serum blocking solution of 0.3% Triton-X in PBS for 1 hr. Samples were then incubated with the primary antibodies overnight at 4°C NF200 1:200 (Sigma Aldrich, N0142), CGRP 1:500 (Rockland, 200–301-DI5) and IB4 1:100 (Invitrogen, I21414). Sections were washed with PBS, and incubated for 1 hr with the secondary antibody 1:1000 (Alexa Fluor 488 and 546 Life technologies) in 5% serum blocking solution. The samples were then mounted with prolong gold (Invitrogen, P36930) for imaging.

Microfluidics

DRG neurons were suspended in 1:1 Matrigel in 10% FBS DMEM and seeded onto a two-chamber microfluidic chip (Xona Microfluidics, SD150). Axons were allowed to grow across the microchannels connecting the two chambers for 3–5 days. On the day of the experiment, media in both the cell body and axon chambers was replaced with media with no serum for 3 hr. 1 µM mono-biotinylated NGF purified in house from eukaryotic cells was coupled with 1 µM streptavidin conjugated quantum dots 655 (Life Technologies, Italy) for 30 min on ice, then diluted to 5 nM in imaging buffer (as above) and then used to replace the media in the axon chamber. A 25% vol difference was kept between the cell body and the axon chamber to avoid backflow from the axon to the cell body chamber. After 1 hr incubation at 37°C in 5% CO2, retrograde transport of NGF-Qdot655 containing endosomes was imaged using a confocal Ultraview Vox (Perkin Elmer) equipped with a 5% CO2 humidified chamber at 37°C. 100 s time lapses were recorded using 300 ms exposure time. Images were analyzed with Imaris software using the particle tracking function and autoregressive motion track generation setting.

FRAP analysis of DRG

DRG were transfected with Piezo2-GFP using a nucleofector device (Amaxa) as described above. After two days FRAP analysis was then carried out on a LEICA SP5 confocal microscope. Cells were imaged for 10 frames pre-bleach before being bleached for a further 10 frames (70% laser power), following this the cells were imaged once every minute for 15 min to measure recovery. Data was analysed and graphs generated using Sigma-Plot.

Superresolution microscopy

The cells were washed once with 3 ml of warm PBS and then fixed and permeabilized for 2 min in cytoskeleton buffer containing 0.3% Glutaraldehyde and 0.25% Triton X-100. Following this, the cells were fixed for 10 min in cytoskeleton buffer containing 2% Glutaraldehyde and treated for 7 min with 2 ml of 0.1% Sodium Borohydride (NaBH4) in PBS. Cells were then washed 3 times for 10 min in PBS. The cells were incubated with primary antibody for 30 min (mouse anti α-tubulin, Neomarker, 1:500) in PBS +2% BSA After washing 3 times for 10 min with PBS, the cells were transferred to the secondary antibody (goat anti mouse Alexa 647, 1:500, Molecular Probes A21236) at room temperature for 30 min. The cells were then washed three times with PBS for 10 min and then mounted for STORM imaging. At the time of imaging cells were overlaid with STORM blinking buffer: 50 mM Tris pH 8.0, 10 mM NaCl, 10% Glucose, 100 U/ml Glucose Oxidase (Sigma-Aldrich), 40 µg/ml Catalase (Sigma-Aldrich).

Superresolution image analysis

The analysis of microtubule (MT) network morphology was done using the open source software CellProfiler (***Carpenter et al., 2006***). The MT signal was enhanced by a top-hat filter and then binarised with the same manual threshold for all images. Binary images were skeletonized using CellProfiler's 'skelPE' algorithm and the resulting skeleton was subjected to branchpoint detection. We

measured MT density by dividing the skeleton length with imaged cell area and we measured MT crossing density by dividing the number of branchpoints with skeleton length. Moreover, we measured the local angular distribution of the MTs in order to assess whether they run in parallel, or in a crossing manner (angular variance). To this end, we subjected each pixel to a rotating morphological filter using a linear structural element with a length of 11 pixels, and recorded at which angle we obtained a maximum response. We computed the response for angles from 0 to 170 degrees at steps of 10 degrees since there is no information on MT polarity. Next we measured the local circular variance of the MT orientations in a sliding window with a diameter of 51 pixels, using angle doubling as it is commonly done for axial data. The circular variance has a value one if the MTs in a given region are completely parallel and has smaller values (down to 0) if the MTs are oriented in various directions. Finally, we computed the average circular variance of all MT pixels in a given cell. If this value were close to one it would mean that locally, on a length scale of 51 pixels, the MTs are parallel in most of the cell.

Atomic force microscopy (AFM)

Force spectroscopy measurements were performed in a similar manner to that described previously (***Qi et al., 2015***). Force spectroscopy measurements were performed by using a NanoWizard AFM (JPK Instruments, Berlin, Germany) equipped with a fluid chamber (Biocell; JPK) for live cell analysis and an inverted optical microscope (Axiovert 200; Zeiss) for sample observation.

DRG cells were seeded on glass coverslips previously coated with a first layer of polylysine (500 µg/ml for about 1 hr room temperature) and a second layer of laminin (20 µg/ml for about 1 hr at 37°C). The cells were then cultured for at least 15 hr before measurements. Then, the sample was inserted into the fluid chamber immersed in culture medium and measurements were carried out at room temperature. The status of cells was constantly monitored by optical microscope.

Indenters for probing cell elasticity were prepared by mounting silica microspheres of 4.5 µm nominal diameter (Bangs Laboratories Inc.) to tipless V-shaped silicon nitride cantilevers having nominal spring constants of 0.32 N/m or 0.08 N/m (NanoWorld, Innovative Technologies) by using UV sensitive glue (Loxeal UV Glue). Silica beads were picked under microscopy control. Before measurements the spring constant of the cantilevers was calibrated by using the thermal noise method.

By using the optical microscope the bead-mounted cantilever was brought over the soma of single DRG and pressed down to indent the cell. The motion of the z-piezo and the force were recorded. On each cell eight-about ten force-distance curves were acquired with a force load of 500 pN and at a rate of 5 µm sec-1 in closed loop feed-back mode.

Cell elastic properties were assessed by evaluating the Young's modulus (E) of the cell. This value was obtained by analysing the approaching part of the recorded F-D curves using the JPK DP software. The software converts the approaching curve into force-indentation curves by subtracting the cantilever bending from the signal height to calculate indentation. Afterwards force-indentation curves were fitted by Hertz-Sneddon model for a spherical indenter according to this equation:

$$F = \frac{E}{1-\nu^2}\left[\frac{a^2+R_s^2}{2}\ln\frac{R_s+a}{R_s-a} - aR_s\right]$$

$$\delta = \frac{a}{2}\ln\frac{R_s+a}{R_s-a}$$

Here, δ is the indentation depth, a is the contact radius of the indenter, R is the silica bead radius, ν is the sample's Poisson ratio (set to 0.5 for cell) (***Rotsch et al., 1999***) and E is Young's modulus. Fitting was performed at different indentations 200, 400 and 600 nm (see SI for examples of fitting curves obtained).

Osmotic shrinking assays

Cultured DRG were loaded with 500 nM SiR Tubulin2 for 1 hr at 37°C and/or 2 µM calcein dye (Invitrogen C3100MP) for 30 min in DRG at 37°C. The cells were then transferred to imaging buffer (10 mM Hepes pH 7.4, 140 mM NaCl, 4 mM KCl, 2 mM CaCl2, 1 mM MgCl2, 5 mM D-glucose) at

320mOsm. Following a 5 min acclimatization period the cells were subjected to a 440mOsm (osmolarity adjusted with mannitol) hyperosmotic shock for 3 min. All imaging was carried out using a Leica SP5 resonant scanner. To increase the permeability and fluorogenicity of the previously described far-red microtubule probe SiR-tubulin2 (***Lukinavičius et al., 2014***) we exchanged the docetaxel in SiR-tubulin with the more hydrophobic cabazitaxel. The molecule was synthesized using the same procedures as described for SiR-tubulin. A detailed characterization of SiR-tubulin2 will be published elsewhere.

Acknowledgements

We thank Maria Kamber and Emerald Perlas of EMBL Monterotondo Mouse and Histology facilities for technical support of our work and Violetta Paribeni for mouse husbandry. Funded by EMBL and DFG.

Additional information

Funding

Funder	Author
Deutsche Forschungsgemeinschaft	Paul A Heppenstall

The funders had no role in study design, data collection and interpretation, or the decision to submit the work for publication.

Author contributions

SJM, JH, PAH, Conception and design, Acquisition of data, Analysis and interpretation of data, Drafting or revising the article; YQ, LI, DG, NK, LC, CT, CP, GB, KS, CMF, AA, FF, MS, UM, ML, JR, YS, Acquisition of data, Analysis and interpretation of data; LA, Acquisition of data, Analysis and interpretation of data, Drafting or revising the article; LR, ADN, LB, KJ, Contributed unpublished essential data or reagents

Author ORCIDs

Jonas Ries, http://orcid.org/0000-0002-6640-9250
Yannick Schwab, http://orcid.org/0000-0001-8027-1836
Paul A Heppenstall, http://orcid.org/0000-0001-7954-5166

Ethics

Animal experimentation: This study was performed in strict accordance with the recommendations in the Guide for the Care and Use of Laboratory Animals of the National Institutes of Health. Mice were maintained at the EMBL Mouse Biology Unit, Monterotondo, Italy, in accordance with Italian legislation (Art. 9, 27. Jan 1992, no 116) under license from the Italian Ministry of Health.

References

Abraira VE, Ginty DD. 2013. The sensory neurons of touch. *Neuron* **79**:618–639. doi: 10.1016/j.neuron.2013.07.051, PMID: 23972592

Akella JS, Wloga D, Kim J, Starostina NG, Lyons-Abbott S, Morrissette NS, Dougan ST, Kipreos ET, Gaertig J. 2010. MEC-17 is an alpha-tubulin acetyltransferase. *Nature* **467**:218–222. doi: 10.1038/nature09324, PMID: 20829795

Bounoutas A, O'Hagan R, Chalfie M. 2009. The multipurpose 15-protofilament microtubules in C. elegans have specific roles in mechanosensation. *Current Biology* **19**:1362–1367. doi: 10.1016/j.cub.2009.06.036, PMID: 19615905

Brohawn SG, Campbell EB, MacKinnon R. 2014a. Physical mechanism for gating and mechanosensitivity of the human TRAAK K+ channel. *Nature* **516**:126–130. doi: 10.1038/nature14013, PMID: 25471887

Brohawn SG, del Mármol J, MacKinnon R. 2012. Crystal structure of the human K2P TRAAK, a lipid- and mechano-sensitive K+ ion channel. *Science* **335**:436–441. doi: 10.1126/science.1213808, PMID: 22282805

Brohawn SG, Su Z, MacKinnon R. 2014b. Mechanosensitivity is mediated directly by the lipid membrane in TRAAK and TREK1 K+ channels. *PNAS* **111**:3614–3619. doi: 10.1073/pnas.1320768111, PMID: 24550493

Carpenter AE, Jones TR, Lamprecht MR, Clarke C, Kang IH, Friman O, Guertin DA, Chang JH, Lindquist RA, Moffat J, Golland P, Sabatini DM. 2006. CellProfiler: image analysis software for identifying and quantifying cell phenotypes. *Genome Biology* **7**:R100. doi: 10.1186/gb-2006-7-10-r100, PMID: 17076895

Castro-Castro A, Janke C, Montagnac G, Paul-Gilloteaux P, Chavrier P. 2012. ATAT1/MEC-17 acetyltransferase and HDAC6 deacetylase control a balance of acetylation of alpha-tubulin and cortactin and regulate MT1-MMP trafficking and breast tumor cell invasion. *European Journal of Cell Biology* **91**:950–960. doi: 10.1016/j.ejcb.2012.07.001, PMID: 22902175

Chalfie M, Thomson JN. 1982. Structural and functional diversity in the neuronal microtubules of Caenorhabditis elegans. *Journal of Cell Biology* **93**:15–23. doi: 10.1083/jcb.93.1.15, PMID: 7068753

Chen JT, Guo D, Campanelli D, Frattini F, Mayer F, Zhou L, Kuner R, Heppenstall PA, Knipper M, Hu J. 2014. Presynaptic GABAergic inhibition regulated by BDNF contributes to neuropathic pain induction. *Nature Communications* **5**:5331. doi: 10.1038/ncomms6331, PMID: 25354791

Chiang LY, Poole K, Oliveira BE, Duarte N, Sierra YA, Bruckner-Tuderman L, Koch M, Hu J, Lewin GR. 2011. Laminin-332 coordinates mechanotransduction and growth cone bifurcation in sensory neurons. *Nature Neuroscience* **14**:993–1000. doi: 10.1038/nn.2873, PMID: 21725315

Choi Y, Yoon YW, Na HS, Kim SH, Chung JM. 1994. Behavioral signs of ongoing pain and cold allodynia in a rat model of neuropathic pain. *Pain* **59**:369–376. doi: 10.1016/0304-3959(94)90023-x, PMID: 7708411

Cox CD, Bae C, Ziegler L, Hartley S, Nikolova-Krstevski V, Rohde PR, Ng CA, Sachs F, Gottlieb PA, Martinac B. 2016. Removal of the mechanoprotective influence of the cytoskeleton reveals PIEZO1 is gated by bilayer tension. *Nature Communications* **7**:10366. doi: 10.1038/ncomms10366, PMID: 26785635

Cramer LP, Mitchison TJ. 1995. Myosin is involved in postmitotic cell spreading. *Journal of Cell Biology* **131**:179–189. doi: 10.1083/jcb.131.1.179, PMID: 7559774

Cueva JG, Hsin J, Huang KC, Goodman MB. 2012. Posttranslational acetylation of α-tubulin constrains protofilament number in native microtubules. *Current Biology* **22**:1066–1074. doi: 10.1016/j.cub.2012.05.012, PMID: 22658592

Davenport AM, Collins LN, Chiu H, Minor PJ, Sternberg PW, Hoelz A. 2014. Structural and functional characterization of the α-tubulin acetyltransferase MEC-17. *Journal of Molecular Biology* **426**:2605–2616. doi: 10.1016/j.jmb.2014.05.009, PMID: 24846647

Delmas P, Hao J, Rodat-Despoix L. 2011. Molecular mechanisms of mechanotransduction in mammalian sensory neurons. *Nature Reviews Neuroscience* **12**:139–153. doi: 10.1038/nrn2993, PMID: 21304548

Elhabazi K, Ayachi S, Ilien B, Simonin F. 2014. Assessment of morphine-induced hyperalgesia and analgesic tolerance in mice using thermal and mechanical nociceptive modalities. *Journal of Visualized Experiments*: e51264. doi: 10.3791/51264, PMID: 25145878

Fukushige T, Siddiqui ZK, Chou M, Culotti JG, Gogonea CB, Siddiqui SS, Hamelin M. 1999. MEC-12, an alpha-tubulin required for touch sensitivity in C. elegans. *Journal of Cell Science* **112**:395–403. PMID: 9885292

Hamm RJ, Pike BR, O'Dell DM, Lyeth BG, Jenkins LW. 1994. The rotarod test: an evaluation of its effectiveness in assessing motor deficits following traumatic brain injury. *Journal of Neurotrauma* **11**:187–196. doi: 10.1089/neu.1994.11.187, PMID: 7932797

Hu J, Chiang LY, Koch M, Lewin GR. 2010. Evidence for a protein tether involved in somatic touch. *The EMBO Journal* **29**:855–867. doi: 10.1038/emboj.2009.398, PMID: 20075867

Hu J, Lewin GR. 2006. Mechanosensitive currents in the neurites of cultured mouse sensory neurones. *Journal of Physiology* **577**:815–828. doi: 10.1113/jphysiol.2006.117648

Kalebic N, Martinez C, Perlas E, Hublitz P, Bilbao-Cortes D, Fiedorczuk K, Andolfo A, Heppenstall PA. 2013a. Tubulin acetyltransferase αTAT1 destabilizes microtubules independently of its acetylation activity. *Molecular and Cellular Biology* **33**:1114–1123. doi: 10.1128/MCB.01044-12, PMID: 23275437

Kalebic N, Sorrentino S, Perlas E, Bolasco G, Martinez C, Heppenstall PA. 2013b. αTAT1 is the major α-tubulin acetyltransferase in mice. *Nature Communications* **4**:1962. doi: 10.1038/ncomms2962, PMID: 23748901

Krieg M, Dunn AR, Goodman MB. 2014. Mechanical control of the sense of touch by β-spectrin. *Nature Cell Biology* **16**:224–233. doi: 10.1038/ncb2915, PMID: 24561618

Krieg M, Dunn AR, Goodman MB. 2015. Mechanical systems biology of C. elegans touch sensation. *BioEssays* **37**:335–344. doi: 10.1002/bies.201400154, PMID: 25597279

Kwan KY, Allchorne AJ, Vollrath MA, Christensen AP, Zhang DS, Woolf CJ, Corey DP. 2006. TRPA1 contributes to cold, mechanical, and chemical nociception but is not essential for hair-cell transduction. *Neuron* **50**:277–289. doi: 10.1016/j.neuron.2006.03.042, PMID: 16630838

Lapatsina L, Jira JA, Smith ES, Poole K, Kozlenkov A, Bilbao D, Lewin GR, Heppenstall PA. 2012. Regulation of ASIC channels by a stomatin/STOML3 complex located in a mobile vesicle pool in sensory neurons. *Open Biology* **2**:120096. doi: 10.1098/rsob.120096, PMID: 22773952

Lewis AH, Grandl J. 2015. Mechanical sensitivity of Piezo1 ion channels can be tuned by cellular membrane tension. *eLife* **4**:e12088. doi: 10.7554/eLife.12088, PMID: 26646186

Lolicato M, Riegelhaupt PM, Arrigoni C, Clark KA, Minor DL. 2014. Transmembrane helix straightening and buckling underlies activation of mechanosensitive and thermosensitive K(2P) channels. *Neuron* **84**:1198–1212. doi: 10.1016/j.neuron.2014.11.017, PMID: 25500157

Lukinavičius G, Reymond L, D'Este E, Masharina A, Göttfert F, Ta H, Güther A, Fournier M, Rizzo S, Waldmann H, Blaukopf C, Sommer C, Gerlich DW, Arndt HD, Hell SW, Johnsson K. 2014. Fluorogenic probes for live-cell imaging of the cytoskeleton. *Nature Methods* **11**:731–733. doi: 10.1038/nmeth.2972, PMID: 24859753

Maksimovic S, Nakatani M, Baba Y, Nelson AM, Marshall KL, Wellnitz SA, Firozi P, Woo SH, Ranade S, Patapoutian A, Lumpkin EA. 2014. Epidermal Merkel cells are mechanosensory cells that tune mammalian touch receptors. *Nature* **509**:617–621. doi: 10.1038/nature13250, PMID: 24717432

Milenkovic N, Wetzel C, Moshourab R, Lewin GR. 2008. Speed and temperature dependences of mechanotransduction in afferent fibers recorded from the mouse saphenous nerve. *Journal of Neurophysiology* **100**:2771–2783. doi: 10.1152/jn.90799.2008, PMID: 18815344

Poole K, Herget R, Lapatsina L, Ngo HD, Lewin GR. 2014. Tuning Piezo ion channels to detect molecular-scale movements relevant for fine touch. *Nature Communications* **5**:3520. doi: 10.1038/ncomms4520, PMID: 24662763

Prager-Khoutorsky M, Khoutorsky A, Bourque CW. 2014. Unique interweaved microtubule scaffold mediates osmosensory transduction via physical interaction with TRPV1. *Neuron* **83**:866–878. doi: 10.1016/j.neuron.2014.07.023, PMID: 25123313

Qi Y, Andolfi L, Frattini F, Mayer F, Lazzarino M, Hu J. 2015. Membrane stiffening by STOML3 facilitates mechanosensation in sensory neurons. *Nature Communications* **6**:8512. doi: 10.1038/ncomms9512, PMID: 26443885

Ranade SS, Woo SH, Dubin AE, Moshourab RA, Wetzel C, Petrus M, Mathur J, Bégay V, Coste B, Mainquist J, Wilson AJ, Francisco AG, Reddy K, Qiu Z, Wood JN, Lewin GR, Patapoutian A. 2014. Piezo2 is the major transducer of mechanical forces for touch sensation in mice. *Nature* **516**:121–125. doi: 10.1038/nature13980, PMID: 25471886

Reed NA, Cai D, Blasius TL, Jih GT, Meyhofer E, Gaertig J, Verhey KJ. 2006. Microtubule acetylation promotes kinesin-1 binding and transport. *Current Biology* **16**:2166–2172. doi: 10.1016/j.cub.2006.09.014, PMID: 17084703

Robison P, Caporizzo MA, Ahmadzadeh H, Bogush AI, Chen CY, Margulies KB, Shenoy VB, Prosser BL. 2016. Detyrosinated microtubules buckle and bear load in contracting cardiomyocytes. *Science* **352**:aaf0659. doi: 10.1126/science.aaf0659, PMID: 27102488

Rotsch C, Jacobson K, Radmacher M. 1999. Dimensional and mechanical dynamics of active and stable edges in motile fibroblasts investigated by using atomic force microscopy. *PNAS* **96**:921–926. doi: 10.1073/pnas.96.3.921, PMID: 9927669

Shida T, Cueva JG, Xu Z, Goodman MB, Nachury MV. 2010. The major alpha-tubulin K40 acetyltransferase alphaTAT1 promotes rapid ciliogenesis and efficient mechanosensation. *PNAS* **107**:21517–21522. doi: 10.1073/pnas.1013728107, PMID: 21068373

Sukharev S. 2002. Purification of the small mechanosensitive channel of Escherichia coli (MscS): the subunit structure, conduction, and gating characteristics in liposomes. *Biophysical Journal* **83**:290–298. doi: 10.1016/S0006-3495(02)75169-2, PMID: 12080120

Sung K, Maloney MT, Yang J, Wu C. 2011. A novel method for producing mono-biotinylated, biologically active neurotrophic factors: an essential reagent for single molecule study of axonal transport. *Journal of Neuroscience Methods* **200**:121–128. doi: 10.1016/j.jneumeth.2011.06.020, PMID: 21756937

Szyk A, Deaconescu AM, Spector J, Goodman B, Valenstein ML, Ziolkowska NE, Kormendi V, Grigorieff N, Roll-Mecak A. 2014. Molecular basis for age-dependent microtubule acetylation by tubulin acetyltransferase. *Cell* **157**:1405–1415. doi: 10.1016/j.cell.2014.03.061, PMID: 24906155

Topalidou I, Keller C, Kalebic N, Nguyen KC, Somhegyi H, Politi KA, Heppenstall P, Hall DH, Chalfie M. 2012. Genetically separable functions of the MEC-17 tubulin acetyltransferase affect microtubule organization. *Current Biology* **22**:1057–1065. doi: 10.1016/j.cub.2012.03.066, PMID: 22658602

Wetzel C, Hu J, Riethmacher D, Benckendorff A, Harder L, Eilers A, Moshourab R, Kozlenkov A, Labuz D, Caspani O, Erdmann B, Machelska H, Heppenstall PA, Lewin GR. 2007. A stomatin-domain protein essential for touch sensation in the mouse. *Nature* **445**:206–209. doi: 10.1038/nature05394, PMID: 17167420

Woo SH, Lukacs V, de Nooij JC, Zaytseva D, Criddle CR, Francisco A, Jessell TM, Wilkinson KA, Patapoutian A. 2015. Piezo2 is the principal mechanotransduction channel for proprioception. *Nature Neuroscience* **18**:1756–1762. doi: 10.1038/nn.4162, PMID: 26551544

Woo SH, Ranade S, Weyer AD, Dubin AE, Baba Y, Qiu Z, Petrus M, Miyamoto T, Reddy K, Lumpkin EA, Stucky CL, Patapoutian A. 2014. Piezo2 is required for Merkel-cell mechanotransduction. *Nature* **509**:622–626. doi: 10.1038/nature13251, PMID: 24717433

Yang G, de Castro Reis F, Sundukova M, Pimpinella S, Asaro A, Castaldi L, Batti L, Bilbao D, Reymond L, Johnsson K, Heppenstall PA. 2015. Genetic targeting of chemical indicators in vivo. *Nature Methods* **12**:137–139. doi: 10.1038/nmeth.3207, PMID: 25486061

Zhang W, Cheng LE, Kittelmann M, Li J, Petkovic M, Cheng T, Jin P, Guo Z, Göpfert MC, Jan LY, Jan YN. 2015. Ankyrin repeats convey force to gate the NOMPC mechanotransduction channel. *Cell* **162**:1391–1403. doi: 10.1016/j.cell.2015.08.024, PMID: 26359990

Zhang Y, Ma C, Delohery T, Nasipak B, Foat BC, Bounoutas A, Bussemaker HJ, Kim SK, Chalfie M. 2002. Identification of genes expressed in C. elegans touch receptor neurons. *Nature* **418**:331–335. doi: 10.1038/nature00891, PMID: 12124626

Zurborg S, Piszczek A, Martínez C, Hublitz P, Al Banchaabouchi M, Moreira P, Perlas E, Heppenstall PA. 2011. Generation and characterization of an Advillin-Cre driver mouse line. *Molecular Pain* **7**:66. doi: 10.1186/1744-8069-7-66, PMID: 21906401